Improving Aptamer Specificity with Novel Counterselection Strategies

By

Jonah C. Rosch

Dissertation

Submitted to the Faculty of the

Graduate School of Vanderbilt University

in partial fulfillment of the requirements

for the degree of

DOCTOR OF PHILOSOPHY

in

Chemical and Biomolecular Engineering

August 31, 2020

Nashville, Tennessee

Approved:

Ethan Lippmann, Ph.D.

Craig Duvall, Ph.D.

Matthew Lang, Ph.D.

John Wilson, Ph.D.

For my family and friends who have given me so much love and support through the years.

ACKNOWLEDGEMENTS

My five years at Vanderbilt University flew by. I started my PhD in 2015 at 21 years old, not knowing what research would be like or what to expect from graduate school. I came in with rose-tinted glasses ready to take on the world but quickly realized the challenges of graduate school. I have learned so much over my time at Vanderbilt and have matured so much as a person. I would not have been successful had it not been for the wonderful people around me.

I would like to thank my committee members Dr. John Wilson, Dr. Craig Duvall, and Dr. Matt Lang for their guidance over the years. In addition to providing me with research expertise, I have gotten to know all of them a little bit outside of a work setting. Each of them has made my graduate school experience so much more manageable. I have had collaborations with graduate students in each of their labs and have appreciated their willingness to discuss anything.

I have had such a great lab experience because of the awesome people I have worked with. I started up our lab with Dr. Emma Hollmann Neal and I always had to push myself to keep up with her work ethic. My lab members over of the years have been so pleasant to work with and I have enjoyed getting to know them inside and outside of a lab setting: Allison Bosworth, Kylie Balotin, Nicholas Marinelli, Yajuan Shi, Ketaki Katdare, Everett Allchin, Alexander Sorets, Lexi Yates, Madison Stiefbold, Brian O'Grady, and Hyosung Kim. I can leave this lab knowing the research projects I have started are in good hands with Everett and Alex. I have had the privilege to mentor two undergraduates directly, Franklin Gong and Nikki Kragt, who have been great helps to me and working with them has taught me how to become a better mentor. I have also enjoyed working with numerous other undergraduate students indirectly, including Michaela Copp, Archit Potharazu, Robbie Weinstein, Amanda Bailey, Riley Knight, Dalton Gullett, Cassie Woolley, Catey Dodson, and Kameron Hagerla.

Two of the most important people to thank are my advisor and postdoc, Dr. Ethan Lippmann and Dr. Daniel Balikov. Ethan and I have learned so much together about starting up a lab and the aptamer field over the past five years. I appreciate his willingness to always be available to talk about research plans or provide emotional support. I feel proud about starting this part of the lab, which wouldn't have been possible without his guidance. Dan was (and still is) a great mentor and friend in my life. Dan started as a postdoc during my second year of graduate school and helped guide me as a scientist. We still chat weekly to keep up with each other's lives. Both Ethan and Dan have been great mentors and I appreciate their guidance in science and in life.

My friends have been such a great support system and I can safely say that we have enjoyed our time in Nashville. I appreciate all of my roommates over the years, including Dushyant Barpaga and Michael Marin, older graduate students who gave me advice in my first few years, and Michael Kosson and Joshua Passantino, who I have been able to pass this guidance onto. I have had the joy of working with one of my best friends, Allison Bosworth, in lab and am thankful to always have her as a karaoke buddy. Through Allison, I have gotten to know Katie Ozgun, who always cheers everyone up around her with her bright personality and who I have yet to ever see not be in a good mood. I have probably spent more time with one of my best friends, Kyle Garland, than anyone else in graduate school. Whether we are out having fun or just sitting in his apartment drinking an espresso, I'm always thankful knowing that he has my back no matter what. I owe so much to one of my best friends, Mohsin Rahim, who started graduate school at the same time as me. I don't know if I would have made it through classes or the rigors of graduate school without knowing that we were always going through it together. Since day 1, we have always been there for each other and I have been so lucky to have him in

my life. Through Mohsin, I have become so close with Prarthana Patil, who is always available for emotional support and who is always better at telling the waiter at a restaurant that I need something fixed. I was lucky enough to meet Ella Hoogenboezem through our research collaboration and she quickly became one of my best friends. As a researcher, she is one of the smartest people I know, and as a friend, she knows me better than anyone else. Words cannot express my gratitude to all of my friends and I look forward to staying friends for life.

Finally, I need to thank my family for their love and support. I have always followed in my brother's footsteps and have looked to him for guidance my whole life. My dad has always provided stability in my life and always makes sure I am becoming the best person I can be. My mom has always been my emotional support and is the most caring and loving woman in the world. I am so fortunate to have such an amazing family and group of friends in my life.

TABLE OF CONTENTS

Page

Abbreviations

AF Buffer: Aptamer folding buffer
BBB: Blood-brain barrier
BMEC: Brain microvascular endothelial cells
Bp: base pair
CRISPR: Clustered regularly interspaced short palindromic repeats
ddPCR: Droplet digital polymerase chain reaction
dsDNA: Double-strand DNA
ePCR: Emulsion polymerase chain reaction
GLUT: Glucose transporter
gRNA: Guide RNA
HTS: High throughput sequencing
iPSC: Induced pluripotent stem cell
ITC: Isothermal calorimetry
IVT: *in vitro* transcription
miRNA: Micro ribonucleic acid
MST: Microscale thermophoresis
NGS: Next-Generation Sequencing
Nt: nucleotide
PDGF: Platelet-derived growth factor
qPCR: Quantitative polymerase chain reaction
SELEX: Systematic evolution of ligands through exponential enrichment
siRNA: Short interfering ribonucleic acid
SPR: Surface plasmon resonance
ssDNA: Single-strand DNA
ssRNA: Single-strand RNA
TIDE: Tracking of indels by decomposition
VEGF: Vascular endothelial growth factor

LIST OF MAIN TABLES

Table Page

LIST OF APPENDIX TABLES

Table Page

LIST OF MAIN FIGURES

Table Page

LIST OF APPENDIX FIGURES

Table Page

Chapter 1

INTRODUCTION

1.1 Aptamer Background

Aptamers are short, single-stranded deoxyribonucleic acids (DNA) or ribonucleic acids (RNA) that are able to fold into unique three-dimensional structures and bind to target molecules with high affinity and specificity [1], [2], summarized in Figure 1.1. Derived from the Latin 'aptus', meaning 'fitting', aptamers adopt complex three-dimensional structures that include hairpins (stems, loops, bulges), pseudoknots, and quadruplexes to bind to a variety of biological targets [3]. Similar to antibody-antigen binding, aptamers bind to target molecules through stacking of aromatic rings, electrostatic interactions, van der Waals interactions, hydrogen bonding, or a combination of these effects [4], [5]. Aptamers were first selected in the early 1990s by Szostak and Ellington and in the decades since, aptamers have been selected for a variety of targets including inorganic materials, small molecules, peptides, proteins, cell surface receptors, whole cells, and even organs of live animals to be used as diagnostic and therapeutic agents [6]. Aptamers have proven to be able to distinguish between structurally similar molecules [7], including conformational isomers [8], targets with different functional groups [9], and a single amino acid mutation [10].

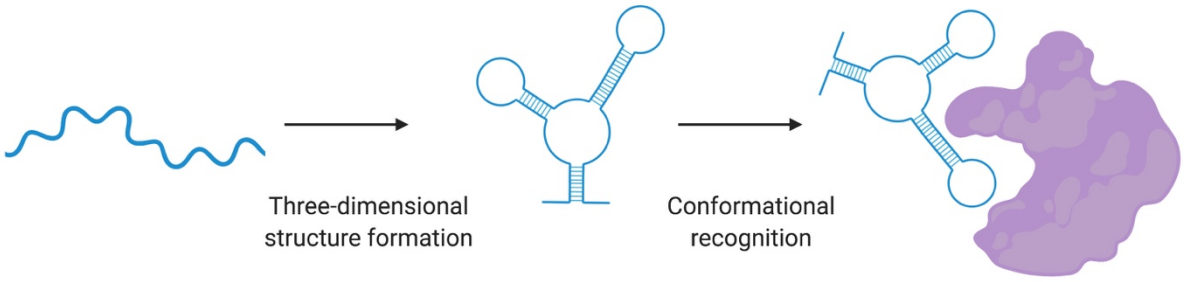

Figure 1.1 Conformational recognition of targets. Aptamers are short, single strand nucleic acid structures which adopt unique tertiary structures to bind to their targets with high affinity and specificity. Figure adapted from Sun, 2014 [11].

Aptamers have drawn interest from the research community due to unique features that make them advantageous over existing affinity reagents, such as monoclonal antibodies (mAbs). Aptamers are similar to antibodies with respect to their binding mechanism and achievable binding affinities [12], [13]. Three key differences between aptamers and antibodies are size, synthesis, and selectivity. Aptamers are comprised of a nucleotide backbone compared to the amino acid backbone of antibodies, with four basic nucleotide members compared to 20 amino acid members. The nucleotide backbone allows for easy chemical modifications and conjugation, as well as a higher tendency to be non-toxic and non-immunogenic. Aptamers are roughly a fifth of the size (~2 nm for aptamers versus ~15 nm for mAb) and molecular weight (~6-30 kDa for aptamers versus ~150-180 kDa for mAb) of a conventional mAb [14]. The small size of aptamers allows for faster tissue uptake and penetration and can theoretically target a wider range of targets due to smaller binding pockets [15]. The chemical solid-phase synthesis of aptamers allows for lower production cost and reduction in batch-to-batch variation, in addition to shorter development time than mAbs (~1-3 months for aptamers versus ~4-6 months for mAbs) [12].

Aptamers have been utilized in numerous therapeutic and diagnostic applications. As therapeutics, aptamers are generally used in three strategies; as an antagonist, an agonist, or

delivery vehicle [16]. The most commonly used strategy for implementing aptamers as therapeutics is using them directly as antagonists [17]. As antagonists, aptamers acts as inhibitors to disrupt the function of a target, such as a protein-protein interactions or receptor-ligand interactions. Typically, aptamers administered directly as antagonists perform poorly, requiring specialized designs or formulations, including fusing with antibodies, cholesterol, nanoparticles, gels, or forming multimers [16]. Aptamers have been isolated for applications as antivirals (ex: HIV reverse transcriptase [18]), anticoagulants (ex: thrombin [19] and Factor VIIa [20]), anti-angiogenic molecules (ex: Vacsular Endothelial Growth Factor (VEGF) [21]), anti-inflammatory molecules (ex: Human Neutrophil Elastase [22] and platelet-derived growth factor (PDGF) [23]), anti-proliferation molecules (ex: prostate-specific membrane antigen (PSMA) [24]), and immune-modulating molecules (ex: acetylcholine receptors [25] and human interferon-gamma [26]). Aptamers are more rarely used as agonists, to activate the function of a target receptor or molecule. Typically, aptamers are used as agonists in cancer immunotherapy, for such targets as human epidermal growth factor receptor 3 (HER3) [27], OX40 [28], CD40 [29], and CD28 [30]. Aptamers can also be used as delivery agents, where the aptamer binds to a cell-type-specific target to delivery other therapeutic agents to target cells and tissues [31]. Aptamers can be conjugated to oligonucleotides, such as shorting-interfering RNAs (siRNAs) [32], microRNAs (miRNAs) [33], and other therapeutic aptamers, drugs, such as chemotherapeutics [34] or toxins [35], [36], and delivery vehicles, such as aptamer-decorated nanomaterials [37].

1.2 Aptamer Limitations

Aptamers were first developed 30 years ago, but have lagged behind other affinity reagents as therapeutic reagents, especially antibodies [13]. Table 1.1 summarizes the current aptamers in

clinical trials. At present, only one aptamer has been approved for therapeutic application, Macugen, which binds VEGF to block abnormal angiogenesis in the eye, and eleven other aptamers are currently in clinical trials [38]. Macugen has been largely superseded by bevacizumab and ranibizumab, VEGF-specific monoclonal antibodies [39]. With all of the potential advantages of aptamers, it may seem surprising that this field has had limited success. The potential for low immunological effects, ease of manufacturing, and unique functional abilities of aptamers would seemingly make them ideal to investigate further for research and clinical applications. There are numerous possible reasons why aptamers still have not become commonly used as therapeutics. First there have been clinical failures of aptamers, which may have hindered investment in their advancement, such as the termination of a phase III clinical trial of an anticoagulant aptamer against factor IXa [40]. Aptamers should have little-to-no toxicity or immunogenic effects when administered *in vivo*; however, availability of this information is limited for administration in humans [41]. Potential toxicity issues may arise from polyanionic effects and nonspecific tissue and organ accumulation [42]. Additionally, conjugations and modifications to the aptamer structure can impart various issues when being administered *in vivo*.

Table 1.1 Aptamers in the clinic. There is currently one FDA-approved aptamer, Macugen, used to treat age-related macular degeneration. Ten other aptamers have undergone clinical trials, all acting as antagonists. Table adapted from Keefe, 2010 [12] and Kaur, 2018 [43].

Name	Target	Composition	Disease	Current Phase
Pepaptanib sodium/ Macugen	Vascular endothelial growth factor	2'-O'methyl purine/ 2'-fluoro pyrimidine with two 2'-ribo purines conjugated to 40 kDa PEG, 3' inverted dT	Age-related macular degeneration	Approved in the US and EU
AS1411/ AGRO001	Nucleolin	G-rich DNA	Acute myeloid leukemia	Phase II
REG1/ RB006 plus RB007	Coagulation factor IXa	2'-ribo purine/ 2'-fluoro pyrimidine/ 40 kDA PEG plus 2'-O-methyl antidote	Percutaneous coronary intervention	Phase II
ARC1779	A1 domain of von Willebrand factor	DNA and 2'-O-methyl with a single phosphorothioate linkage conjugated to 20 kDa PEG, 3' inverted dT	Thrombotic microangiopathies and carotid artery disease	Phase II
NU172	Thrombin	Unmodified DNA aptamer	Cardiopulmonary bypass to maintain steady state of anticoagulation	Phase II
NOX-H94	Hepcidin	PEGylated L-sterioisomer RNA aptamer	Anemia	Phase 2
ARC1905	Complement component 5	2'-ribo purine/ 2'-fluoro pyrimidine conjugated to 40 kDa PEG, 3' inverted dT	Age-related macular degeneration	Phase 1
E10030	Platelet-derived growth factor	DNA and 2'-O-methyl 5'-conjugated to 40 kDA PEG, 3' inverted dT	Age-related macular degeneration	Phase 1
NOX-A12	CXCL12	L-RNA with 3'-PEG	Multiple myeloma and non-Hodgkin's lymphoma	Phase 1
NOX-E36	CCL2	L-RNA with 3'-PEG	Type 2 diabetes, diabetic nephropathy	Phase 1
ARC1779	A1 domain of von Willebrand Factor	PEGylated, unmodified DNA/ 2'O-methyl RNA/ 3' inverted dT	Von Willebrand Disease	Phase 1
BX499	Tissue Factor Pathway	RNA with 3'-inverted dT, 40-kDa PEG, and 5'-hexylamine linker	Hemophilia	Phase 1

The size of aptamers make them easily excreted from the bloodstream through renal filtration of molecules less than 30 kDa [44]. Nucleases in biological media hinder the *in vivo* applications of aptamers; for example, oligonucleotides are typically degraded in blood within several minutes, making them impractical without degradation protection mechanisms. Additionally, there is a steep learning curve and lack of standardized protocols that prohibit researchers from easily developing aptamers for personal research use [41], [45]. The process for identifying aptamers can be laborious and difficult, with conventional procedures only having a 30% success rate to develop high affinity and specificity aptamers [11]. Each selection procedure is inherently different due to unique characteristics of the target molecule, requiring laborious evaluation and optimization. Furthermore, aptamers can fail to recognize primary targets and bind to molecules with similar structures, even with seemingly high specificity [46]. There are no benchmarks to determine if a certain degree of specificity will prohibit side-effects *in vivo*. Even if aptamers with high affinity are identified from a selection procedure, cross-reactivity can diminish clinical relevance.

Advancements in oligonucleotide technologies and manufacturing have been used to address some of these limitations with aptamers. Modified nucleotides have been used in aptamer selections to reduce the effects of nuclease degradation, including 2'-amino pyrimidine, 2'-fluorine pyrimidine, 2'-O-methyl purine and pyrimidine, locked nucleic acids, and inverted thymidine capping on the 3' end [44], [47]. Furthermore, two new classes of modified bases have been specifically developed to be incorporated into aptamer selections; SOMAmers (slow off-rate modified aptamers) and Spiegelmers [48]. SOMAmers are modified deoxyuracil bases with a hydrophobic functional group at the C5 position, often improving the affinity and functional abilities with incorporated bases over unmodified bases [49]. Spiegelmers are L-form RNA

aptamers that are chiral inversions of natural D-forms, which improve *in vivo* biostability by avoiding nuclease degradation [50]. Conjugations with bulky groups, such as polyethylene glycol (PEG) [51], proteins [52], cholesterol [53], and liposomes [54] have been used to increase the molecular weight and size of aptamers to avoid rapid excretion through renal filtration. Designing multivalent aptamers with complementary linkers or polyethylene spacers can also be used to increase the size of the molecule [55].

An oft-cited roadblock for the development of aptamers is the numerous issues associated with the selection workflow. Aptamers are direct products of their selection environment, meaning that experimental conditions, such as buffer components, pH, and incubation temperatures, and inherent target properties, such as pI charge and hydrophilicity, directly affect their applications [1], [13]. Additionally, the off-targets introduced into the selection workflow directly affect the affinity and specificity of the aptamers that can be obtained. Understanding how they are selected is a crucial component in isolating aptamers with the best chance for successful applications, as discussed in the next section.

1.3 Overview of SELEX

Aptamers are selected using an *in vitro* selection process called Systematic Evolution of Ligands by Exponential Enrichment (SELEX) [6], in which high affinity aptamers are selected from a random starting oligonucleotide library through iterative rounds of selection. Figure 1.2 shows the general steps to performing a DNA aptamer selection. The starting library usually consists of aptamers with 20-60 random bases, flanked by primer regions of about 20 bases. Our lab uses a starting single-strand DNA (ssDNA) library of 40 random nucleotides flanked by 20 nucleotides in the 5'- and 3'-end constant regions, which theoretically yields 10^{24} unique

sequences, but realistically yields 10^{15} unique sequences [56], [57]. Every aptamer selection varies to some degree, but each round includes three key steps: (1) a binding step, where the aptamer library is incubated with the target molecule, (2) a partitioning step, where weakly bound aptamers are removed from the selection pool through washing, and (3) an amplification step, where bound aptamers are eluted and PCR amplified. After PCR amplification in a DNA selection, double-strand DNA is regenerated to ssDNA through bead separation or with the use of an exonuclease. This *in vitro* selection method emulates Darwinian evolution where the "strongest", high-affinity aptamers are retained through the rounds and the "weakest", low-affinity aptamers are removed from the selection process. This iterative process is continued until the researcher determines that the final pool has converged on individual aptamers with desired properties.

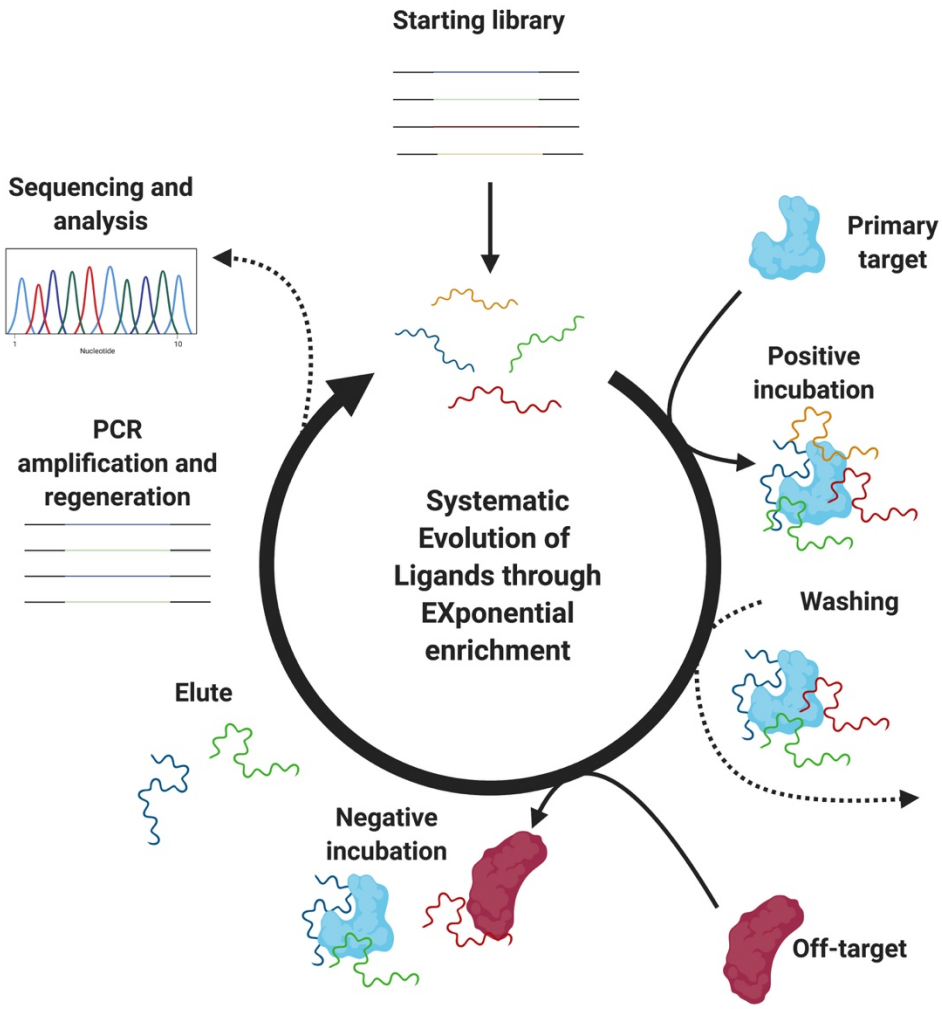

Figure 1.2 Overview of SELEX workflow. In a standard DNA aptamer selection, the initial library is incubated with the primary target and washed, followed by introduction of off-targets in a counterselection. Bound aptamer sequences are eluted, PCR amplified, and regenerated to ssDNA, to be used in the next round of selection. At the end of the selection, individual sequences are isolated for characterization. Figure adapted from Darmostuk, 2016 [58].

A crucial part of an aptamer selection to impart specificity is the counterselection step, also referred to as the negative selection. The positive selection imparts affinity toward the target molecule, whereas the negative selection imparts specificity against undesired off-targets. Aptamers bound to the primary target in the positive selection are eluted and introduced to the off-

targets to be removed from the selection system. Selection pressure of the positive and negative selections are increased through the rounds to allow for the selection of aptamers with higher affinity toward the primary target and higher specificity against off-targets. Increasing selection pressure involves increasing the time of washing, the amount and concentration of off-targets, and the time of the counterselection, while decreasing the amount of primary target and the time of the positive incubation [59]. The selection process is complete when the researcher determines that the pools have converged with a high probability to identify high affinity sequences from the final pool.

Two methods can be used to identify individual sequences from the final pool: conventional bacterial cloning and high throughput sequencing (HTS). Conventional cloning requires the aptamer selection to converge to a high affinity pool to ensure that the clones that are isolated are representative of the pool. More recently, HTS has been used as a powerful tool to identify aptamers from selection pools more rapidly [7], [60]. HTS allows researchers to track the evolution and enrichment of over 10 million sequences from each pool, as opposed to the less than 100 colonies that are usually picked from bacterial cloning. Computer analysis has helped researchers in sorting through HTS data to identify aptamers within three rounds and with up to 8-fold higher affinity than those obtained with traditional cloning techniques [7]. Once individual aptamer sequences have been identified through cloning or HTS, the aptamers are analyzed for their binding kinetics, including affinity, specificity, and on/off rates. There are numerous assays that can be used to analyze the binding kinetics with varying levels of difficulty and precision, including fluorescent-based assays, such as flow cytometry or quantitative PCR (qPCR), anisotropy, surface plasmon resonance (SPR), microscale thermophoresis (MST), and isothermal titration calorimetry (ITC) [61].

There are many different methods of selecting aptamers, all with benefits and limitations. Common methods for purified-target SELEX include nitrocellulose filter binding, coupling-chemistry beads, capillary electrophoresis, and microfluidics. For nitrocellulose filter binding, proteins are immobilized on nitrocellulose filters, incubated with the library, and washed to remove weakly bound aptamers [62]. However, nucleic acids can also bind nonspecifically to nitrocellulose, which can confound the selection process. For coupling-chemistry beads, agarose, polystyrene, and magnetic beads have been used to tether proteins and other targets to their surfaces using various chemical reactions, such as EDC-NHS and streptavidin [56]. Beads can be separated from the library with magnetic separation or centrifugation. However, there can be difficulty handling these beads and nonspecific binding to the beads surface. For capillary electrophoresis, an electric current is applied to aptamers bound to targets, separating weakly bound aptamers from the target [63]. Fewer rounds of selection are required with capillary electrophoresis, but its use is limited to targets that will cause an electrophoretic shift. Microfluidic methods require only a few rounds of selection, but require specialized micromanufacturing techniques [64].

Aptamer selections can also be performed using whole cells and animals, though much more uncommonly performed. Figure 1.3 summarizes the types of aptamer selections performed in the literature. In cell-based SELEX, aptamers are bound to the surface of whole cells, either targeting a specific cell type or cell surface receptor [65]. Aptamers have been generated that can distinguish between different cell lineages and healthy versus tumor cells [66], [67], [34]. However, due to the complex surface of cells, generating aptamers with high specificity for a particular target can be difficult. For *in vivo* SELEX, aptamer libraries are injected into whole animals and tissues or organs of interest are removed [68]–[70]. Aptamers in these tissues or

organs are extracted and amplified for the next round of selection. Typically, cell-based SELEX and *in vivo* SELEX require more rounds of selection than purified-target SELEX due to increased complexities of the system. However, the benefit of performing these selections is the target displaying its correct conformation for more translatable applications.

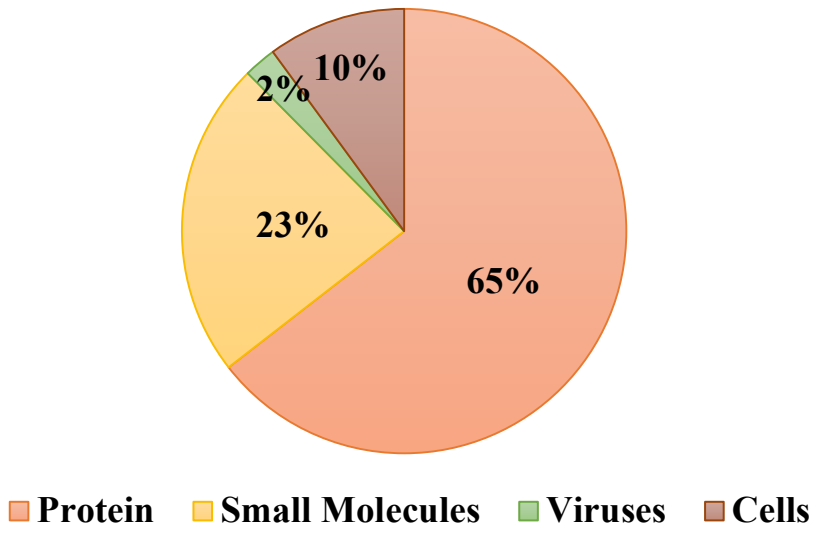

Figure 1.3 Summary of types of aptamer selections performed. The majority of aptamer selections are performed on proteins and small molecules. Cell-based selections account for only 10% of aptamer selections performed. Figure modified from Cruz-Toledo, 2012 [71].

In any form of aptamer selection, there are two particular challenges that influence aptamer isolation: poor partitioning during selection and washing, which is critical for removing weakly bound aptamers from the selection, and spurious PCR amplification, which can lead to the formation of byproducts and amplification artifacts [41], [72]. Many issues associated with the SELEX workflow have been addressed by research labs, such as increasing the number of rounds of a selection and using emulsion PCR (ePCR) or ddPCR to reduce the chance of byproduct formation during the amplification [73], [74]. More stringent washing steps have been

incorporated into workflows for removing weakly bound aptamers with the use of microfluidic devices or capillary electrophoresis, as well as improved buffers, passivated surfaces, and removal of binding interference by the fixed primer regions in the nucleic acid library. Despite these advances, the necessary devices, equipment, and/or technical expertise (e.g. microfluidic cartridges, ddPCR machines, capillary electrophoresis setups/expertise) are not always readily accessible to the broader research community. Additionally, the canonical route for imparting selectivity during SELEX is through additional rounds of negative selection against off-target molecules, which increases the amount of labor and reagent costs required to perform successful selections. As such, in this dissertation, we sought to address these issues to more broadly enable the isolation of aptamers. We explored whether certain principles from advanced SELEX workflows, particularly the use of dynamic flow conditions during selection and washing and compartmentalized PCR techniques during sequence recovery and amplification, could be incorporated into more traditional platforms. We also explored an expedited approach to counterselection, whereby off-targets were included during the washing stage, thus establishing an environment for competitive binding of prospective aptamers between the immobilized target and soluble off-targets while eliminating the need for a separate counterselection step.

This dissertation outlines the design of a novel selection in an attempt to improve the SELEX workflow and the specificity of aptamers. Aptamers were isolated for four different targets, including two proteins, one peptide, and one cell-surface transporter. Both DNA, RNA, and modified-base RNA nucleic acids were used in these selections. The four targets were chosen to test the ability of this dynamic flow selection workflow to isolate aptamers with high affinity and specificity. The first selection was performed to isolate DNA aptamers for the PDGF family of proteins which has five structurally similar homodimers and heterodimer. Figure 1.4 shows the

PDGF family and binding receptors for each homodimer and heterodimer. The next selection was performed to isolate RNA aptamers for the kinesin-12 coverstrand, which has similar function as other coverstrands in the kinesin family. Figure 1.5 shows the general structure of a kinesin molecule. The next selection was performed to isolate modified-base RNA aptamers for serum albumin, to backpack aptamers off the long half-life of albumin in an effort to improve therapeutic delivery of siRNA. Figure 1.6 shows the general mechanism for delivery of siRNA into the interference pathway using an aptamer. The final selection was performed to isolate DNA aptamers for Glucose Transporter 1 (GLUT1) using a whole-cell based selection workflow. Figure 1.7 shows the general structure of a GLUT transporter, part of a family of 14 structurally similar members. The first chapter details the selection workflow, using the PDGF family of proteins for proof-of-concept, and the following three selections used this selection workflow to develop aptamers for use as therapeutics.

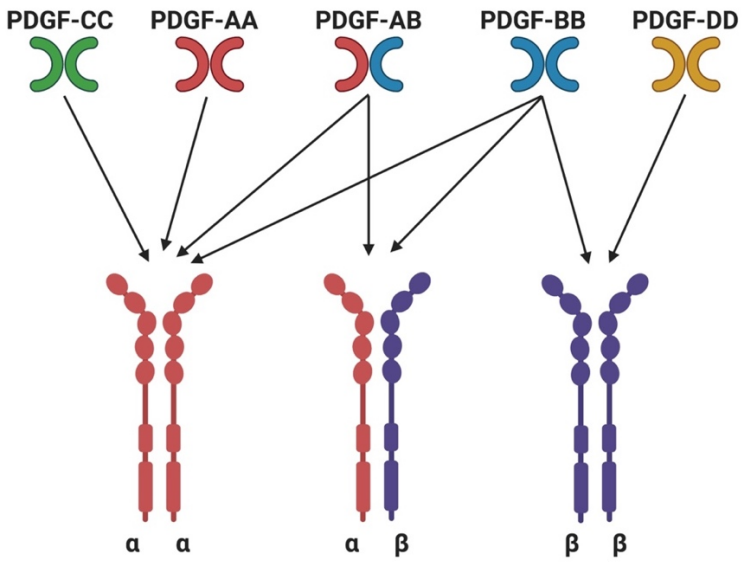

Figure 1.4 Homodimers and heterodimer in the PDGF family of proteins. The PDGF family of protein consists of four homodimers (AA, BB, CC, DD) and one heterodimer (AB), which are structurally similar. Figure modified from Canalis, 2008 [75].

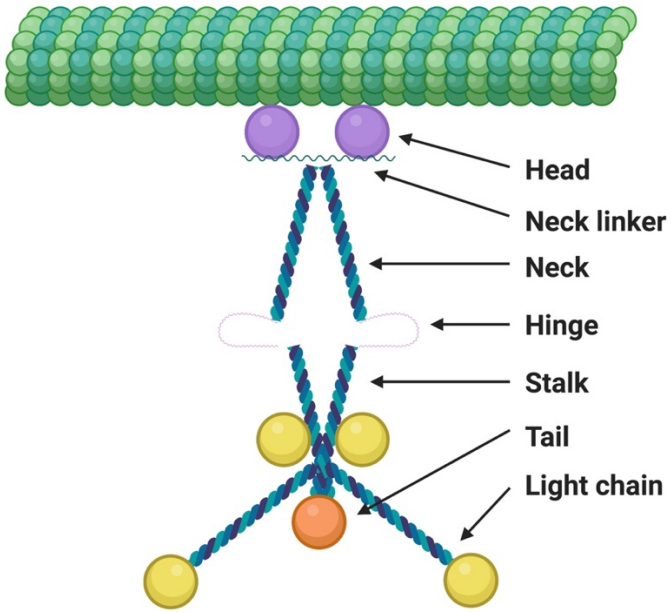

Figure 1.5 Kinesin domain structure interacting with a microtubule. A kinesin molecule consists of a motor domain that binds to microtubules, a neck linker which causes a conformation change when binding to ATP, a α-helical neck, and a stalk. Figure modified from Mandelkow, 2002 [76].

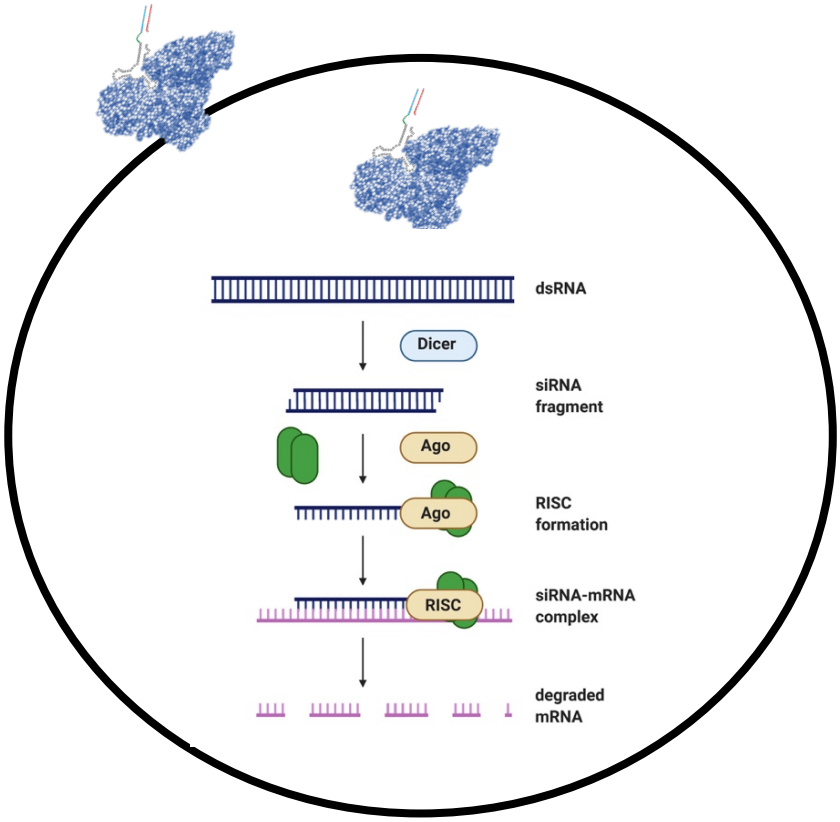

Figure 1.6 Albumin aptamer delivering siRNA payload. Aptamer-siRNA chimeras bind to endogenous albumin and enter cells. Aptamer chimeras enter the siRNA pathway to downregulate gene expression.

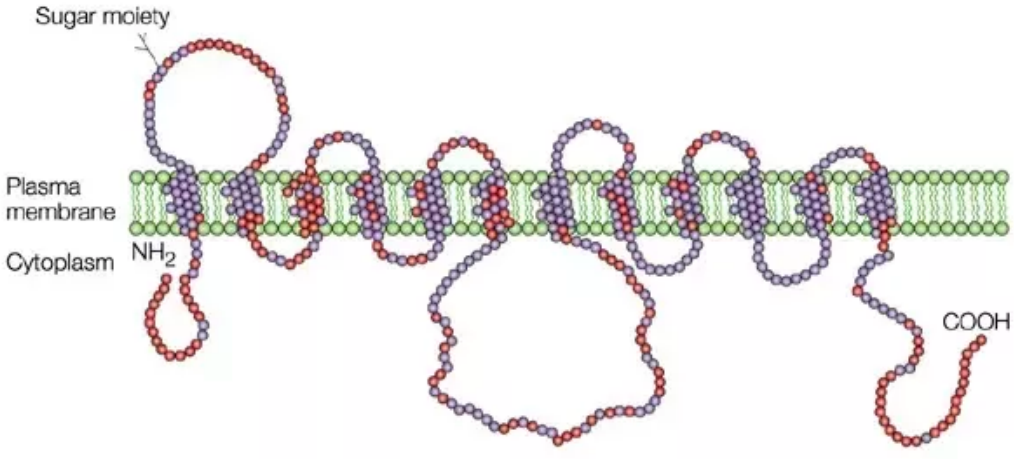

Figure 1.7 GLUT structure. The GLUT family of transporters is comprised of 14 members, which all span the plasma membrane 12 times. Amino acids in blue are unique to each GLUT member. Figure adopted from Bryant 2002, with permission from Springer Nature [77].

1.4 Organization of Dissertation

This dissertation consists of 5 chapters.

Chapter 2 details the development of a novel selection platform for isolating high affinity aptamers for purified-protein targets. In this selection platform, dynamic flow is used to increase partitioning and enhance selection stringency. Aptamers with high affinity and moderate specificity were identified for the PDGF homodimer BB (PDGF-BB) with specificity against structurally similar homodimers (PDGF-AA, -CC, and -DD). Components of this selection platform are used throughout each chapter of this dissertation.

Chapter 3 uses the dynamic flow system described in Chapter 2 to isolate RNA aptamers for the kinesin-12 coverstrand peptide. Two aptamers with micromolar affinity were isolated for the kinesin-12 coverstrand peptide, with one aptamer having moderate specificity over the kinesin-1 coverstrand peptide. This chapter highlights the ability to use the dynamic flow system to successfully isolate RNA aptamers for applications as antimitotics.

Chapter 4 uses the dynamic flow system described in Chapter 2 to isolate modified-base RNA aptamers for serum albumin. Two high affinity aptamers were isolated and fused with siRNAs. Fusion of siRNAs with these aptamers form complexes, termed chimeras, which confer siRNA with the ability to bind to albumin, thereby improving their circulation times and bioavailability for therapeutic delivery.

Chapter 5 details a novel aptamer selection platform that utilizes isogenic pairs of cells generated via Clustered Regularly Interspaced Short Palindromic Repeats (CRISPR) techniques. Aptamers were isolated for GLUT1 using these custom engineered cell lines. One aptamer was isolated with high affinity to GLUT1 and high specificity against other similarly structured glucose transporters.

Chapter 6 provides conclusions for the work discussed in this dissertation as well as future areas of focus for this research.

Chapter 2

A SYSTEMATIC EVOLUTION OF LIGANDS BY EXPONENTIAL ENRICHMENT WORKFLOW WITH CONSOLIDATED COUNTERSELECTION TO EFFICIENTLY ISOLATE HIGH-AFFINITY APTAMERS

Adopted from: Rosch JC, Balikov DA, Gong F, & Lippmann ES. A systematic evolution of ligands by exponential enrichment workflow with consolidated counterselection to efficiently isolate high-affinity aptamers. Engineering Reports. 2020;2:e12089 *with permission from Wiley Online Library.*

2.1 Summary

Efficient selection of nucleic acid aptamers with high affinity and specificity for a broad range of targets remains challenging. Historically, aptamer selections have been protracted and tedious processes, often requiring double-digit rounds of selection to converge nucleic acid pools into a small number of prospective high-affinity aptamers. More recently, the use of microfluidic devices and specialized equipment has helped streamline the aptamer selection process, but these platforms are not necessarily accessible to the broad research community. Here, we demonstrate that aptamers with high affinity and moderate specificity can be obtained with a conventional selection workflow that is modified to include facile methods for increasing partitioning and enhancing selection stringency. This process exposes an immobilized protein target to a single-stranded DNA library, followed by washing with buffer that contains the undesired off-target(s), with both steps occurring under constant perfusion using a standard peristaltic pump. Prospective aptamers are then eluted, amplified by an emulsion polymerase chain reaction, regenerated to single strands by enzymatic digestion, and resubjected to the selection procedure. We validated this selection scheme using the PDGF family of proteins, whereby we successfully isolated nanomolar affinity aptamers against PDGF-BB with specificity comparable to an aptamer selected using a microfluidics-based approach.

2.2 Introduction

Aptamers are single-stranded DNA or RNA molecules that individually form unique tertiary structures that can bind to a variety of targets, including proteins, small molecules, inorganic compounds, and cell membrane receptors [6]. Since their initial discovery [4], [5], research interest in aptamers for therapeutic and diagnostic applications has increased primarily owing to the potential benefits of aptamers relative to other affinity reagents including, but not limited to, their smaller size, low immunogenicity, high stability, ease of chemical modifications, and ability to be produced *in vitro* [12]. In addition, aptamers offer the chemical flexibility of small molecules, while retaining the strong specific binding of antibodies. However, despite their apparent promise, aptamers lag behind other affinity reagents in terms of widespread use [13].

One oft-cited roadblock for the development of aptamers is the numerous issues associated with the selection workflow. Aptamers are isolated from random or partially structured nucleic acid libraries through iterative rounds of selection in a process termed systemic evolution of ligands by exponential enrichment (SELEX). In a typical round of selection, a positive incubation step is first employed, where the aptamer library is incubated with a primary target molecule. Next, the nucleic acids are subjected to a partitioning step, whereby weakly bound aptamers are removed from the selection pool through washing, amplified by PCR, and regenerated from double-stranded DNA into single strands for the next round of selection. To impart specificity into a selection workflow, the library is exposed to undesired or similarly structured secondary targets to remove non-specific aptamers. This step typically occurs in separate selection rounds by collecting the aptamers that do not bind to the immobilized off-targets. When an aptamer pool has converged through iterative rounds, individual sequences are identified by Sanger sequencing and subsequently characterized for their affinity and specificity to the targets and off-targets.

Historically, conventional SELEX has required double-digit selection rounds to converge a library, such that when the final pool is cloned into a plasmid and analyzed by Sanger sequencing, the resulting hits are likely to be high-quality aptamers rather than contaminating nucleic acid strands [3]. More recently, to bypass this need for nucleic acid pool convergence, high throughput sequencing (HTS) has improved the ability of researchers to identify high affinity aptamers more rapidly [7], [60], [78]. This method is particularly powerful because the most abundant and/or most enriched sequences can be tracked in early rounds of selection, and these sequences typically have high affinity for the target of interest.

Within the overall SELEX process, two particular challenges that influence aptamer isolation are poor partitioning during selection and washing, which is critical for removing weakly bound aptamers from the selection, and spurious PCR amplification, which can lead to the formation of byproducts and amplification artifacts [74]. Increasing the total number of rounds counteracts these issues and improves the chances of isolating high affinity aptamers, but increases the workload and overall time required to obtain useful aptamers. To address these issues and shorten the SELEX workflow, several research groups have developed novel strategies and/or devices. For example, to overcome poor partitioning, more stringent washing steps have been incorporated to remove weakly bound aptamers within microfluidic devices [7], [56], [79]. Another method, capillary electrophoresis, does not require target immobilization and uses low reaction volumes [80], [81]. Improved buffers, passivated surfaces, and removal of binding interference by the fixed primer regions in the nucleic acid library have also been employed to enhance partitioning [82], [83]. In addition, to reduce the chance of byproduct formation during the amplification step, droplet digital PCR [82], which employs emulsion PCR principles to compartmentalize individual nucleic acid sequences, has been incorporated into selections [73].

However, despite these advancements, several concerns remain with respect to SELEX workflows. First, the necessary devices, equipment, and/or technical expertise described above (e.g. microfluidic cartridges, ddPCR machines, capillary electrophoresis setups/expertise) are not always readily accessible to the broader research community. Second, as previously mentioned, the canonical route for imparting selectivity during SELEX is through additional rounds of negative selection against off-target molecules, which increases the amount of labor and reagent costs required to perform successful selections. As such, in this work, we sought to address these issues to more broadly enable the isolation of aptamers. We explored whether certain principles from advanced SELEX workflows, particularly the use of dynamic flow conditions during selection and washing and compartmentalized PCR techniques during sequence recovery and amplification, could be incorporated into more traditional platforms. We also explored an expedited approach to counterselection, whereby off-targets were included during the washing stage, thus establishing an environment for competitive binding of prospective aptamers between the immobilized target and soluble off-targets while eliminating the need for a separate counterselection step. Using the PDGF family as a model system, we demonstrate that this integrated SELEX workflow is able to isolate aptamers to the primary target (PDGF-BB) with low nanomolar affinity and moderate specificity relative to other PDGF homodimers. Ultimately, these aptamers were identified without the need for a microfluidics-based selection or uncommon PCR equipment, and the highest quality aptamers are comparable to ones selected against PDGF-BB using microfluidics. Because all of the materials and assays used in this workflow are easily accessible to researchers, we suggest that the techniques described herein may be broadly adapted for performing aptamer selections.

2.3 Materials and Methods

2.3.1 Materials and Instruments

Recombinant human PDGF-AA, -BB, and –CC were purchased from Peprotech (Rocky Hill, NJ) and recombinant human PDGF-DD was purchased from R&D Systems (Minneapolis, MN). All chemicals were purchased from Fisher Scientific (Hampton, NH). The starting DNA library, primers, and custom aptamer sequences were purchased from Integrated DNA Technologies (San Jose, CA) with HPLC purification. The starting DNA library was synthesized with 40 nucleotide random bases flanked by 20 nucleotide primer ends required to perform PCR amplification (forward fixed region: TCGCACATTCCGCTTCTACC, reverse fixed region: CGTAAGTCCGTGTGTGCGAA). The starting library was designed with a A:C:G:T molar ratio of 3:3:2:2.4 to adjust for equimolar amounts of nucleotide incorporation and primers; forward primer: TCGCACATTCCGCTTCTACC, 5'-phosphorylated reverse primer: /5Phos/TTCGCACACACGGACTTACG. Complementary blocking regions were used during library preparation to block the primer regions during incubation steps (5'-complementary: GGTAGAAGCGGAATGTGCGA, 3'-complementary: TTCGCACACACGGACTTACG), similar to previous descriptions [82]. Dynabeads M-270 Carboxylic Acid were purchased from Thermo Fisher Scientific (Waltham, MA), along with N-hydroxysuccinimide (NHS) and 1-ethyl-3-(3-dimethylaminopropyl) carbodiimide hydrochloride required for magnetic bead activation. Binding buffer used throughout the selection was prepared with 20 mM tris-HCl (pH 7.4), 140 mM NaCl, 5 mM KCl, 1 mM $MgCl_2$, and 1 mM $CaCl_2$. Washing buffer was comprised of binding buffer supplemented with 0.005% Tween-20.

2.3.2 Preparation of Target-Immobilized Beads

$1x10^8$ M-270 Carboxylic Acid Dynabeads were conjugated with PDGF-BB before each round of selection according to the manufacturer's instructions. The magnetic beads were washed with MES buffer (25 mM 2-(N-morpholino)-ethane sulfonic acid, pH 6.0), activated with EDC/NHS chemistry for 30 minutes, and incubated with PDGF-BB for 1.5 hours with rotation at room temperature. After incubation, the beads were washed with 50 mM Tris-HCl (pH 7.4) buffer and incubated with the same buffer for 1 hour to ensure that all unreacted groups on the magnetic beads were quenched. The beads were finally washed with PBS buffer with 0.005% Tween-20 and suspended in binding buffer and stored at 4°C until utilized. Beads were prepared fresh for each round of selection, and immediately prior to their use, beads were washed three times with wash buffer and resuspended in binding buffer.

2.3.3 SELEX Process

A single well of a hydrogel bonded, ultra-low attachment 96-well plate (Corning, St. Louis, MO) was plumbed by drilling two holes into the lid, inserting dispensing needles (Jensen, North Andover, MA), and circulating fluid using a peristaltic pump (Fisher Scientific) (Figure 2.1). Manifold pump tubing (PVC, 0.51 mm ID, Fisher Scientific) was flushed with washing buffer containing 100 mg/mL of yeast tRNA (Thermo Fisher) and 0.1% bovine serum albumin (RPI, Mt. Prospect, IL) to passivate the lines before introducing the aptamer pools. Beads were trapped at the bottom of the plumbed well using a neodymium magnet. The selection was initiated with 1 nmole ($\sim10^{14}$ sequences) of starting random DNA library. The starting library pool was mixed with equimolar amounts of complementary blockers, heated to 95°C for 5 minutes, and slowly

cooled down to 25°C in a standard thermocycler at a rate of 0.5°C/min. Aptamer pools were circulated over the magnetically trapped beads at a rate of 20 mL/h. Wash buffer was then circulated at a rate of 50 mL/h to continuously remove unbound and weakly bound aptamers. After washing, aptamers bound to the beads were resuspended in 100 µL of ultrapure water and heated at 95°C for 10 minutes to elute the bound nucleic acids. Round 1 only included a positive incubation step with PDGF-BB. Round 2 and beyond included both positive incubation and negative counterselection, where soluble PDGF-AA, -CC, and –DD were included in the wash buffer solution for the integrated counterselection step.

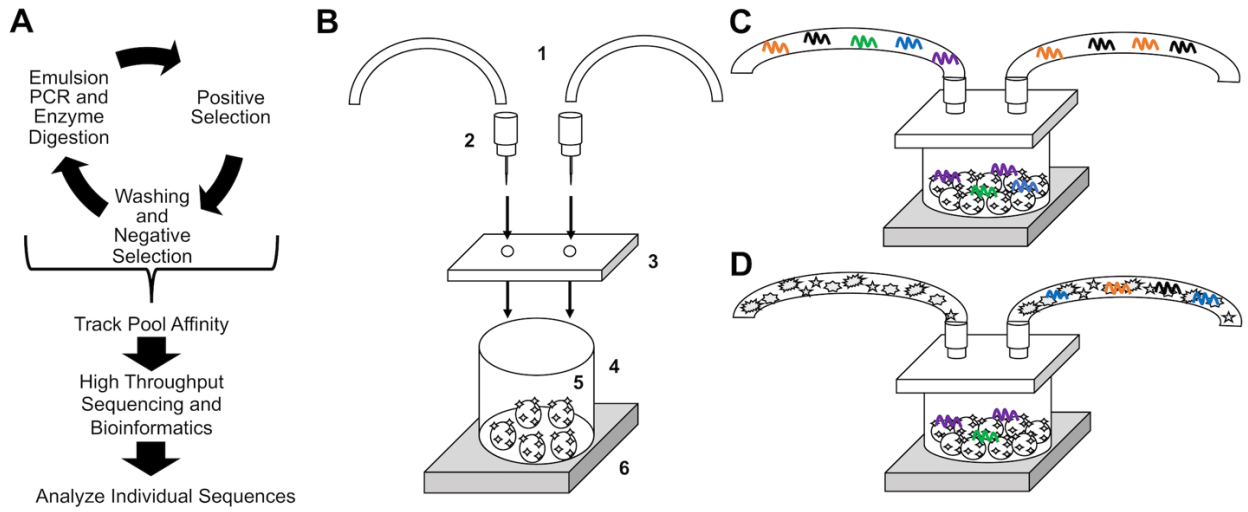

Figure 2.1 SELEX workflow. (A) Conceptual overview of the integrated SELEX process. Iterative cycles of positive selection, combined washing and negative selection, and emulsion PCR and enzyme digestion are repeated to converge a starting nucleic acid library. When the pool is determined to have high affinity for the primary target, high throughput sequencing is used to identify individual aptamer sequences to test for affinity and specificity. **(B)** Schematic for the setup of the flow system. Manifold pump tubing (1) is inserted into dispensing needles (2). Dispensing needles are inserted through drilled out holes in the lid of a 96-well plate (3). The lid with dispensing needles is placed over the wells of a 96-well plate (4) where the micromagnetic beads (5) are immobilized by a magnet (6) underneath the plate. Fluid with either the aptamer pool or soluble off-targets are perfused unidirectionally through one dispensing needle and removed from the well through the other dispensing needle with the use of a peristaltic pump (not shown). **(C)** Schematic showing a positive selection round, where an aptamer pool is circulated

over immobilized protein-conjugated magnetic beads. **(D)** Schematic showing a negative selection step, where soluble off-target proteins are circulated over the aptamers bound to the primary target on the immobilized magnetic beads.

2.3.4 Emulsion PCR

Emulsion PCR protocols were modified for larger-scale preparations [73]. Emulsion PCR oil was prepared in 20 mL glass scintillation vials with a mixture of 900 μL of Span-80, 80 μL of Tween-80, and 10 μL of Triton X-100 in mineral oil. The oil mixture was blended with a magnetic stir bar at 1500 rpm for 10 minutes in 4°C. The aqueous PCR mixture was prepared with 10X PCR buffer, 500 nM forward and reverse primers, 400 nM dNTPs, 5 U/μL of VAPRase (produced by Vanderbilt Antibody and Protein Resource (VAPR) core facility at Vanderbilt University), nuclease-free H_2O, and 10 pM of template DNA from each round of SELEX. 1 mL of the aqueous PCR mixture was slowly added to 2 mL of the emulsion PCR oil over two minutes, while continuously spinning at 1500 rpm. The oil/aqueous PCR mixture was stirred for an additional 10 minutes at 4°C, continuously spinning at 1500 rpm. Once emulsions were formed, the 3 mL volume of emulsion mixture was pipetted into 30 separate PCR tubes (100 μL/tube) and run at optimized PCR settings on a standard thermocycler (2 minutes denaturation at 98°C, 15 cycles of [30 seconds of denaturation at 98°C, 10 seconds of annealing at 56°C, 15 seconds of extension at 72°C], final 5 minutes of annealing at 72°C). The PCR products were then pooled and broken with the use of 1-butanol [84]. After adding butanol, the mixture was vortexed for 1 minute until the solution became clear, signifying that the emulsions were broken. The solution was centrifuged at 16000xg for 10 minutes at room temperature to pellet the DNA. The DNA pellet was then dried and resuspended in ultrapure water.

2.3.5 Regeneration of Single-Strand DNA

Emulsion PCR products were run on a 3% agarose gel to ensure correct band size and to check for any smearing from over-amplification and high molecular weight byproduct formation. Single-strand DNA was regenerated after PCR by incubating double-strand DNA with 5 U of λ-exonuclease (NEB, Ipswich, MA) at 37°C for 1 hour, followed by heat inactivation at 75°C for 10 minutes in a standard PCR thermocycler [82]. The single-strand product was purified through phenol/chloroform/isomayl alcohol extraction (Thermo Fisher Scientific) and ethanol precipitated. Single-strand DNA was resuspended in binding buffer before being used in the next round of selection.

2.3.6 Pool Affinity Characterization

After five rounds of selection, the eluted aptamer pool was prepared and characterized with a quantitative PCR (qPCR)-based bulk affinity assay.16 The round 5 pool was 2-fold serially diluted into eight concentrations spanning 200 to 0 nM. 2×10^7 of PDGF-BB immobilized magnetic beads were added to each dilution and incubated at room temperature for 1 hour with gentle mixing using a spinning tube rotator. After the incubation, beads were washed three times with washing buffer and incubated at 95°C for 10 minutes in a standard heat block to elute bound aptamers. The eluted aptamer pools were mixed with iQ SYBR Green Supermix (Bio-Rad, Hercules, CA) and 250 nM of forward and reverse primers. The pools were amplified according to the manufacturer's instructions: 30 seconds at 95°C and 40 cycles of 15 seconds of denaturation at 95°C and 30 seconds of annealing/extension at 60°C. Bound aptamer fractions were determined through comparison to a standard curve made from the starting DNA library. ΔCq values were nonlinearly fitted to the Langmuir equation to determine the bulk dissociation

constant (K_D) of the round five pool. In addition, the round 5 eluted aptamer pool was characterized for its specificity to the primary target PDGF-BB against the surface of the magnetic beads. The round 5 pool and starting library were PCR-amplified with FAM-labeled forward primer and digested with λ-exonuclease. These ssDNA samples were incubated with either 2×10^7 PDGF-BB immobilized magnetic beads or 2×10^7 quenched beads for 1 hour. Beads were washed three times with washing buffer and bound aptamers were eluted from the beads at 95°C for 10 minutes in a standard heat block. The fluorescence intensity of the eluted sequences was measured with a standard plate reader.

2.3.7 High-throughput DNA Sequencing

The round five-aptamer pool was prepared for sequencing on the Illumina HiSeq platform 2 × 150 bp configuration with ~350-M raw paired-end reads per lane (Genewiz, South Plainfield, NJ). To prepare the sample, the aptamer pool was amplified by emulsion PCR for 10 cycles to generate ~1-μg double-strand DNA. The sample was examined on a 2% agarose gel and extracted using the Qiaquick Gel Extraction Kit (Qiagen, Hilden, Germany). After sequencing, the data were analyzed using a custom script generated from Vanderbilt Technologies for Advanced Genomics Analysis and Research Design (Figure A.2.1). Raw sequences were cut around the forward primer and reverse primer fixed regions, which includes the 40-mer random region, and sorted based on relative abundance.

2.3.8 Affinity and Specificity Measurements

Single-stranded 40-mer DNA sequences lacking primer regions were ordered from IDT with a 5'-FAM fluorophore attachment. Affinity against each soluble protein was measured via microscale thermophoresis (MST) using the Monolith NT.115 device (Nanotemper Technologies, Munchen, Germany) [85], [86]. Briefly, 16 2-fold serial dilutions of soluble protein were prepared from concentrations of 300 nM to 9.15 pM in binding buffer. 40-nM solutions of each 5'-FAM-labeled aptamer was prepared by diluting the aptamer in binding buffer, heating the mixture to 95◦C for 5 minutes, snap-cooling on ice, and incubating at room temperature for 10 minutes. The folded aptamers were mixed with each dilution of protein and incubated in the dark for 1 hour at room temperature. Then, a standard Monolith NT.115 capillary was dipped into each serially diluted solution and fluorescent dose-response was measured at 20% MST excitation power. Equilibrium binding constants were fitted using the MO. Affinity Analysis software (Figure A.2.2). Specificity is reported as affinity for the primary target vs each individual off-target.

2.4 Results and Discussion

2.4.1 Choice of Target and Outline of SELEX Process

To facilitate our studies, we chose the PDGF family as a model system, with PDGF-BB used as the primary target and PDGF-AA, -CC, and -DD as the off-targets. Aptamers have previously been reported against PDGF-BB with binding affinities in the low nanomolar range, suggesting its utility as a model target. In particular, microfluidic SELEX coupled with HTS has

been used to identify aptamers that bind to PDGF-BB with high affinity and moderate specificity relative to PDGF-AA [7]. Thus, by using the PDGF family, our SELEX approach can be quantitatively benchmarked against other methods.

As previously stated, our selection scheme was designed to integrate certain concepts from other SELEX procedures into a workflow that is manageable without highly specialized techniques or equipment. First, we incorporated fluid flow for each step of the selection using magnetic immobilization of targets and an inexpensive peristaltic pump, building off concepts established in microfluidic devices [7], [56] (Figure 2.1). Flow also allows for the recirculation of the library and subsequently enriched nucleic acid pools over the immobilized target; in this selection scheme, the total volume is circulated through the system roughly five times in one hour, thus yielding multiple opportunities for the prospective aptamers to interact with the target. In addition, as previously described, fluid flow increases the stringency of the washing steps to remove weakly bound aptamers from the primary target [56]. To validate the initial flow rate and circulation time used for SELEX, we employed a previously reported aptamer against PDGF-BB and analyzed real-time binding via fluorescence. In these experiments, the PDGF-BB aptamer was labeled with a fluorophore, diluted in binding buffer to a concentration of 2 nM, and circulated over three wells of a 96-well plate at 20 mL/h. One well contained immobilized PDGF-BB, the second well contained immobilized mouse IgG, and the third well was fully passivated without any added protein. The aptamer was circulated for 60 minutes and fluorescence was measured every 10 minutes by disconnecting the plate from the pump and assaying on a plate reader (each well was briefly washed with washing buffer before every measurement) (Figure 2.2). After the first reading, fluorescence was noticeably increased in the well where PDGF-BB was immobilized but not in the control wells. Within 20 minutes, the fluorescence in the PDGF-BB well reached a

plateau, potentially indicating that all of the PDGF-BB target proteins in the well were saturated with bound aptamer, whereas no significant changes in fluorescence were observed in the control wells throughout the remainder of the experiment. This result validated the ability of high affinity aptamers to bind a target under active flow and demonstrates that unbound aptamers are not retained against nonspecific targets.

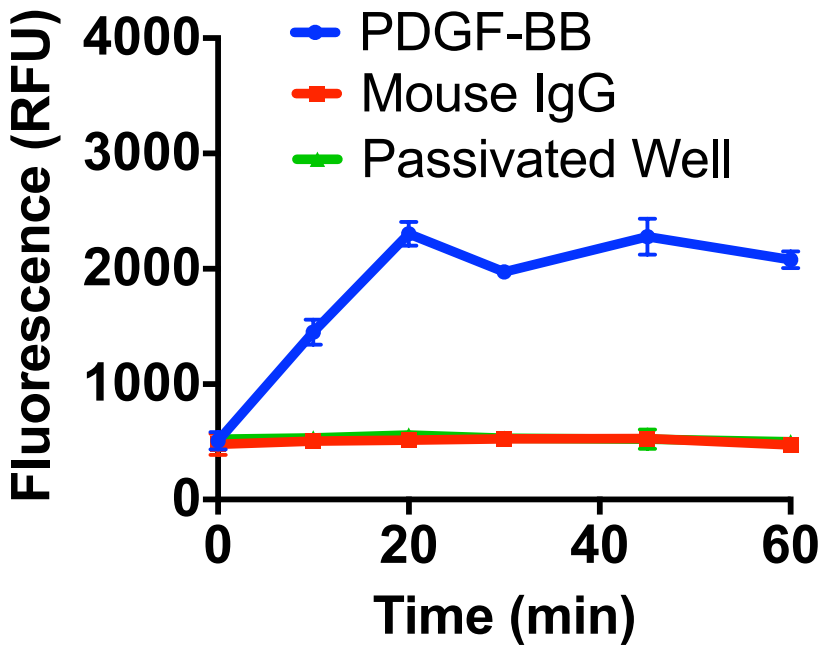

Figure 2.2 Validation of aptamer binding under active flow. The Alexa Fluor 488-conjugated anti-PDGF-BB aptamer was circulated over wells containing immobilized PDGF-BB, immobilized mouse IgG, or no protein (passivated well). Fluorescence was measured every 10 minutes using a plate reader. Data points represent mean ± SD from technical triplicate wells.

Next, we incorporated emulsion PCR for all amplification steps of the workflow to reduce byproduct formation and high molecular weight artifacts. Several research groups have incorporated the use of emulsion PCR into their selection workflow to improve the yield of product amplification and reduce the formation of larger molecular weight byproducts that are

evident after high cycle amplification of random nucleic acid libraries. Emulsion PCR has also been shown to reduce the amount of amplification artifacts and byproducts through rounds of amplification [73], [87]. This selection workflow uses emulsion PCR in every round of selection as described in the methods section. Byproduct formation from amplification of random nucleic acid libraries can be observed on an agarose gel after only 10 cycles, whereas our adjusted emulsion PCR protocol does not show evidence of byproduct formation, even up to 35 cycles (Figure 2.3 A, B). Following emulsion PCR amplification, the dsDNA aptamers were restored to ssDNA with a λ-exonuclease enzymatic digestion, as previously described (Figure 2.3 C).

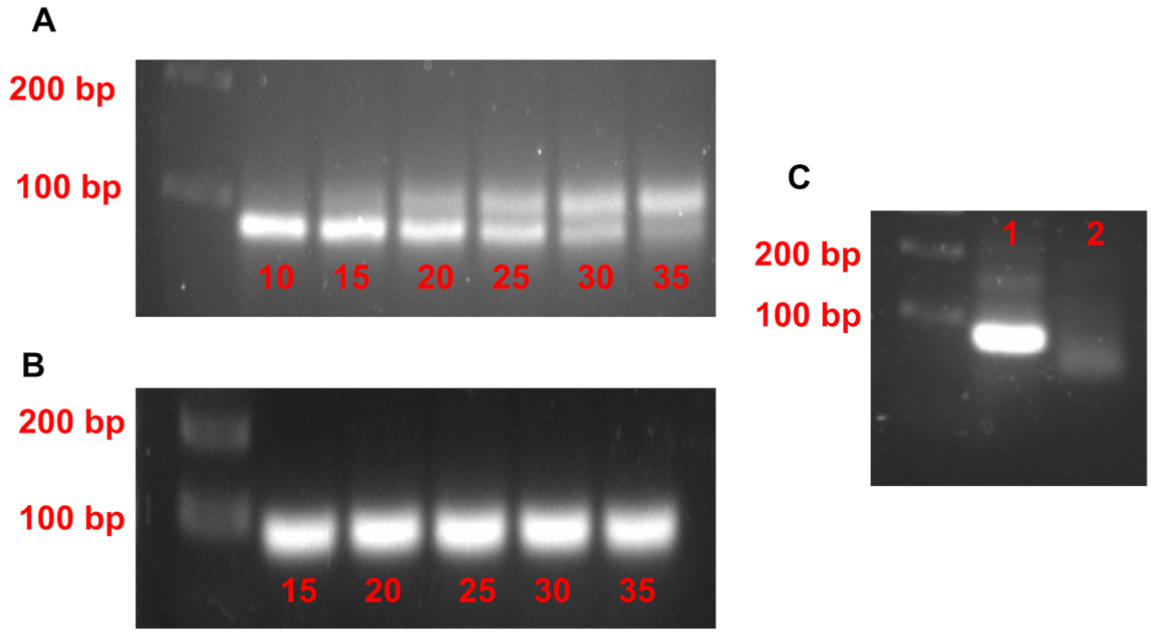

Figure 2.3 Recovery, amplification, and enzymatic digestion to ssDNA. (A-B) Comparison between conventional solution PCR (panel A) and emulsion PCR (panel B). Cycle numbers are indicated in red. Conventional PCR of a random nucleic acid library yields spurious amplification and byproduct formation within 10 cycles, whereas emulsion PCR shows little to no byproduct formation up to 35 cycles. **(C)** 3% agarose gel image of λ-exonuclease digestion to restore ssDNA after each round of selection. Lane 1 is the 80 bp dsDNA product prior to digestion and lane 2 is the 80 bp ssDNA product after digestion. ssDNA exhibits lower band due to lower molecular weight relative to dsDNA.

Finally, we utilized a consolidated counterselection strategy, where off-targets are introduced into the system during washing steps and therefore exposed to prospective aptamers that are still bound to the primary target. In this manner, the aptamers bound to the immobilized target are exposed to all off-targets simultaneously during the negative selection, providing a competitive binding atmosphere to enrich for specificity. This approach eliminates the need for separate rounds of counterselection, thereby benefiting SELEX workflows by shortening the overall procedure.

2.4.2 SELEX Workflow

Five rounds of selection were completed with the PDGF family of proteins as described in the methods section. The first round of selection performed only involved a positive selection with the primary target PDGF-BB. In rounds 2 to 5, a negative selection step was performed immediately after positive selection by including PDGF-AA, -CC, and -DD during the washing stage. Through the five rounds, the amount of primary target and the time of positive incubation were decreased, while the amount of off-targets, the time of washing, and the time of negative selection were increased (Table A.2.1). The aim was to increase the ratio of the primary target to off-targets to increase the selection pressure through each round of selection, eventually increasing to a ratio of 1:100. After the fifth round of selection, we labeled the enriched pool with a FAM fluorophore to show preferential binding against PDGF-BB-coated beads but not quenched beads (Figure 2.4 A). The pool affinity toward PDGF-BB was then assayed with a qPCR assay. The bulk pool affinity was measured to be 24±17 nM, compared to the starting library which had insignificant binding to PDGF-BB (Figure 2.4 B).

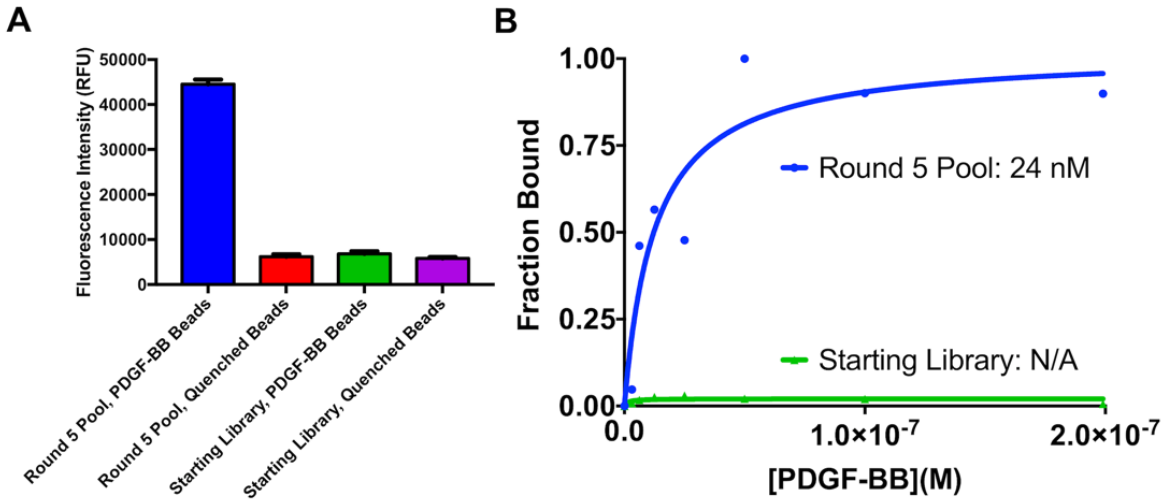

Figure 2.4 Bulk affinity of aptamer pool after five rounds of selection. (A) Binding experiment measuring mean fluorescence intensity of the round 5 pool to platelet-derived growth factor (PDGF)-BB-coated beads and quenched beads, compared to the starting library. Data are presented as mean±SD from technical triplicates. (B) quantitative polymerase chain reaction (qPCR) measurements of dissociation constants in the round five-aptamer pool and starting nucleic acid library. The plots represent a single qPCR run, and results were verified across biological triplicates. The average KD of the round five pools is 24±17 nM

2.4.3 Identification and Characterization of Prospective Aptamers

We utilized HTS and bioinformatics analysis to identify the most abundant aptamers in the round 5 pool; as described earlier, this approach is becoming increasingly common for identifying high-affinity aptamers without pool convergence and laborious molecular cloning [7]. A total of 8,171,212 prospective aptamer sequences were identified, and analysis revealed that the pool was not highly converged after five rounds of selection, with only 11.91% of the pool represented as duplicate sequences. The most abundant sequence represented 2.52% of the total population of the round 5 pool, with the top 10 sequences representing less than 7% of the total population (Table A.2.2). In addition, there was little structural homogeneity between the top sequences analyzed in this study (Figure A.2.3). The most abundant sequences from the pool

were tested for their affinity to PDGF-BB using MST, and the sequences with the highest affinity for PDGF-BB were also tested for their specificity against PDGF-AA, -CC, and -DD. The 10 assayed aptamers possessed affinities for PDGF-BB ranging from 49 to 155 nM, compared to the affinity of 16 nM of the previously reported aptamer that was used to validate initial flow rates (Figure 2.5). The aptamers were then tested for their specificity against the other homodimers used in the counterselection step of the workflow. Overall, the aptamers exhibit moderate specificity against the off-targets. For example, one aptamer, PDGF-2, with an affinity of 49 nM to primary target PDGF-BB, exhibited 2.3-, 11.8-, and 10.7-fold specificities against off-targets PDGF-AA, -CC, and -DD, respectively (Figure 2.6 B). Another aptamer, PDGF-6, with an affinity of 50 nM to primary target PDGF-BB, exhibited 6.0- and 5.6-fold specificities against off-targets PDGF-AA and -CC, with no change in specificity against PDGF-DD (Figure 2.6 C). Binding specificities of the other aptamer sequences are reported in Figure S4. Meanwhile, the previously reported aptamer, A2, exhibited 5.0-, 24.0-, and 12.0-fold specificities against PDGF-AA, -CC, and -DD, respectively (Figure 2.6 A), which are reasonably similar to aptamer PDGF-2 in this study. We do note that specificity for the selected aptamers in this study seems to be stochastic. On the other hand, we used three off-targets during counterselection, and in most cases, specificity was only observed against one or two of the off-targets. Interestingly, the selection scheme for A2 only included PDGF-AA during counterselection, yet this aptamer exhibits specificity over PDGF-CC and PDGF-DD similar to the aptamers from our study. Thus, while our results do indicate that the competitive counterselection approach is effective, more steps need to be taken to further drive specificity. We expect to explore modulation of the counterselection parameters and other variables that could impact selection fidelity (such as flow rates) in future studies.

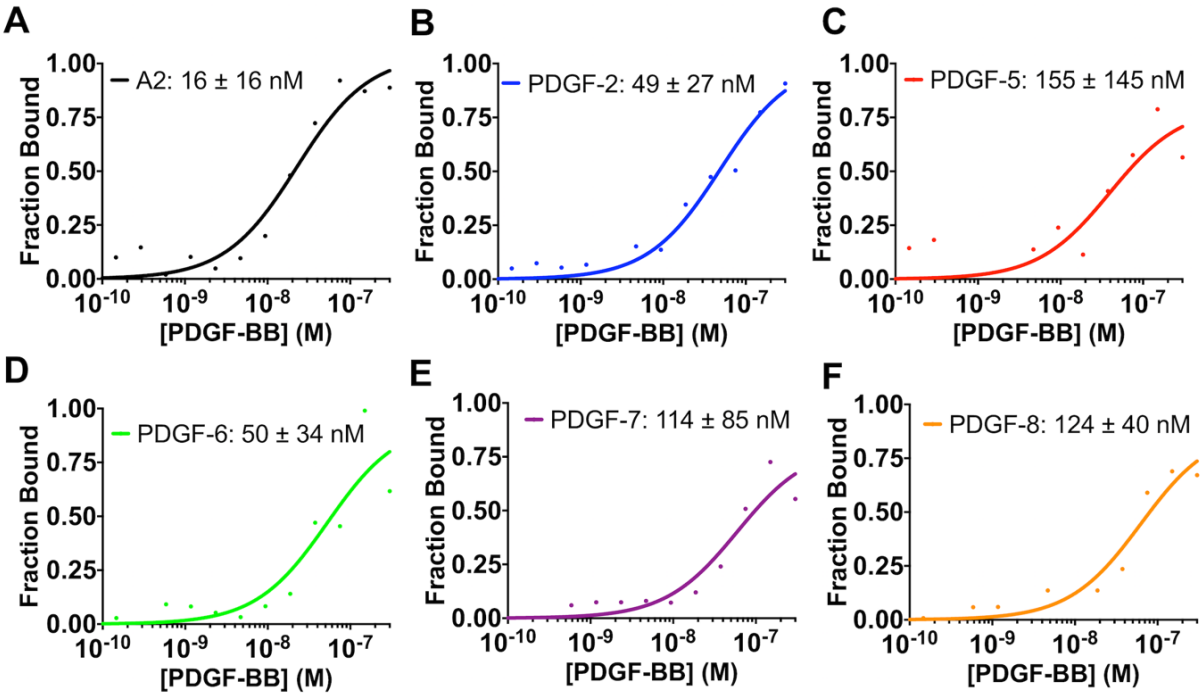

Figure 2.5 Affinity of individual aptamers for platelet-derived growth factor (PDGF)-BB. The most abundant sequences from high throughput sequencing (HTS) were measured for affinity to PDGF-BB via microscale thermophoresis (MST) binding measurements (A)-(F). The plots represent binding isotherms from triplicate MST experiments, with final affinities reported as mean±SD.

A

GATACTGAGCATCGTACATGATCCCGCAACGGGCAGTATT

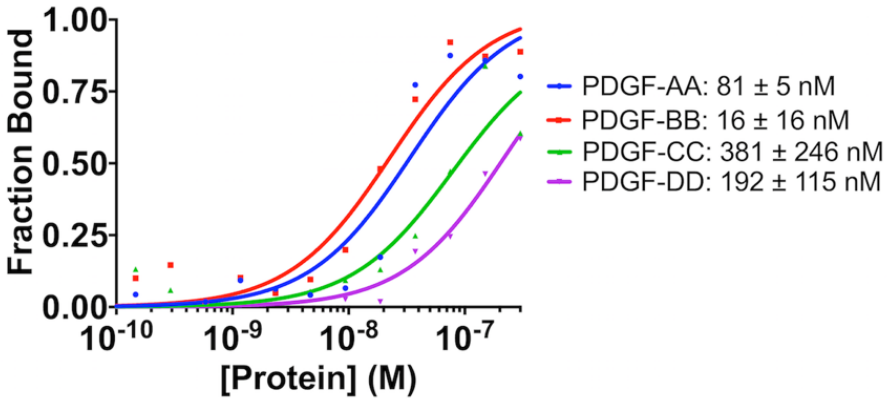

B

CCAGATCCGAGGAGCGTTTCGTTAATGGATCGGGCGTCCA

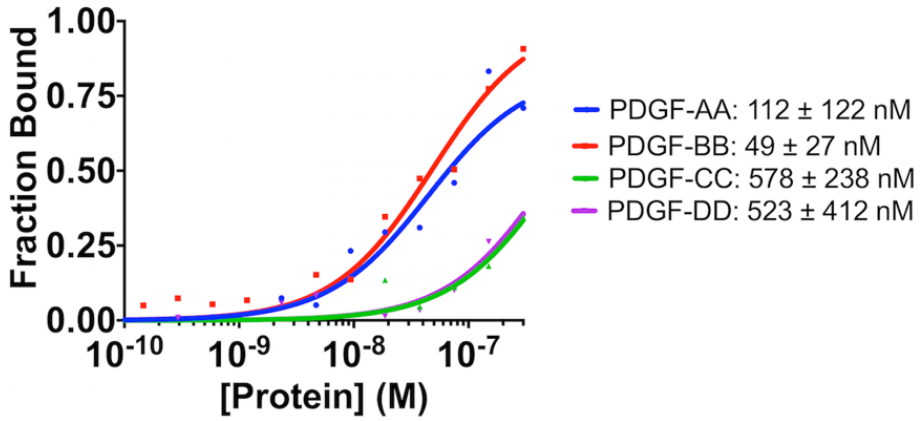

C

GACCGCGGGGTGGGTGGGAGGGTTTGTGGCCGGGCCGTG

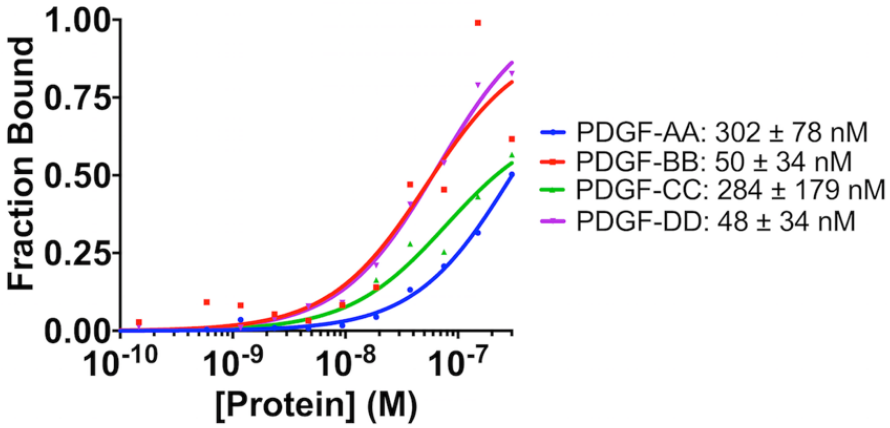

Figure 2.6 Specificity measurements. Select aptamers were measured for affinity to platelet-derived growth factor (PDGF)-AA, PDGF-CC, and PDGF-DD via microscale thermophoresis (MST) binding measurements. The plots represent binding isotherms from single MST experiments, and the final affinities are mean±SD from biological triplicates. (A) A2 aptamer from a previous study. (B) Aptamer PDGF-2 from this study. (C) Aptamer PDGF-6 from this study.

2.5 Conclusions

In this work, we describe a selection approach that builds off previous SELEX advancements, as well as incorporates a consolidated counterselection strategy, thereby generating high-affinity and moderate specificity aptamers. We recently reported the design of a custom-built multichannel peristaltic pump that could be used for this purpose, continuing on the theme of bringing novel ideas and low-cost resources to the aptamer community [88]. Overall, once improvements are made to the selection workflow to better impart specificity, we envision that such an array-based system could provide diverse sets of aptamers for researchers aiming to develop therapeutic and diagnostic tools.

2.6 Appendix

```
##06/06/2017 By CQS Vangard
##fastq data input. sequence_head_43pb as
"GTATAATACGACTCACTATAGGGTCGCACATTCCGCTTCTACC".
sequence_tail_20pb as "CGTAAGTCCGTGTGTGCGAA"
##Run code as
##sh aptamerSeq40_stat.sh 14-JR-4_S51_R1.fastq
fastq=$1
sed -e '1 i \+\tBeginning' $fastq |tr '\n' '\t'|tr '\+' '\n' >${fastq}_reformat
cut  -f 4 ${fastq}_reformat >${fastq}_reformat_seq.tmp
cut  -f 3 ${fastq}_reformat >${fastq}_reformat_name.tmp
cut  -f 2 ${fastq}_reformat >${fastq}_reformat_QC.tmp

sed -i '/^$/d' ${fastq}_reformat_seq.tmp
sed -i '/^$/d' ${fastq}_reformat_name.tmp
sed -i '/^$/d' ${fastq}_reformat_QC.tmp
sed -i '/Beginning/d' ${fastq}_reformat_QC.tmp
wc -l *.tmp

head -n 1000 ${fastq}_reformat_seq.tmp|tail -n 10 >seq_for_length.tmp
sgl=`cat seq_for_length.tmp`;for n in $sgl;do echo ${#n};done

cut -b -43 ${fastq}_reformat_seq.tmp>seq_b43_head.tmp
cut -b 84-103 ${fastq}_reformat_seq.tmp >seq_b20_tail.tmp
sort seq_b43_head.tmp|uniq -c|sort -rn >seq_b43_head_uniq.stat
sort seq_b20_tail.tmp|uniq -c|sort -rn >seq_b20_tail_uniq.stat
head *.stat

grep -P "^GTATAATACGACTCACTATAGGGTCGCACATTCCGCTTCTACC"
${fastq}_reformat_seq.tmp|grep "CGTAAGTCCGTGTGTGCGAA"
>${fastq}_reformat_seq_matched.tmp
cut -b 44-83 ${fastq}_reformat_seq_matched.tmp|sort|uniq -c|sort -rn
>${fastq}_reformat_seq_matched_aptamer_seq40.stat
wc -l *_reformat_seq_matched.tmp
wc -l *_aptamer_seq40.stat
head *_aptamer_seq40.stat

echo -e "${fastq}______aptamer_______done!!!"
```

Figure A.2.1 Custom script used to sort the HTS data by clipping the head and tail regions of the .fastq files, pairing duplicate sequences, and sorting based on abundance.

$$f(Concentration) = Unbound + \frac{(Bound - Unbound) \times \left(Concentration + TargetConc + K_d - \sqrt{(Concentration + TargetConc + K_d)^2 - 4xConcentrationxTargetConc}\right)}{2xTargetConc}$$

Figure A.2.2 Fraction bound equation used to determine apparent dissociation constants of aptamers tested in the MST binding assay. Fraction bound graphs and dissociation constant values were generated using the MO.Affinity analysis software (Nanotemper).

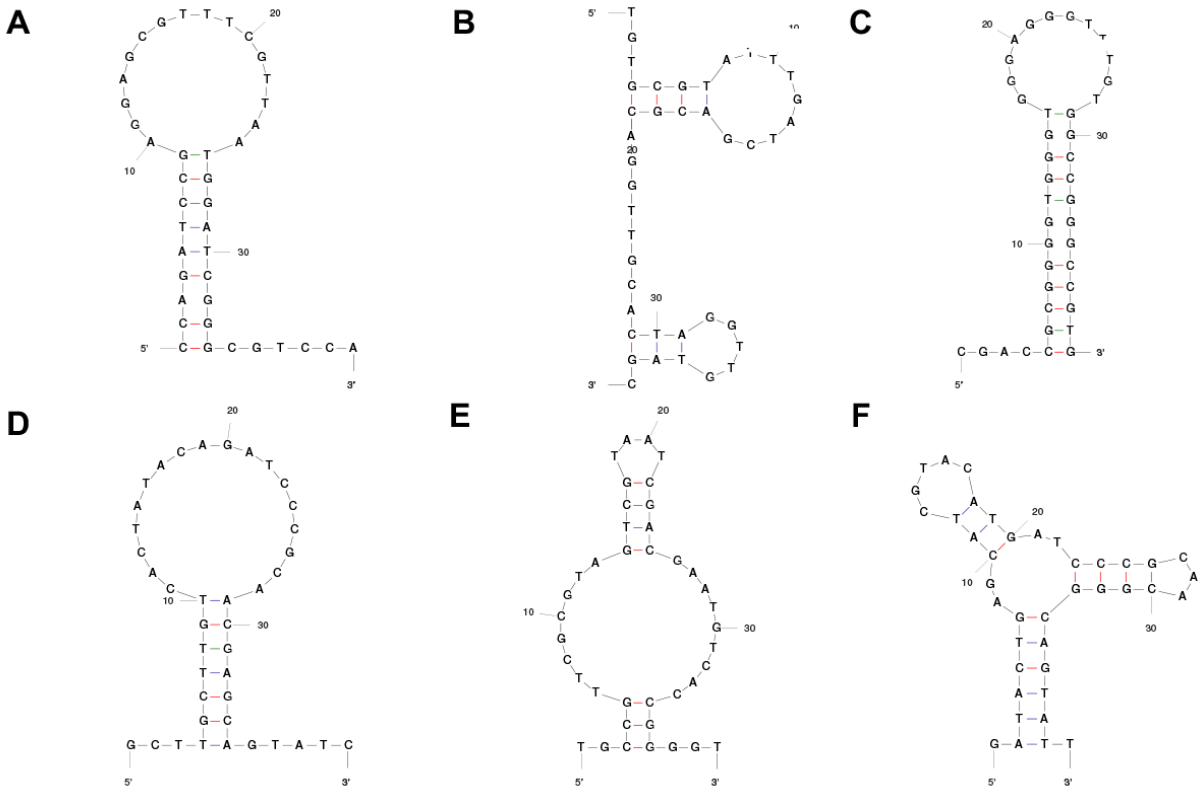

Figure A.2.3 Predicted secondary structures for aptamers using Mfold software. **(A)** PDGF-2. **(B)** PDGF-5. **(C)** PDGF-6. **(D)** PDGF-7. **(E)** PDGF-8. **(F)** Previously reported A2 aptamer.

A

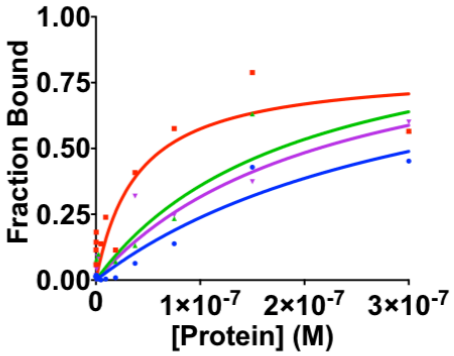

TGTGCGTATTTGATCGACGCAGGTTGCACTAGGTTGTAGC

- PDGF-AA: 305 ± 7 nM
- PDGF-BB: 155 ± 145 nM
- PDGF-CC: 164 ± 150 nM
- PDGF-DD: 202 ± 188 nM

B

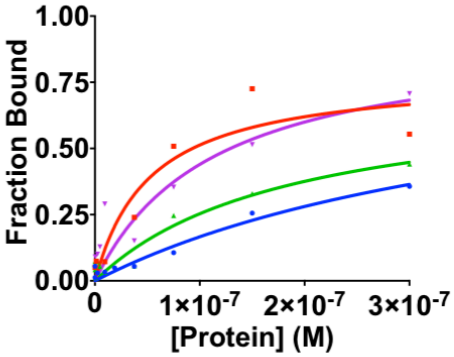

GCTTGCTTGTCACTATACAGATCCCGCAACGAGCAGTATC

- PDGF-AA: 576 ± 245 nM
- PDGF-BB: 115 ± 85 nM
- PDGF-CC: 435 ± 255 nM
- PDGF-DD: 148 ±95 nM

C

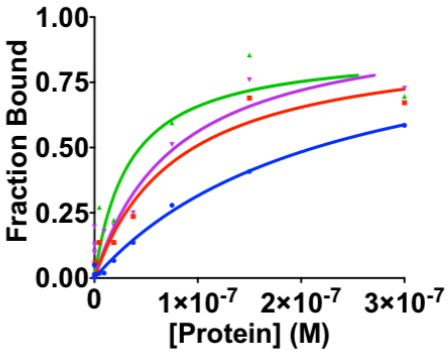

TGCCGTTCGCGTAGTCGTAATCGACGAATGTCACCGGGGT

- PDGF-AA: 204 ± 14 nM
- PDGF-BB: 124 ± 40 nM
- PDGF-CC: 66 ± 22 nM
- PDGF-DD: 140 ±110 nM

Figure A.2.4 Affinity and specificity of aptamers **(A)** PDGF-5, **(B)** PDGF-7, **(C)** PDGF-8.

Table A.2.1 Parameters for each round of SELEX.

Round	Primary Target PDGF-BB	Off targets PDGF-AA, CC, DD (each)	Molar Ratio of PDGF-BB to Off-Targets	Time of Positive Selection	Time of Washing & Counterselection
1	40 pmol	-	-	1 hr	-
2	4 pmol	4 pmol	1:1	50 min	30 min
3	4 pmol	40 pmol	1:10	45 min	45 min
4	0.4 pmol	40 pmol	1:100	40 min	50 min
5	0.4 pmol	40 pmol	1:100	30 min	1 hr

Table A.2.2 Top ten most abundant nucleic acid sequences determined by HTS.

Aptamer ID	Sequence (5' to 3')	Abundance (total reads)	Prevalence (%)
PDGF-1	ATTGCATTCCTGCCGCTACGTAGCTAAGCTAGGCTAATAG	205915	2.52
PDGF-2	CCAGATCCGAGGAGCGTTTCGTTAATGGATCGGGCGTCCA	94929	1.16
PDGF-3	CTATCGAAAACAGCAGCCGGCTTCTCACCACAGACATAGC	79984	0.98
PDGF-4	GCACGTGATGTTACAATTAAGTCGATCCTCCAACCACCTT	31618	0.39
PDGF-5	TGTGCGTATTTGATCGACGCAGGTTGCACTAGGTTGTAGC	31600	0.39
PDGF-6	GACCGCGGGGTGGGTGGGAGGGTTTGTGGCCGGGCCGTG	29856	0.37
PDGF-7	GCTTGCTTGTCACTATACAGATCCCGCAACGAGCAGTATC	28383	0.35
PDGF-8	TGCCGTTCGCGTAGTCGTAATCGACGAATGTCACCGGGGT	21693	0.27
PDGF-9	ACCACTAACGGACGCATTTGGTTTACCCTTGTTACGCCAT	14121	0.17
PDGF-10	CTACGTGTTCCGGCACTATCCGCTACACCTGCTTGGACAA	13946	0.17

Chapter 3

ISOLATING RNA APTAMERS FOR THE KINESIN-12 COVERSTRAND

3.1 Summary

The dynamic flow system used to isolate DNA aptamers for the PDGF family of proteins was investigated for its application in isolating RNA aptamers. Here, we demonstrate that RNA aptamers can successfully be isolated using this workflow for the kinesin-12 coverstrand peptide. Aptamers for the kinesin-12 (K12) coverstrand are predicted to inhibit formation of the cover-neck bundle in an effort to block centrosome separation and halt mitosis. This chapter describes efforts to generate an RNA aptamer library, perform an RNA aptamer selection, and characterize the affinity and specificity of the top isolated aptamers. Two aptamers with micromolar affinity were successfully isolated, with one aptamer having moderate specificity over a similarly structured kinesin-1 (K1) coverstrand peptide. Plans for further *in vitro* characterization of these isolated aptamers are discussed.

3.2 Introduction

RNA aptamers have been previously reported to bind to various targets with high affinity and specificity. Starting RNA libraries theoretically have more diversity than starting DNA libraries due to their 5'-hydroxyl group [89],[10]. In addition, RNA aptamers are smaller in size and can enter cells more readily than DNA aptamers of the same length in nucleotides [90]. These unique characteristics of RNA aptamers aid in their ability *in vivo*, such as carrying additional ligands for specific targeting or therapeutic agents for intracellular drug delivery [91],[92].

However, RNA aptamer selections are more laborious to perform as they require additional steps to convert between RNA, ssDNA, and dsDNA (Fig 3.1). An RNA aptamer library cannot be purchased for use, requiring an RNA library to be generated from a ssDNA library. The ssDNA library is PCR amplified with a forward primer containing the T7 promoter region, which is required for polymerase recognition during *in vitro* transcription (IVT). dsDNA with the T7 promoter region allows for transcription to occur, thereby converting the dsDNA library to a ssRNA library.

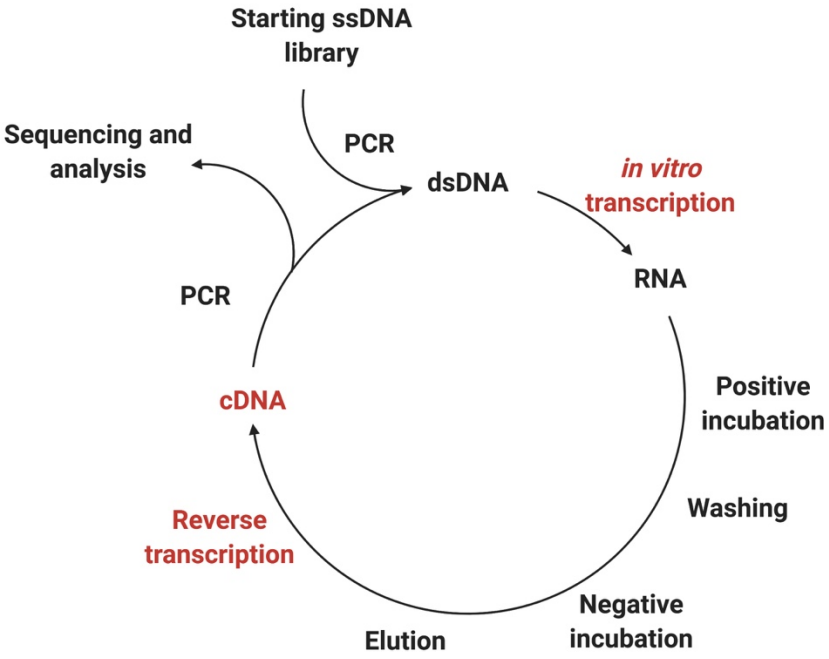

Figure 3.1 Overview of RNA SELEX workflow. RNA libraries are transcribed from ssDNA libraries. RNA is incubated with the primary target in a positive selection step and off-targets in a negative selection step. Following incubations, washing and elution steps are performed. Eluted RNA is converted to ssDNA with reverse transcription and PCR amplified into dsDNA with the T7 promoter region. dsDNA is transcribed back to RNA for the next round of selection.

In an RNA selection, RNA is heat prepped, incubated with the target molecule, washed, and eluted similar to DNA selections. However, RNA selections have two unique steps. After RNA aptamers are eluted from the target, they need to be reverse transcribed into ssDNA to perform PCR amplification, using a reverse transcription kit to generate cDNA. ssDNA is converted to dsDNA with PCR amplification; again using the T7-modified forward primer. Performing an IVT reaction generates ssRNA, so there is no requirement for an additional separation step such as using λ-exonuclease in a DNA selection. Furthermore, RNA aptamer selections require more care to ensure an RNase-free work area and RNase-free reagents, as unmodified RNA is more susceptible to nuclease degradation.

The previously described dynamic flow system used to isolate DNA aptamers for the PDGF family of proteins was used to isolate RNA aptamers for the kinesin-12 coverstrand peptide. Antimitotics are therapeutics that target spindle microtubule dynamics, leading to mitotic arrest and apoptosis [93]. In recent years, mitotic kinesins have attracted attention as drug targets due to their specific function in mitosis. Inhibitors have been developed to target the microtubule motor Eg5 (kinesin5) in an attempt to halt mitosis [94]. However, kinesin-12 (K12/Kif15/Hklp2) can still drive centrosome separation during bipolar spindle assembly if Eg5 is partially inhibited [95]. K12 can replace all essential functions of Eg5 and thus, a lone inhibitor for Eg5 cannot completely halt mitosis. A combination of inhibitors for Eg5 and K12 has the potential to completely halt mitosis as a cancer therapeutic strategy. We aimed to develop an aptamer that could target the K12 coverstrand to block the formation of the cover-neck bundle, which is yielded when a N-terminal cover strand forms a β-sheet with the neck linker cover [96]. We aimed to develop aptamers with high affinity and specificity in an effort to target the K12 coverstrand without interfering with other kinesin activity, which would limit cellular toxicity [93].

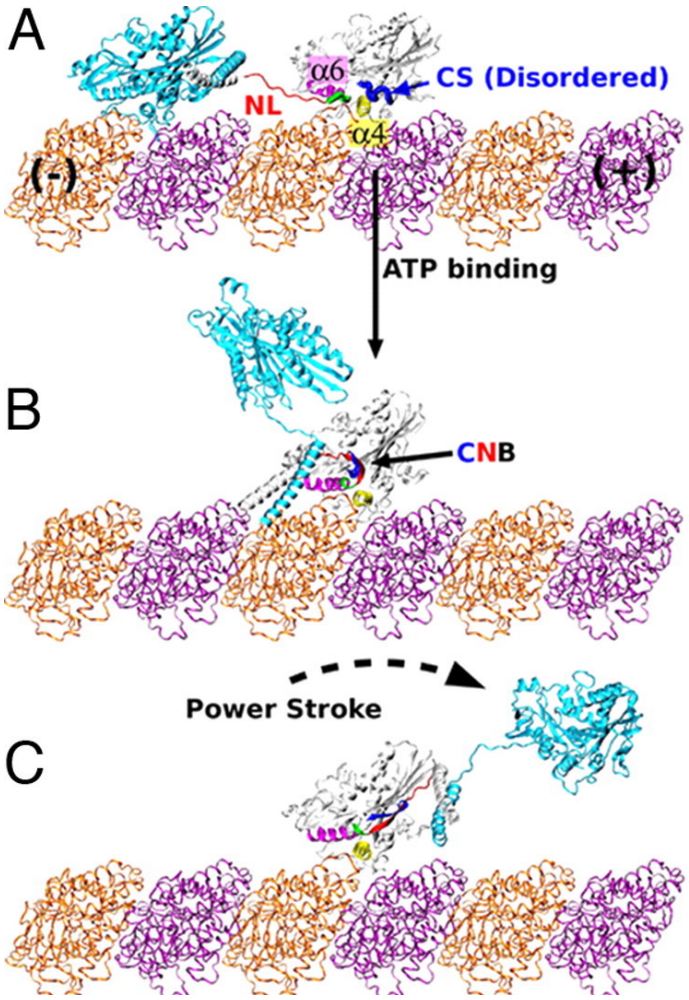

Figure 3.2 Model for kinesin's power stroke. ATP binding results in bringing the necklinker and coverstrand into a favorable position to form a β-sheet, known as the coverneck bundle. The coverneck bundle is responsible for delivering a power stroke, which propels the trailing head forward, and the new leading head searches for the next microtubule binding site. Figure adopted from Khalil, 2008, with permission from PNAS [96].

3.3 Materials and Methods

3.3.1 Materials and Instruments

Kinesin-12 and kinesin 1 peptides were synthesized from Genscript (Piscataway, NJ) (K12: QPSNEGDAIGK, K1: REIPAEDSIGK). N-terminal FITC-labeled peptides were also ordered

from Genscript. The starting DNA library, primers, and custom aptamer sequences were purchased from Integrated DNA Technologies (San Jose, CA) with HPLC purification. The starting DNA library was synthesized with 40 nucleotide random bases flanked by 20 nucleotide primer ends required to perform PCR amplification (forward fixed region: TCGCACATTCCGCTTCTACC, reverse fixed region: CGTAAGTCCGTGTGTGCGAA). The starting library was designed with a A:C:G:T molar ratio of 3:3:2:2.4 to adjust for equimolar amounts of nucleotide incorporation and primers; forward primer: GTATAATACGACTCACTATAGGG, reverse primer: TTCGCACACACGGACTTACG. Dynabeads M-270 Carboxylic Acid were purchased from Thermo Fisher Scientific (Waltham, MA), along with N-hydroxysuccinimide (NHS) and 1-ethyl-3-(3-dimethylaminopropyl) carbodiimide hydrochloride required for magnetic bead activation. All RNA work was performed in RNA-designated areas following RNA workflow guidelines. All materials used were RNase-free (pipet tips, reagents, conicals, microcentrifuge tubes, etc.). All glassware was baked at 300°C for 2 hours in a standard oven. RNA workspaces were maintained with RNase Zap (Thermo, AM9780) to remove RNases. All buffers used were RNase-free. Binding buffer used throughout the selection was prepared with 20 mM tris-HCl (pH 7.4), 140 mM NaCl, 5 mM KCl, 1 mM $MgCl_2$, and 1 mM $CaCl_2$. Washing buffer was comprised of binding buffer supplemented with 0.005% Tween-20. Elution buffer was prepared with 50 mM Tris-HCl, 140 mM NaCl, 50 mM EDTA, pH 7.4.

3.3.2 Generating an RNA Aptamer Library

To generate an RNA aptamer library, 1 nmol of 80-bp starting DNA library (N40) was prepared for transcription into RNA form. 60 standard Taq PCR reactions were prepared to

amplify the starting DNA library in a total reaction volume of 3 mL (300 μL of Taq Buffer, 60 μL of dNTP, 180 μL of unmodified reverse primer, 180 μL of T7 forward primer, 10 μL of 100 μM N40 Library, 15 μL of standard Taq Polymerase, 2255 μL of ultrapure water) [cycling conditions: 95°C 30 seconds, 8 cycles of (95°C 30 seconds, 60°C for 60 seconds, 68°C for 1 min), 68°C for 5 minutes]. PCR reactions were pooled and standard phenol-chloroform extraction and ethanol precipitation of the dsDNA product were performed. The dsDNA pellet was resuspended in 100 μL of ultrapure water, concentration was measured with Qubit Fluorometer (Thermo, Q33238), and correct band size was confirmed with gel electrophoresis on a 3% agarose gel. The total size of the dsDNA library was correctly visualized at 103 bp. The dsDNA library was then converted to RNA using the Ampliscribe T7 High Yield Transcription Kit (Lucigen, AS3107). 1 μg of dsDNA template was loaded into each IVT reaction. 10 transcription reactions were performed (20 μL of reaction buffer, 15 μL of ATP, 15 μL of CTP, 15 μL of UTP, 15 μL of GTP, 20 μL of DTT, 5 μL of RNase inhibitor, 20 μL of T7 Enzyme solution, bring total volume to 200 μL with dsDNA template and ultrapure water). Reactions were incubated at 37°C overnight, followed by incubation with 1 μL of DNase I per reaction for 15 minutes. RNA product was ethanol precipitated and resuspended in RNase-free AF Buffer.

3.3.3 SELEX Process

To begin, $1x10^8$ M-270 Carboxylic Acid Dynabeads were conjugated with K12 peptide before each round of selection according to the manufacturer's instructions. The magnetic beads were washed with MES buffer (25 mM 2-(N-morpholino)-ethane sulfonic acid, pH 6.0), activated with EDC/NHS chemistry for 30 minutes, and incubated with K12 peptide for 1.5 hours with

rotation at room temperature. After incubation, the beads were washed with 50 mM Tris-HCl (pH 7.4) buffer and incubated with the same buffer for 1 hour to ensure that all unreacted groups on the magnetic beads were quenched. The beads were finally washed with PBS buffer with 0.005% Tween-20 and suspended in binding buffer and stored at 4°C until utilized. Beads were prepared fresh for each round of selection, and immediately prior to their use, beads were washed three times with wash buffer and resuspended in binding buffer.

A single well of a hydrogel bonded, ultra-low attachment 96-well plate (Corning, St. Louis, MO) was plumbed by drilling two holes into the lid, inserting dispensing needles (Jensen, North Andover, MA), and circulating fluid using a peristaltic pump (Fisher Scientific). Manifold pump tubing (PVC, 0.51 mm ID, Fisher Scientific) was flushed with washing buffer containing 100 mg/mL of yeast tRNA (Thermo Fisher Scientific) and 0.1% bovine serum albumin (RPI, Mt. Prospect, IL) to passivate the lines before introducing the aptamer pools. Beads were trapped at the bottom of the plumbed well using a neodymium magnet. The selection was initiated with 5 nmole of starting RNA library. The starting library pool was heated to 95°C for 5 minutes and slowly cooled down to 25°C in a standard thermocycler at a rate of 0.5°C/min. Aptamer pools were circulated over the magnetically trapped beads at a rate of 20 mL/h. RNase-free wash buffer was then circulated at a rate of 50 mL/h to continuously remove unbound and weakly bound aptamers. After washing, aptamers bound to the beads were resuspended in 100 μL of elution buffer and heated at 95°C for 10 minutes to elute the bound nucleic acids. Round 1 only included a positive incubation step with K12 peptide. Round 2 and beyond included both positive incubation and negative counterselection, where soluble K1 peptide was included in the wash buffer solution for the integrated counterselection step.

After elution, elution buffer was ethanol precipitated and resuspended in 10 μL of ultrapure water. Sunscript Reverse Transcriptase RNaseH (Expedeon, 422050) was used to convert the eluted RNA to cDNA (10 μL of resuspended RNA, 2 μL of 10 μM reverse primer, 4 μL of 5X reaction buffer, 2 μL of 0.1 M DTT, 1 μL of 10 mM dNTP, 1.5 μL of Sunscript RT Enzyme) [65°C for 10 min, 70°C for 10 min, 75°C for 40 min, 95°C for 10 min]. The cDNA product was PCR amplified with emulsion PCR using the T7 forward primer, as previously described. dsDNA product was run on a 2% agarose gel and extracted with the Qiaex II Gel Extraction Kit (Qiagen, 20021). dsDNA was transcribed into RNA using 10 reactions of the Ampliscribe transcription kit, heated at 37°C overnight, incubated with DNase I at 37°C for 15 minutes, followed by phenol-chloroform extraction and ethanol precipitation. RNA product was resuspended in binding buffer and prepared for the next round of selection.

After round 1, a counterselection step was incorporated into the workflow using K1 peptide-coated micromagnetic beads. Through the selection, the amount of K12 peptide-coated magnetic beads was decreased and the amount of K1 peptide-coated magnetic beads was increased. The time of washing was increased, the time of positive incubation was decreased, and the amount of RNA introduced into the next round of selection was decreased. At the end of five rounds of selection, the TOPO-TA Cloning kit (Thermo 460572) was used to isolate individual aptamer sequences. The cloning reaction was set up with 4 μL of PCR product from the round 5 pool, 1 μL of salt solution, and 1 μL of TOPO vector. The reaction was gently mixed, incubated for 5 minutes at room temperature, and then placed on ice. One Shot Top10 Competent Cells were thawed on ice, 2 μL of the TOPO cloning reaction was added to the cells, and incubated on ice for 30 minutes. Cells were then heat-shocked for 30 seconds at 42°C, placed on ice, and then mixed with 250 μL of SOC medium. The cells were rotated at 37°C for 1 hour, followed by spreading

onto a pre-warmed ampicillin-selective plate, and incubated at 37°C overnight. The following day, individual colonies were picked and incubated overnight in 5 mL of LB broth with 50 μg/mL of ampicillin. dsDNA was extracted using the Plasmid Miniprep Kit (Qiagen, 27104). dsDNA concentration was measured using a Nanodrop (Thermo, ND-2000) and sequences were sent to Genewiz (Plainfield, NJ) for Sanger Sequencing. Sanger Sequencing files were analyzed with SnapGene.

3.3.4 Screening Aptamer Candidates

Seven aptamers were isolated with the TOPO TA cloning kit and ordered from IDT as 40 nt ssDNA. These ssDNA aptamer sequences were PCR amplified into dsDNA with T7 forward primer, as previously described. dsDNA aptamers were transcribed into RNA, as previously described. To screen RNA aptamer candidates binding to K12 peptide, the Monolith Microscale Thermophoresis system was used (Nanotemper NT.115). These seven RNA aptamer candidates were screened for their response amplitude and signal to noise ratio to fluorescently labeled K12 peptide at a concentration of 20 nM of unlabeled aptamer.

3.3.5 Measuring Aptamer Affinity and Specificity

The RNA aptamer candidates with the top response amplitude and signal to noise ratio (Clone 3, Clone 5) were then tested for their affinity to the K12 peptide and specificity against the K1 peptide. Briefly, 16 2-fold serial dilutions of RNA aptamer were prepared from a starting concentration of 2.5 μM in binding buffer. Aptamers were prepared by heating the mixture to 95°C for 5 minutes, snap-cooling on ice, and incubating at room temperature for 10 minutes. 40

nM solutions of fluorescently-labeled soluble peptide were prepared by diluting the peptide in binding buffer. The fluorescently-labeled peptide was mixed with each dilution of aptamer and incubated in the dark for 1 hour at room temperature. A standard Monolith NT.115 capillary was dipped into each serially diluted solution and fluorescent dose-response was measured at 20% MST excitation power. Equilibrium binding constants were fitted using the MO. Affinity Analysis software [85].

3.4 Results and Discussion

3.4.1 Choice of Target and Generating RNA Library

The primary target used in this RNA selection was the K12 coverstrand peptide and the off-targets used were K1 peptide and quenched micromagnetic beads. This is the first known selection performed with these coverstrand peptides. An RNA aptamer library was generated from a starting ssDNA N40 library ordered from IDT, with a 20 nt forward primer region, 40 random nucleotides, and a 20 nt reverse primer region. This ssDNA library was PCR amplified into dsDNA with a T7 promoter region on the 5' primer, with a GGG repeat spacer between the promoter and aptamer sequence (Figure 3.3). dsDNA was transcribed into RNA using the Ampliscribe Transcription kit. The concentration of ssDNA template, PCR cycle numbers, and PCR cycling parameters were optimized to generate a single, clear band on a 3% agarose gel (Figure 3.4). The optimized parameters show a clear band at 103 bp, compared to a standard 80 bp dsDNA library (Figure 3.5).

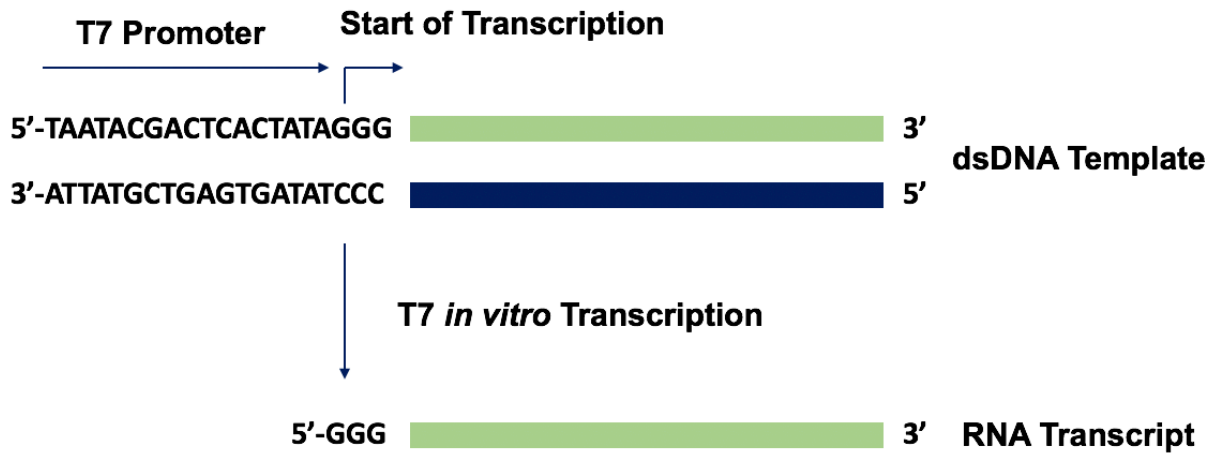

Figure 3.3 T7 promoter region required for *in vitro* transcription. dsDNA with the T7 promoter region is required for polymerase recognition to begin *in vitro* transcription. ssRNA is generated from the top strand of the DNA template [97].

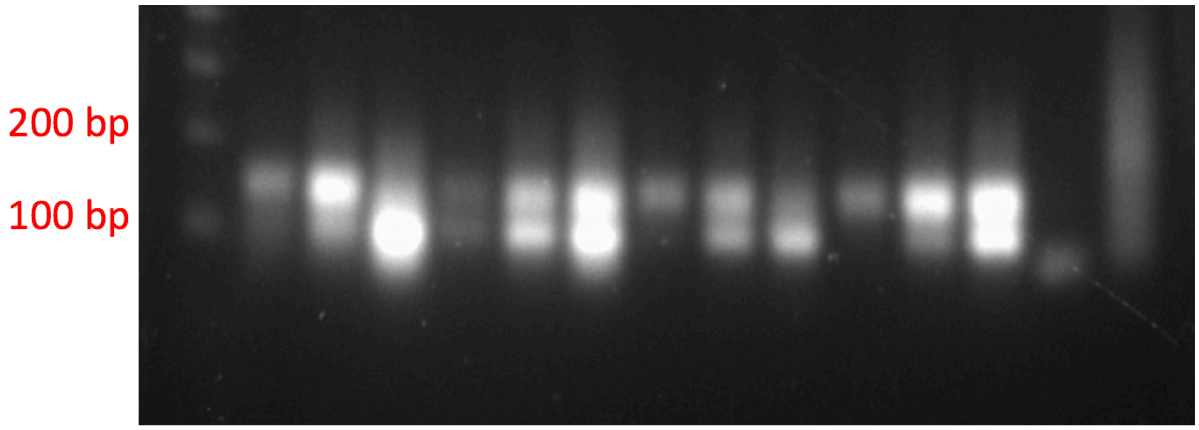

Figure 3.4 Optimization of PCR amplification of dsDNA library. The concentration of ssDNA template, PCR cycle numbers, and PCR cycling parameters were optimized to generate a single, clear band on a 3% agarose gel.

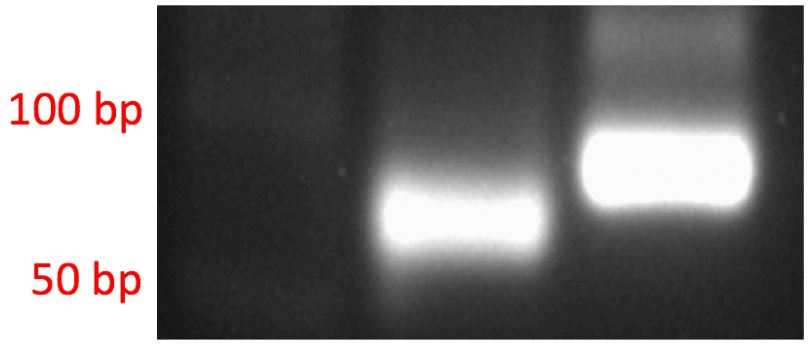

Figure 3.5 Optimized dsDNA Library. Lane 1: dsDNA ladder, Lane 2: 80-bp dsDNA library used for PDGF aptamer selection, Lane 3: 103-bp dsDNA library with T7 promoter region used to generate RNA aptamer library.

3.4.2 SELEX Workflow

Five rounds of positive selection were completed with the K12 coverstrand peptide as the primary target and four rounds of negative selection were completed with the K1 coverstrand, as described in the methods section. The first round of selection performed only involved a positive selection with the primary target K12 peptide. In rounds 2 to 5, a negative selection step was performed immediately after positive selection with the K1 peptide and quenched micromagnetic beads. Through the five rounds, the amount of primary target and the time of positive incubation were decreased, while the amount of off-targets, the time of washing, and the time of negative selection were increased (Table 3.1). The aim was to increase the ratio of the primary target to off-targets to increase the selection pressure through each round of selection, eventually increasing to a ratio of 1:100. After the fifth round of selection, the TOPO TA cloning kit was used to isolate individual aptamer sequences from the round 5 converged pool. These sequences are summarized in Table 3.2.

Table 3.1 Summary of kinesin-12 SELEX workflow. Five rounds of selection were performed to isolate aptamers for the kinesin-12 coverstrand peptide. The amount of primary target was decreased and the amount of off-targets were increased, reaching a ratio of 1:100 of primary target to off-targets. Additionally, time of positive incubation was decreased, while the time of washing and counterselection were increased.

Round	Primary Target: K12	Off-targets: K1, Quenched Beads	Ratio of Primary Target to Off-targets	Time of Positive Selection (min)	Time of Washing and Counterselection (min)
1	2 μg	-	-	60	-
2	1 μg	1 μg	1:1	50	30
3	500 ng	2 μg	1:4	45	45
4	100 ng	5 μg	1:50	40	50
5	100 ng	10 μg	1:100	30	60

Table 3.2 Isolated aptamers from TOPO TA cloning kit. Seven aptamers were isolated from the TOPO TA cloning kit (Clones 1-7).

Aptamer Name	40-nt Aptamer Sequence
Clone 1	CUCUUAGCUGCCGCCAGCCCGGCUCAGAGCAAUACCAAGU
Clone 2	UUCCCACACCAACUCGUGCAAACCGUGCGGCUGGAAAAUC
Clone 3	AGUCCUAAUUAGAGCAACGACUAAACGACCAGUGCCGCUG
Clone 4	GCCAGGGAAACCUCGAGGCUGCUACUACUGGUUUUAAACU
Clone 5	CUAUCGAAAACAGCAGCCGGCUUCUCACCACAGACAUAGC
Clone 6	CUACGUGUUCCGGCACUAUCCGCUACACCUGCUUGGACAA
Clone 7	AGAGCAUAAAUAACCAUCAGGCUAAAACUCUACCAGUACG

3.4.3 Screening Aptamer Candidates

The top seven aptamer candidates identified through cloning were screened for their binding to the K12 coverstrand peptide using MST, and compared to the starting RNA library. Performing a screen with MST measures two parameters: response amplitude, which is the signal difference between the bound and unbound states, and signal to noise ratio, which is the difference

in fluorescent signal of the fluorescent molecule alone. A true binding signal should have a response amplitude and signal to noise ratio of at least 5 response units. Clone 3 had a response amplitude of 9.8±1.7 fluorescent units with the highest signal to noise ratio of 17.0±1.6. Clone 5 had the highest response amplitude of 14.0±1.7 fluorescent units and a signal to noise ratio of 5.0±0.7.

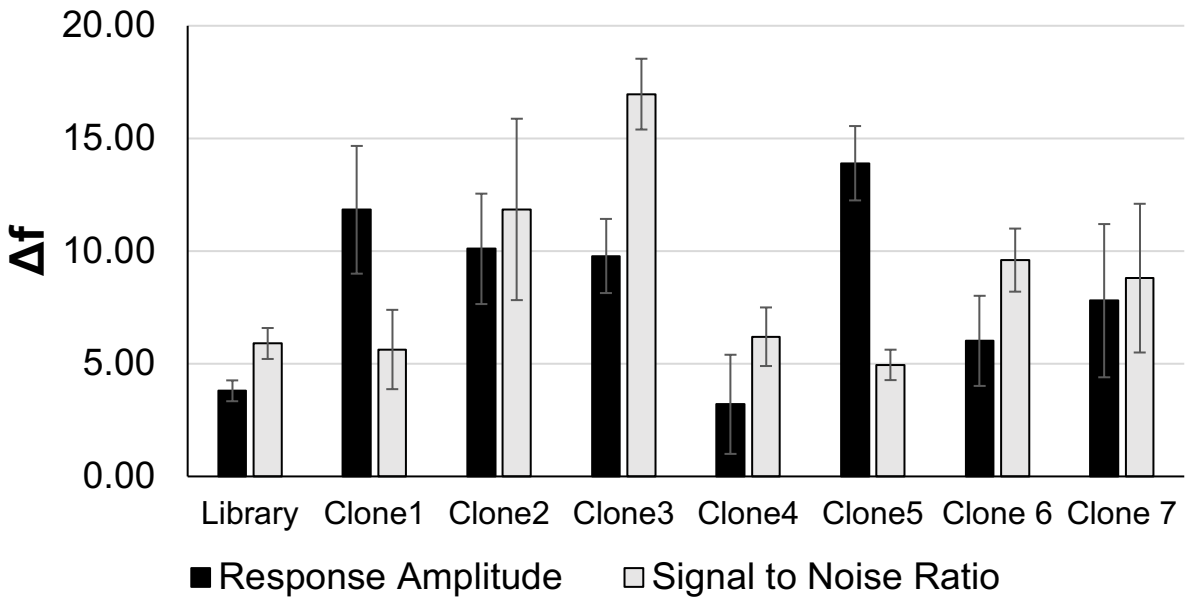

Figure 3.6 Screening aptamer candidates. MST was used to screen the seven aptamer candidates (Clones 1-7) for their response amplitude and signal to noise ratio to the fluorescently-labeled K12 coverstrand peptide. Starting RNA aptamer library was used as the negative control. Data are presented as mean±SD from biological triplicates.

3.4.4 Characterization of Prospective Aptamers

The starting library, Clone 3, and Clone 5 were transcribed into RNA and checked for correct sized bands on a 3% agarose gel. The RNA bands showed clear bands for the three sample groups (Fig 3.7). MST was used to determine the affinity of these sample groups to the primary

target K12 coverstrand peptide. Clone 3 is reported to have an affinity of 2.7±1.0 μM to the primary target (Figure 3.8) and Clone 5 is reported to have an affinity of 1.2±0.3 μM (Figure 3.9), with the starting library having negligible binding (data not shown). The aptamers were then tested for their specificity against the K1 coverstrand peptide used in the counterselection step of the workflow. No specificity is reported for Clone 3 to the off-target kinesin-1 peptide. However, a 2.6-fold specificity is reported for Clone 5 to the off-target kinesin-1 peptide (data not shown). NUPAC software was used to determine the structure of the 40-nt region of Clone 3 and Clone 5 (Figure 3.10 A,B). This RNA aptamer selection was able to isolate two aptamers with micromolar affinity to the primary target peptide, with one of the two aptamers exhibiting specificity over the off-target introduced in the selection workflow.

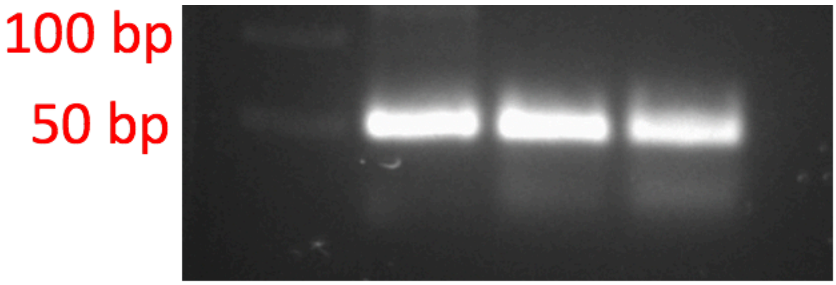

Figure 3.7 Checking quality of RNA samples used for affinity measurements. Lane 1: dsDNA ladder, lane 2: starting RNA library, lane 3: RNA Clone 3 aptamer, lane 4: RNA Clone 5 aptamer. Single, clear bands are confirmed on a 3% agarose gel for the RNA samples used for affinity measurements.

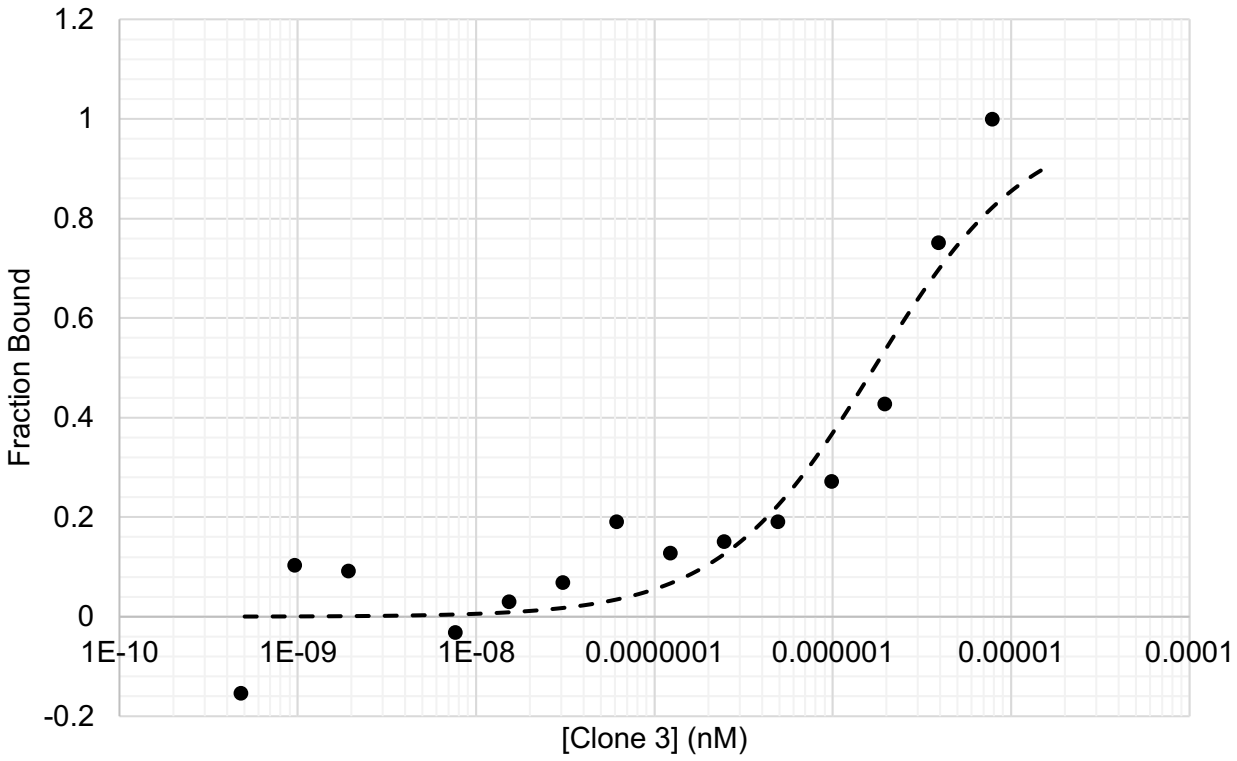

Figure 3.8 Affinity of Clone 3. MST was used to measure the affinity of Clone 3 to the fluorescently-labeled primary target K12 coverstrand peptide. An affinity of 2.7±1.0 μM is reported, with no specificity to the off-target K1 coverstrand peptide. Affinity values were obtained from biological triplicates.

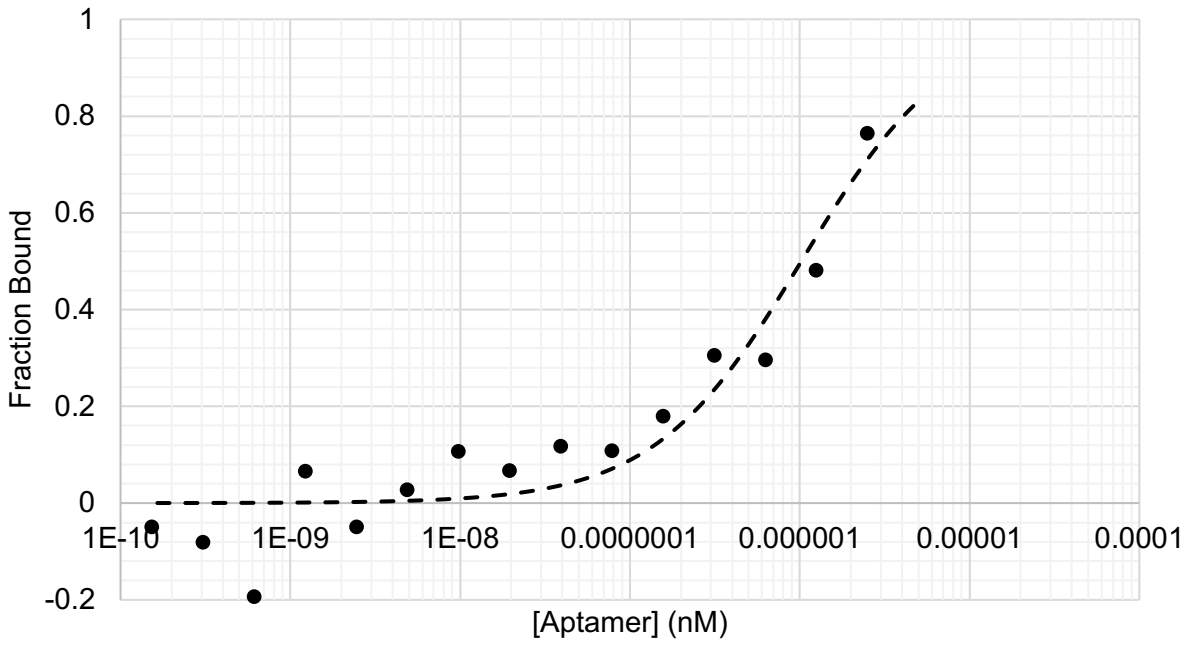

Figure 3.9 Affinity of Clone 3. MST was used to measure the affinity of Clone 3 to the fluorescently-labeled primary target K12 coverstrand peptide. An affinity of 1.2±0.3 μM is reported, with a 2.6-fold specificity to the off-target K1 coverstrand peptide. Affinity values were obtained from biological triplicates.

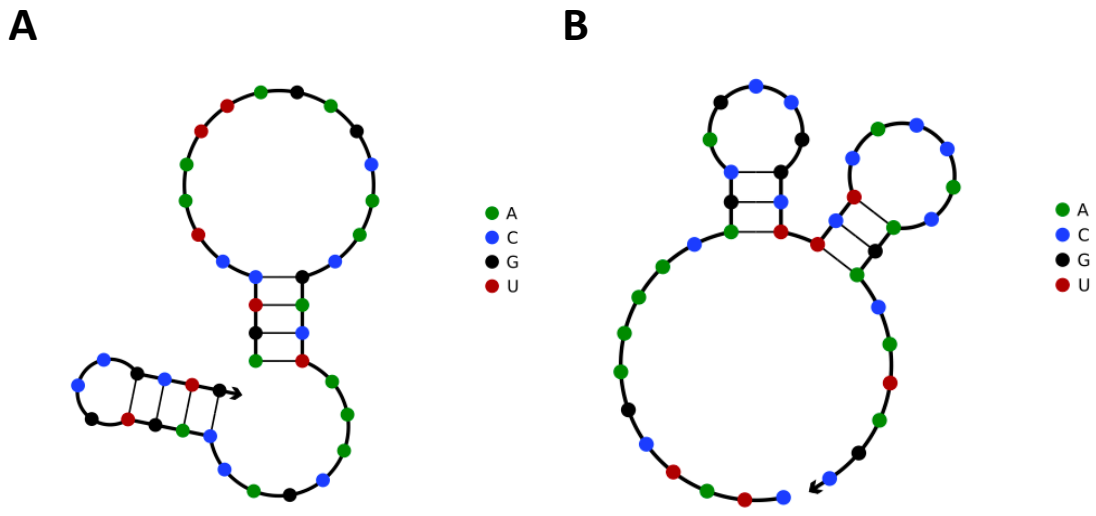

Figure 3.10 Predicted structures of Clone 3 and Clone 5. NUPAC software was used to predict the structure of (A) Clone 3 and (B) Clone 5.

3.5 Conclusions and Future Work

The same selection workflow used to isolate DNA aptamers for the PDGF family of proteins was used to isolate RNA aptamers for the kinesin-12 coverstrand peptide. Five rounds of positive selection and four rounds of negative selection were performed to isolate seven aptamer sequences through conventional bacterial cloning. Two of the top aptamers, Clone 3 and Clone 5, are reported to have micromolar affinity to the kinesin-12 coverstrand peptide. While Clone 3 did not show any specificity against the introduced off-target, Clone 5 is reported to have a 2.6-fold specificity against the kinesin-1 coverstrand peptide. Further *in vitro* functional assays will be performed, including a fluorescently-labeled necklinker inhibition assay. In this assay, kinesin cover-neck bundles will be incubated with increasing concentrations of aptamers to determine an inhibitory effect on coverneck bundle formation. This assay will be performed with both kinesin-12 and kinesin-1 cover-neck bundles to further validate the specificity of these aptamers. Further *in vitro* functional assays and characterizations will be completed to further validate the efficacy of these kinesin-12 coverstand peptide aptamers.

Chapter 4

ALBUMIN-BINDING APTAMER SIRNA-CHIMERAS TOWARD IMPROVED BIOAVAILABILITY

4.1 Summary

Short interfering RNA (siRNA) are potent nucleic acid-based drugs that interfere with disease driving genes that may otherwise be undruggable [98]. The potential of administering therapeutic siRNA *in vivo* is limited due to poor pharmacokinetic properties, including rapid renal clearance and nuclease degradation [99]. siRNA-nanocarriers and -conjugates have been explored as means to improve these properties; however, these methods often involve complex synthesis, lack of specificity, and toxicity issues [100]. In this work, we investigate the use of aptamer-siRNA chimeras to improve these limitations. Aptamers are short single-stranded DNA or RNA molecules that can be selected to have high affinity and specificity for biological targets using SELEX (Systematic Evolution of Ligands through Exponential Enrichment). We sought to identify new aptamers that target endogenous albumin, the most abundant serum protein that has an extraordinary circulation half-life of 19 days [101]. Fusion of siRNAs with these aptamers form complexes, termed chimeras, which confer siRNA with the ability to bind to albumin, thereby improving their circulation times and bioavailability for therapeutic delivery.

4.2 Introduction

Short interfering RNA (siRNA) is a powerful gene silencing platform that can silence traditionally undruggable targets [102]. In this RNA interference cellular mechanism, long double-stranded RNA is cleaved by the endoribonuclease, Dicer, into small siRNA fragments (20-25 bp) (Figure 4.1) [103]. These siRNAs are incorporated into the RNA-induced silencing complex (RISC), which creates single-strand RNA (ssRNA) [104]. The RISC complex containing either the sense or antisense strand binds to complementary mRNA sequences in cells. The enzyme, Argonaute, recognizes bound mRNA sequences within the RISC complex and signals it for degradation. This leads to downmodulation of the mRNA sequence and prevention of translation into protein, thus silencing the gene that encodes that mRNA [68].

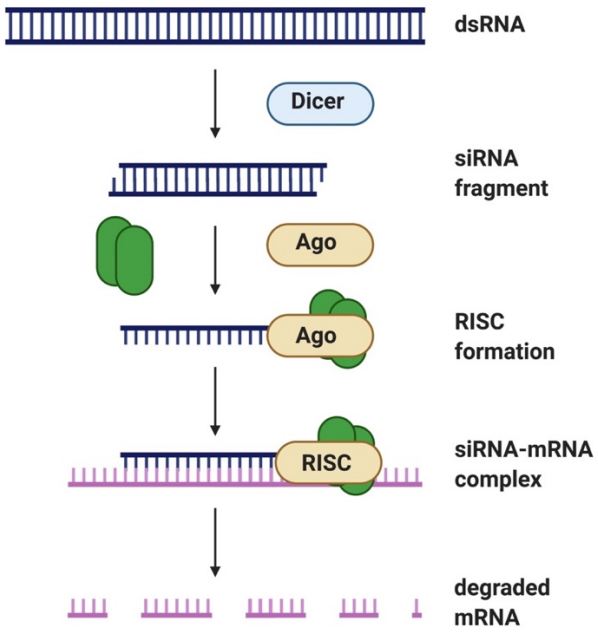

Figure 4.1 siRNA cellular mechanism. Dicer cleaves long dsRNA into small siRNA fragments, which are then incorporated into the RISC complex to create ssRNA. ssRNA binds to complementary mRNA, triggering degradation from the enzyme, Argonaute. Figure adapted from Dana, 2017 [103].

Systemic delivery of siRNA remains elusive. Despite the potent and powerful potential of siRNAs as a gene silencing platform, they are limited by their rapid degradation and clearance, lack of innate targeting, and inability to escape the endolysosomal pathway in their native form [105], [106]. Nanocarriers and conjugates have been explored as a means to improve these properties, but these mediums often involve complex synthesis, lack specificity, and can have toxicity issues [105], [107]. Sarett *et al.* has previously reported a siRNA conjugated to a diacyl lipid moiety (siRNA-L_2) that binds rapidly to endogenous serum protein albumin [108]. By utilizing albumin as a carrier, the circulation half-life and bioavailability of the siRNA were increased, while renal accumulation was reduced. In addition, this siRNA-L_2 conjugate was also able to achieve greater tumor accumulation and an increase in per-tumor-cell uptake in mouse models, compared to standard jetPEI. The dissociation constant of the lipid conjugate was determined to be 1.38 μM using isothermal calorimetry.

Aptamers are single stranded DNA or RNA molecules that can be selected to have excellent affinity and specificity for biological targets through SELEX. Fusions of siRNA and RNA aptamers have been previously reported to confer targeting ability to siRNA and siRNA-carriers [109], [110]. Though these platforms benefit from the high specificity targeting conferred by aptamers, they are still subject to the poor circulation time and rapid clearance characteristic of RNA-based treatments [93]. In this research, we sought to leverage targeting to endogenous albumin, the most abundant protein in blood, with RNA aptamers to imbue our platform with long-circulating properties. Albumin's extraordinary circulation half-life of 19 days and concentration of 40 mg/mL in blood make it an ideal target for an aptamer that can both improve the bioavailability and targeting of its cargo [112], [113]. We have leveraged 2'-fluorine modified pyrimidines (Figure 4.2) to obtain superior serum stability over unmodified-base RNA and

ultimately present a synthetically simple and elegant design that can be applied to a wide variety of siRNA payloads [114]. The implications of this aptamer are far reaching in that it can be used for a wide spectrum of nanomedicines that are limited by clearance or targeting ability. Herein, we demonstrate the excellent affinity of the aptamer, the preserved activity of siRNA once appended to this aptamer, extended circulation half-life of these chimeras, and improved knockdown *in vitro* of a target gene.

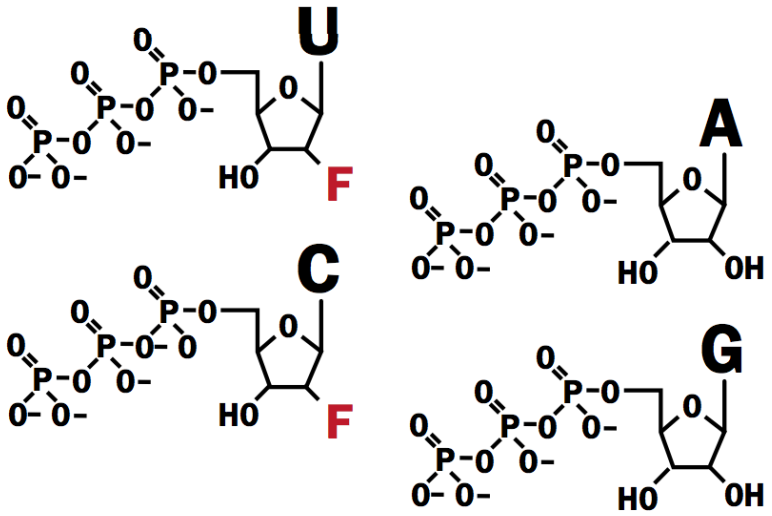

Figure 4.2 Modified RNA bases used in aptamer selection. The Durascribe transcription kit incorporates 2'-fluorine-modified RNA bases into the aptamer selection workflow to improve serum stability. [115]

Five rounds of SELEX were completed to identify high affinity albumin-binding aptamers. The SELEX procedure was able to isolate 2'-fluoro modified pyrimidine bases to confer superior serum stability over unmodified DNA and RNA counterparts [116],[117]. Chimeras were generated by transcribing the 40 nt RNA aptamer with the antisense strand of the siRNA separated by a two uracil base linker [118]. The sense strand is transcribed separately and the two

complementary strands are annealed, allowing for cellular Dicer/RISC-complex recognition. Two albumin-binding aptamers were isolated and fused with siRNA targeting the luciferase gene for *in vitro* characterization. Knockdown potency of firefly luciferase-interfering chimeras was confirmed *in vitro* following 24 hour incubation with luciferase-expressing cells. Additionally, the aptamers improved the *in vivo* pharmacokinetics of the appended siRNA. Following tail vein injection, half-lives of chimeras were measured in mice using fluorescent intravital microscopy. Further studies will be performed to validate the findings of this research.

4.3 Materials and Methods

4.3.1 Materials and Instruments

Human serum albumin (A1653) and mouse serum albumin (A3139) were purchased from Sigma (St Louis, MO). Fluorescently-labeled human serum albumin (HS1-S5-1) was purchased from NANOCS (New York, NY). The starting DNA library, primers, and custom aptamer sequences were purchased from Integrated DNA Technologies (San Jose, CA) with HPLC purification. The starting DNA library was synthesized with 40 nucleotide random bases flanked by 20 nucleotide primer ends required to perform PCR amplification (forward fixed region: TCGCACATTCCGCTTCTACC, reverse fixed region: CGTAAGTCCGTGTGTGCGAA). The starting library was designed with a A:C:G:T molar ratio of 3:3:2:2.4 to adjust for equimolar amounts of nucleotide incorporation and primers. Table A.4.1 summarizes the primers used in these studies. Dynabeads M-270 Carboxylic Acid were purchased from Thermo Fisher Scientific (Waltham, MA), along with N-hydroxysuccinimide (NHS) and 1-ethyl-3-(3-

dimethylaminopropyl) carbodiimide hydrochloride required for magnetic bead activation. All RNA work was performed in RNA-designated areas following RNA workflow guidelines. All materials used were RNase-free (pipet tips, reagents, conicals, microcentrifuge tubes). All glassware was baked at 300C for 2 hours in a standard oven. RNA worksapces were maintained with RNase Zap (Thermo Fisher, AM9780) to remove RNases. All buffers used were RNase-free. Binding buffer used throughout the selection was prepared with 20 mM tris-HCl (pH 7.4), 140 mM NaCl, 5 mM KCl, 1 mM $MgCl_2$, and 1 mM $CaCl_2$. Washing buffer was comprised of binding buffer supplemented with 0.005% Tween-20. Elution buffer was prepared with 50 mM Tris-HCl, 140 mM NaCl, 50 mM EDTA, pH 7.4.

4.3.2 Generating 2'-Fluorine Pyrimidine RNA Library

To generate the 2'-fluorine pyrimidine RNA aptamer library, 1 nmol of 80-nt starting DNA library (N40) was prepared for transcription into RNA form. 60 standard Taq PCR reactions were prepared to amplify the starting DNA library in a total reaction volume of 3 mL (300 μL of Taq Buffer, 60 μL of dNTP, 180 μL of unmodified reverse primer, 180 μL of T7 forward primer, 10 μL of 100 μM N40 Library, 15 μL of standard Taq Polymerase, 2255 μL of ultrapure water) [cycling conditions: 95°C 30 seconds, 8 cycles of (95°C 30 seconds, 60°C for 60 seconds, 68°C for 1 min), 68°C for 5 minutes]. PCR reactions were pooled and the dsDNA was phenol-chloroform extracted and ethanol precipitated. The dsDNA pellet was resuspended in 100 μL of ultrapure water, concentration was measured with Qubit Fluorometer (Thermo Fisher, Q33238), and correct band size (103 bp) was confirmed with gel electrophoresis on a 3% agarose gel. The dsDNA library was then converted to modified-base RNA using the Durascribe T7 Transcription Kit (Lucigen, MA170E). This kit produces RNA that is resistant to RNase A degradation through

the replacement of canonical CTP and UTP with 2'-fluorine-dCTP (2'-F-dCTP) and 2'-fluorine-dUTP (2'-F-dUTP). The Durascribe kit uses a mutant T7 RNA polymerase that is able to efficiently incorporate 2'-F-dCTP, 2'-F-dUTP, ATP, and GTP into RNA transcription. 1 μg of dsDNA template was loaded into each IVT reaction. 10 transcription reactions were performed (20 μL of reaction buffer, 20 μL of ATP, 20 μL of 2'-F-dCTP, 20 μL of 2'-F-dUTP, 20 μL of GTP, 20 μL of DTT, 20 μL of T7 Enzyme solution, and bringing the total volume to 200 μL with dsDNA template and ultrapure water). Reactions were incubated at 37°C overnight, followed by incubation with 20 μL of DNase I for 15 minutes. RNA product was ethanol precipitated and resuspended in RNase-free AF Buffer.

4.3.3 SELEX Workflow

To begin, $1x10^4$ M-270 Carboxylic Acid Dynabeads were conjugated with human albumin and $1x10^4$ M-270 Carboxylic Acid Dynabeads were conjugated with mouse albumin before each round of selection according to the manufacturer's instructions. The magnetic beads were washed with MES buffer (25 mM 2-(N-morpholino)-ethane sulfonic acid, pH 6.0), activated with EDC/NHS chemistry for 30 minutes, and incubated with protein for 1.5 hours with rotation at room temperature. After incubation, the beads were washed with 50 mM Tris-HCl (pH 7.4) buffer and incubated with the same buffer for 1 hour to ensure that all unreacted groups on the magnetic beads were quenched. The beads were finally washed with PBS buffer with 0.005% Tween-20 and suspended in binding buffer and stored at 4°C until utilized. Beads were prepared fresh for each round of selection, and immediately prior to their use, beads were washed three times with wash buffer and resuspended in binding buffer.

A single well of a hydrogel bonded, ultra-low attachment 96-well plate (Corning, St. Louis, MO) was plumbed by drilling two holes into the lid, inserting dispensing needles (Jensen, North Andover, MA), and circulating fluid using a peristaltic pump (Fisher Scientific). Manifold pump tubing (PVC, 0.51 mm ID, Fisher Scientific) was flushed with washing buffer containing 100 mg/mL of yeast tRNA (Thermo Fisher Scientific) to passivate the lines before introducing the aptamer pools. Beads were trapped at the bottom of the plumbed well using a neodymium magnet. The selection was initiated with 5 nanomole of starting RNA library. The starting library pool was heated to 95°C for 5 minutes and slowly cooled down to 25°C in a standard thermocycler at a rate of 0.5°C/min. Aptamer pools were circulated over the magnetically trapped beads at a rate of 20 mL/h. RNase-free wash buffer was then circulated at a rate of 50 mL/h to continuously remove unbound and weakly bound aptamers. After washing, aptamers bound to the beads were resuspended in 100 μL of elution buffer and heated at 95°C for 10 minutes to elute the bound nucleic acids. Round 1 only included a positive incubation step with human and mouse albumin. Round 2 and beyond included both positive incubation and negative counterselection, where aptamer pools were circulated over quenched Dynabeads to remove aptamers binding to the surface of the beads.

After elution, elution buffer was ethanol precipitated and resuspended in 10 μL of ultrapure water. Sunscript Reverse Transcriptase RNaseH (Expedeon 422050) was used to convert the eluted RNA to cDNA (10 μL of resuspended RNA, 2 μL of 10 μM reverse primer, 4 μL of 5X reaction buffer, 2 μL of 0.1 M DTT, 1 μL of 10 mM dNTP, 1.5 μL of Sunscript RT Enzyme) [65°C for 10 min, 70°C for 10 min, 75°C for 40 min, 95°C for 10 min]. The cDNA product was PCR amplified with emulsion PCR using the T7 forward primer, as previously described. dsDNA product was run on a 2% agarose gel and extracted with the Qiaex II Gel Extraction Kit (Qiagen,

20021). dsDNA was transcribed to RNA using 5 reactions of the Durascribe transcription kit, heated at 37°C overnight, incubated with DNase I at 37°C for 15 minutes, followed by ethanol precipitation. RNA product was resuspended in AF Buffer and prepared for the next round of selection.

After round 1, a counterselection step was incorporated into the workflow using quenched micromagnetic beads. Through the selection, the amount of albumin-coated magnetic beads and the amount of RNA introduced into the next round of selection were decreased. Also, the amount of quenched magnetic beads introduced in the negative selection and the time of washing were increased. At the end of five rounds of selection, the TOPO-TA Cloning kit (Thermo Fisher, 460572) was used to isolate individual aptamer sequences. The cloning reaction was set up with 4 μL of PCR product from the round 5 pool, 1 μL of salt solution, and 1 μL of TOPO vector. The reaction was gently mixed, incubated for 5 minutes at room temperature, and then placed on ice. One Shot Top10 Competent Cells were thawed on ice, 2 μL of the TOPO cloning reaction was added to the cells, and incubated on ice for 30 minutes. Cells were then heat-shocked for 30 seconds at 42°C, placed on ice, and then mixed with 250 μL of SOC medium. The cells were rotated at 37°C for 1 hour, followed by spreading onto a pre-warmed ampicillin antibiotic selective plate, and incubated at 37°C overnight. The following day, individual colonies were picked and incubated overnight in 5 mL of LB broth with 50 μg/mL of ampicillin. dsDNA was extracted using the Plasmid Miniprep Kit (Qiagen, 27104). dsDNA concentration was measured using a Nanodrop (Thermo, ND-2000) and sequences were sent to Genewiz for Sanger Sequencing. Sanger Sequencing files were analyzed with SnapGene.

4.3.4 Screening Aptamer Candidates

Nine aptamers were isolated with the TOPO TA cloning kit and ordered from IDT as 40 nt ssDNA. These ssDNA aptamer sequences were PCR amplified into dsDNA with T7 forward primer, as previously described. dsDNA aptamers were transcribed into RNA, as previously described. To screen RNA aptamer candidates binding to fluorescently-labeled human serum albumin, the Monolith Microscale Thermophoresis system was used (Nanotemper NT.115). These nine RNA aptamer candidates were screened for their response amplitude and signal to noise ratio to Cy5-labeled human albumin at a concentration of 20 nM of aptamer.

4.3.5 Confirming Chimera Annealing to Sense Strand

Cy5-labeled sense strands were synthesized using the MerMade 12 Oligonucleotide synthesizer (BioAutomation). In brief, amidites were dissolved at 0.1 M in anhydrous acetonitrile and oligonucleotides were synthesized using standard coupling conditions. Mass fidelity was confirmed by LC ESI on a Waters Synapt. dsDNA antisense strands were transcribed into ssRNA and then annealed to the synthesized Cy5-labeled sense strands to create the aptamer-siRNA chimera (Figure A.4.1). Aptamer antisense strands were annealed to sense strands by heating to 95°C for 5 minutes and slow cooling to room temperature for 1 hour. Annealing of aptamer antisense strand to sense strand was confirmed on a 3% agarose gel, comparing nucleic acid migration between the annealed chimeras and sense strand alone (Figure A.4.2). Annealing of Cy5-labeled sense strand was similarly checked by visualizing nucleic acid migration on the IVIS Lumina III imaging system (Caliper Life Science, Hopkinton, MA) (Figure A.4.3).

4.3.6 Measuring Aptamer Affinity

The RNA aptamer candidates with the top response amplitude and signal to noise ratio (Clone 1, Clone 3) were then tested for their affinity to human albumin. Briefly, 16 2-fold serial dilutions of RNA aptamer were prepared from a starting concentration of 1.0 μM in binding buffer. Aptamers were prepared by heating the mixture to 95°C for 5 minutes, snap-cooling on ice, and incubating at room temperature for 10 minutes. 40 nM solutions of Cy5-labeled soluble albumin were prepared by diluting the protein in binding buffer. The Cy5- labeled protein was mixed with each dilution of aptamer and incubated in the dark for 1 hour at room temperature. Then, a standard Monolith NT.115 capillary was dipped into each serially diluted solution and fluorescent dose-response was measured at 20% MST excitation power. Equilibrium binding constants were fitted using the MO. Affinity Analysis software.

The affinities of the top aptamers were also tested with a plate-based assay. Briefly, Maleic Anhydride Amine-Binding Wells (Thermo Fisher, 15100) were washed three times with PBS with 0.05% Tween-20. Mouse albumin and human albumin were dissolved in immobilization buffer (PBS, pH 8.8) at a concentration of 10 μg/mL. 100 μL of protein solution were incubated in each amine-binding well at 37°C for 1 hour. Protein solution was then removed and 200 μL of Protein Blocking Buffer (Thermo Fisher, 37515) was incubated in each well for 1 hour at room temperature. Blocking buffer was removed and washed three times with wash buffer. 2-fold serial dilutions of Cy5-labeled aptamer chimeras were prepared from 2 μM to 0 μM. Chimera dilutions were incubated in albumin-conjugated wells for 2 hours, washed three times with AF washing buffer, and mean Cy5-fluorescence was measured on a Tecan Infinite M1000 Pro plate reader.

4.3.7 in vitro Gene Knockdown Using Aptamer Chimeras

Table A.4.2 summarizes all antisense and sense strands used in these studies. 4,000 Luciferase-expressing MDA-MB-231 cells were seeded into a black 96 well plate and adhered overnight. 25 nM of aptamer chimeras were complexed with standard Lipofectamine 3000 reagent (Thermo Fisher, L3000001) in Opti-MEM Media (Thermo Fisher, 31985062). Transfection complexes were incubated with cells for 24 hours in normal culture media. Following the 24 hour incubation, media was replaced with luciferin-containing media (150 μg/mL) (Sigma, L9504) and luminescence was evaluated by IVIS imaging.

4.3.8 Determining Aptamer Serum Stability

To determine the serum stabilities of Clone1 and Clone 3, 1 μg of aptamer was incubated with 60% FBS at 37°C for the following time points: 0, 0.5, 2, 4, 8, and 24, and 30 hours. Following the incubation, the DNA was run on a 3% agarose gel and visualized using an Odyssey Fc Imager.

4.3.9 Measuring Chimera Half-Lives

Prior to tail vein injection, the mouse ear was placed on a glass coverslip and an artery within the ear was set in focus, on the Nikon C1si+ confocal microscope system. 2 nmol of Cy5-labeled aptamer chimeras were injected into the tail vein of CD-1 mice (4-6 weeks old, Charles Rivers Laboratories). Images of the artery were collected every 2 seconds for 30 minutes per sample. Maximum initial fluorescence of the artery was set to a time of 0 seconds. Aptamer chimera fluorescence was evaluated in the artery by averaging pixel intensity values within a

circular region of interest located within the vessel. Data were fit to a one-phase exponential decay model in Graphpad Prism. Half-life and area under the curve data were determined from these fits. Figure A.4.4 shows example images of an artery visible with the microscope, with decaying fluorescence over the measurement time.

4.3.10 Carrier-free in vitro knockdown using chimeras

4,000 Luciferase-expressing MDA-MB-231 cells were seeded into a black 96 well plate and adhered overnight. 100 nM of aptamer chimeras or siRNA alone were precomplexed with 1:10 molar ratio of human serum albumin for 30 minutes at room temperature. RNA-albumin complexes were added to normal culture media for 24 hours. Following the 24 hour incubation, media was replaced with luciferin-containing media (150 μg/mL) and luminescence was evaluated by IVIS imaging.

4.4 Results and Discussion

4.4.1 Choice of Target and Outline of SELEX Process

Five rounds of selection were completed with human and mouse serum albumin as the primary targets, with quenched micromagnetic beads used as the counterselection, as described in the methods section. In the first round of selection, only a positive selection with the primary targets human and mouse albumin was performed. In rounds 2 to 5, a negative selection step was performed immediately after positive selection with quenched micromagnetic beads. Through the five rounds, the amount of primary target and the time of positive incubation were decreased, while

the amount of off-targets, the time of washing, and the time of negative selection were increased (Table 4.1). The aim was to increase the ratio of the primary target to off-targets, thereby increasing the selection pressure through each round of selection. After the fifth round of selection, the TOPO TA cloning kit was used to isolate individual aptamer sequences from the Round 5 pool. These sequences are summarized in Table 4.2.

Table 4.1 Overview of albumin SELEX workflow. Primary targets human and mouse albumin were decreased over five rounds, while the amount of quenched beads were increased. The time of positive incubation was decreased from 60 minutes to 30 minutes, while the time of washing and counterselection were increased to 60 minutes.

Round	Primary target: human, mouse albumin	Off-targets: quenched beads	Time of positive selection (min)	Time of washing and counterselection (min)
1	2 μg	-	60	-
2	1 μg	1 μg	50	30
3	500 ng	2 μg	45	45
4	100 ng	5 μg	40	50
5	100 ng	10 μg	30	60

Table 4.2 Albumin aptamers isolations from cloning. The round 5 pool was cloned with the TOPO TA cloning kit and individual colonies were identified with Sanger sequencing. Nine aptamers were chosen for further characterization (Clones 1-9).

Aptamer Name	40 nt Aptamer Sequence
Clone 1	GCGCCGCAACAGGUGUGACUGCCCUAGCCUCCGCUGUACC
Clone 2	UGUCCUAACGCACGACAAACUGGCUUGCCAGUAUACUUUC
Clone 3	UGGUAACCCUUUCCGGCUACGGCUACUAAAGACUUUUAUG
Clone 4	GAAACGAAAGGUUGAUCGUAGGUGGCAUCUAUGGAGGGAC
Clone 5	GUGACCCUGGCAAGCAUCAACAUUUAAUCAUCGGGAUCAG
Clone 6	GAUCGGAAAAGCCUUACACAAUCAUCAGAAAACUUGUUUG
Clone 7	UGAUAAAAGUUACUUAAGCGUGUACCAGAGCGAGAGUAUU
Clone 8	GUACCCUAGCAGGUCGUGGGUAUGCUAGAUACUAUGUUGC
Clone 9	ACCACUAACGGACGCAUUUGGUUUACCCUUGUUACGCCAU

4.4.2 Identification and Characterization of Prospective Aptamers

The top nine aptamer candidates identified through cloning were screened for their binding to Cy5-labeled human albumin using MST and compared to the starting RNA library (Figure 4.3). Performing a screen with MST measures two parameters: response amplitude, which is the signal difference between the bound and unbound states, and signal to noise ratio, which is the difference in fluorescent signal of the fluorescent molecule alone. A true binding signal should have a response amplitude and a signal to noise ratio of at least 5 response units. Clone 3 had the highest response amplitude of 10.8±2.2 fluorescent units with the highest signal to noise ratio of 10.1±1.2. Clone 1 had the second highest response amplitude of 8.4±1.8 fluorescent units and a signal to noise ratio of 5.2±2.0. Clone 1 and Clone 3 were chosen for further characterization. NUPAC software was used to determine the structure of the 40 nt region of Clone 1 and Clone 3 (Figure 4.4 A, B).

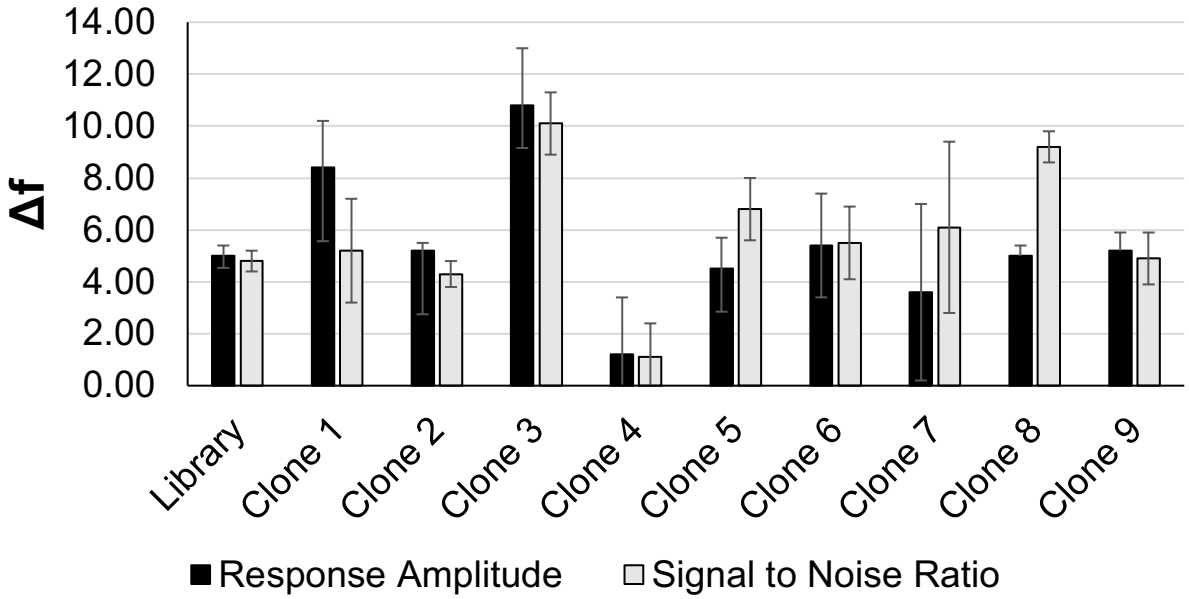

Figure 4.3 Screening aptamer candidates. MST was used to screen the nine aptamer candidates (Clones 1-9) for their response amplitude and signal-to-noise ratio to Cy5-labeled human albumin. The starting RNA aptamer library was used as a negative control. Data are presented as mean±SD from biological triplicates.

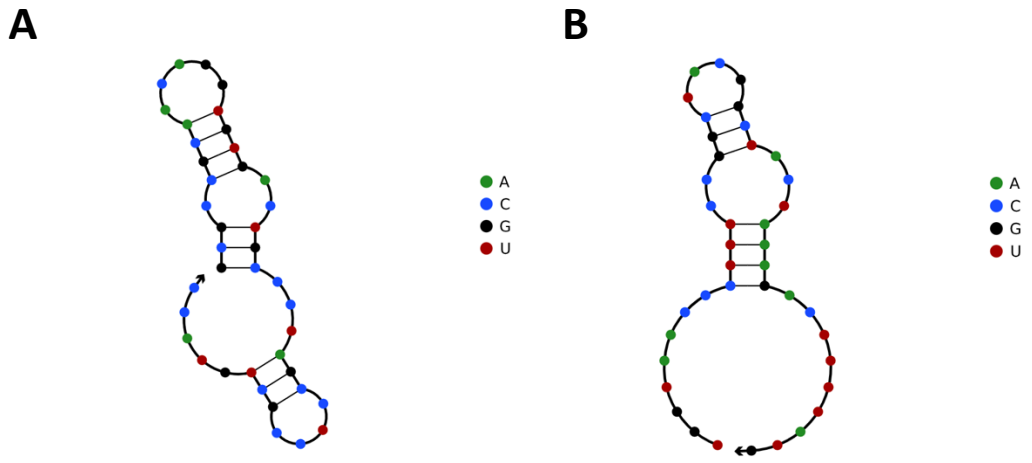

Figure 4.4 Predicted structures of Clone 1 and Clone 5 aptamers. NUPAC software was used to predict the structures of (A) Clone 1 and (B) Clone 3.

The starting library, Clone 1, and Clone 3 were transcribed into RNA and checked for correct sized bands on a 3% agarose gel (Figure A.4.4). The RNA sequences showed clear bands for the three sample groups. Two different assays were used to determine the affinities of Clone 1 and Clone 3: MST and a plate-based assay. For MST, unlabeled, annealed chimeras were measured for their binding to Cy5-labeled human serum albumin. Clone 1 was is reported to have an affinity of 46±12 nM and Clone 3 is reported to have an affinity of 480±120 nM (Figure 4.5 A,B). A plate-based affinity assay was used to further validate the affinities of the chimeras. For this assay, Cy5-labeled sense strands were annealed to the chimeras and unlabeled human and

mouse serum albumin were conjugated to amine-binding 96-well plates. Clone 1 is reported to have an affinity of 272±84 nM and Clone 3 is reported to have an affinity of 369±142 nM (Figure 4.5 C,D). Differences in the affinities measured could be due to the species of albumin used and the change in location of the Cy5 fluorescent label.

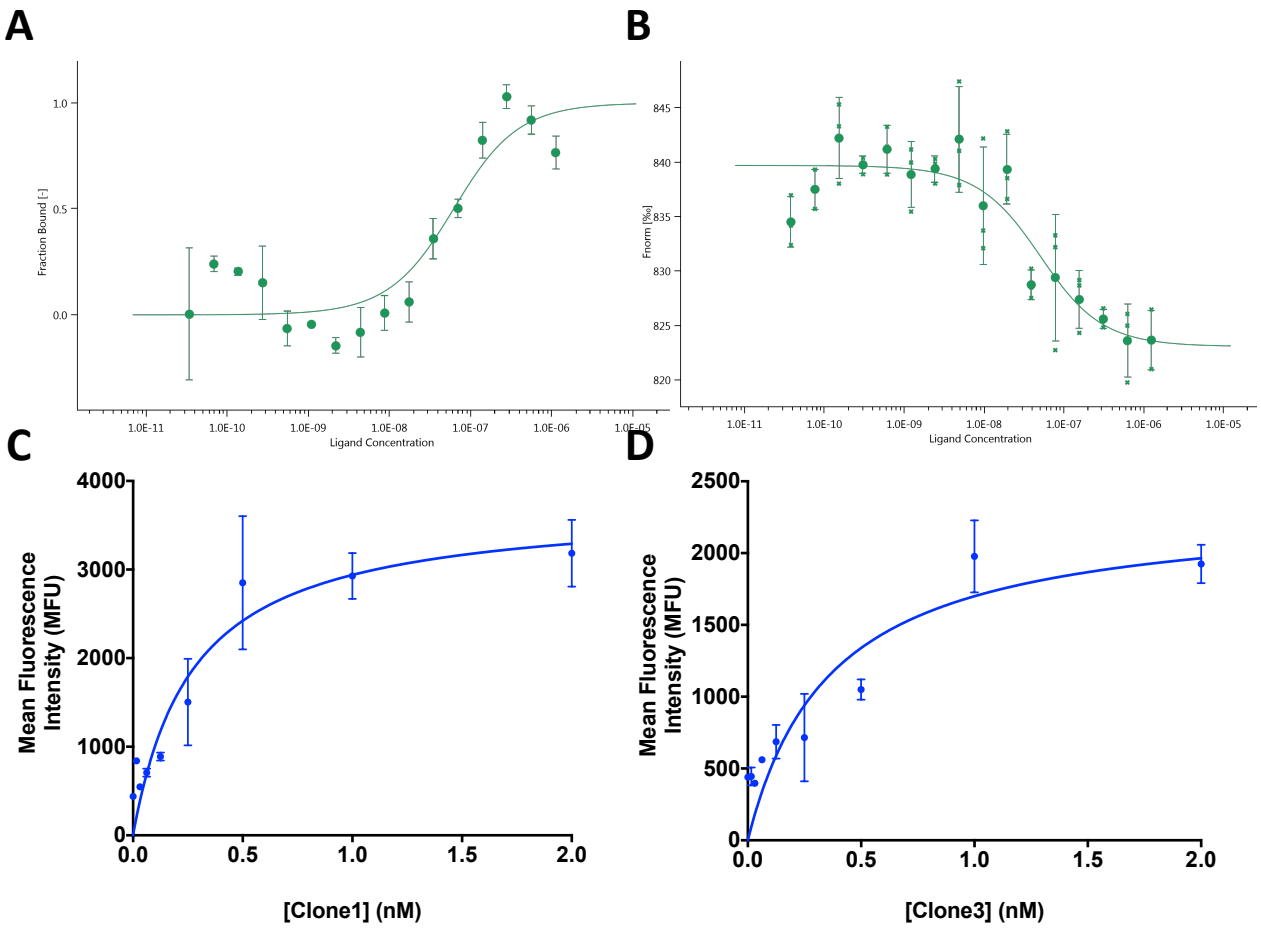

Figure 4.5 Measuring aptamer affinity to human albumin. Two methods were used to measure the affinity of the aptamers to albumin; MST and a plate-based assay. (A) Clone 1 is reported to have an affinity of 46±12 nM to Cy5-labeled albumin, using MST. (B) Clone 3 is reported to have an affinity of 480±120 nM to Cy5-labeled albumin, using MST. (C) Clone 1 is reported to have an affinity of 272±84 nM to unlabeled mouse and human albumin, using a plate-based affinity assay. (D) Clone 3 is reported to have an affinity of 369±142 nM to unlabeled mouse and human albumin, using a plate-based affinity assay.

4.4.3 in vitro Characterization of Top Aptamers

Aptamer-siRNA chimeras can be designed with either the antisense strand or sense strand appended to the aptamer [24]. An *in vitro* knockdown experiment with luciferase-expressing MDA-MB-231 cells was used to compare the knockdown efficiency of the chimeras with either the antisense strand or sense strand appended. No significant difference is reported between either formulation of the chimera (Figure A.4.5). All proceeding experiments used chimeras with the antisense appended to the aptamer and annealed to the sense strand. Aptamer-siRNA chimeras are able to retain their silencing potency *in vitro* with about 50% knockdown efficiency compared to the scrambled controls (Figure 4.6). Additionally, the serum stability of the 2'-fluorine-modified chimeras was measured over 24 hours. Modified-base chimeras are able to resist degradation over the 24 hour incubation, while unmodified-base RNA chimeras are degraded rapidly in serum (Figure 4.7).

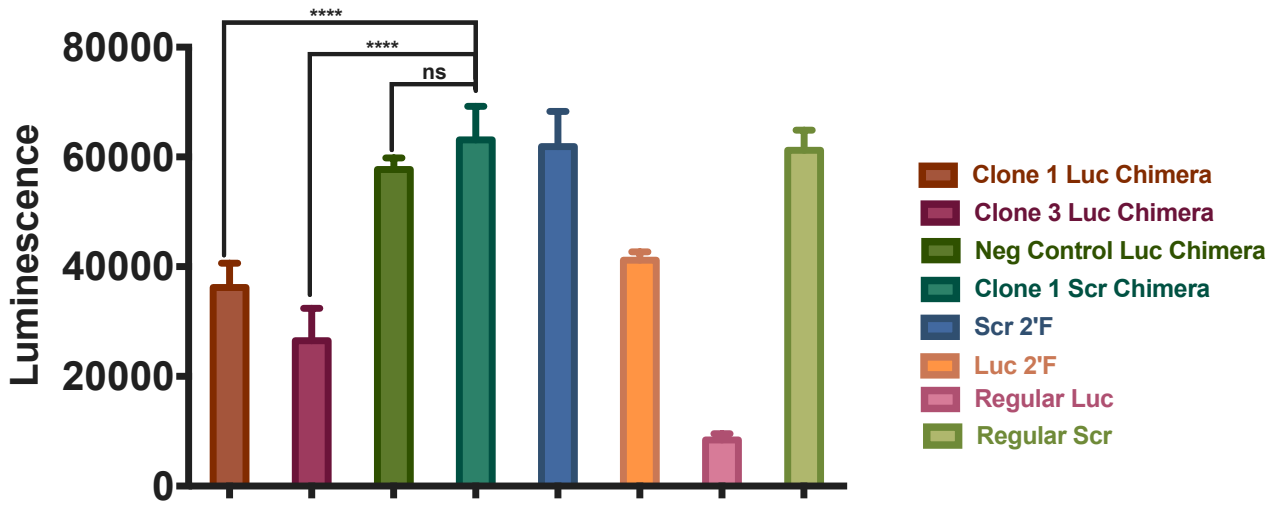

Figure 4.6 *in vitro* knockdown of luciferase-expressing MDA-MB-231 cells with aptamer chimeras. Aptamer Chimeras maintain similar luciferase-knockdown potency as siRNA alone, compared to scramble chimera and scramble siRNA. ****, P <0.0001. Data are presented as mean±SD from biological triplicates.

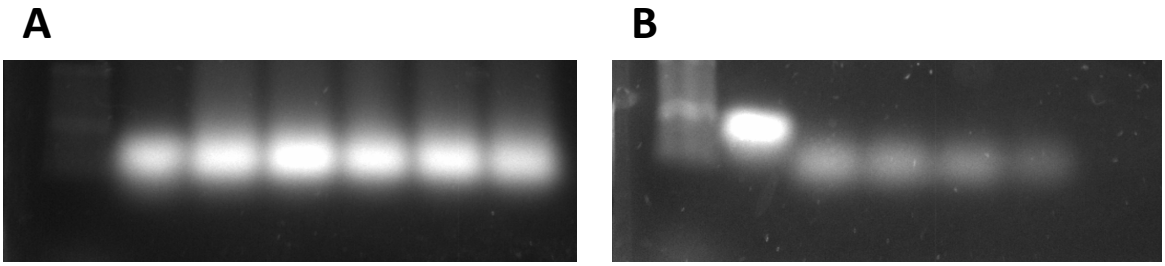

Figure 4.7 Aptamer serum stability. Degradation of aptamers were measured in 60% serum for up to 24 hours. Lanes: (1) Ladder, (2) 0 hours, (3) 30 minutes, (4) 2 hours, (5), 4 hours, (6) 8 hours, (7) 24 hours. Clone 1 aptamer with modified-base RNA (A) showed drastically improved serum stability over an unmodified base RNA aptamer (B), on a 3% agarose gel.

4.4.4 in vitro knockdown of target gene using aptamer chimeras

Aptamer chimeras were tested for their ability to deliver siRNA *in vitro* without the use of transfection reagents. Aptamer chimeras were pre-complexed with human albumin and incubated with luciferase-expressing MDA-MB-231 cells in normal culture media. A decrease in luciferase expression was used to measure the percent knockdown. Clone 1 and Clone 3 chimeras are reported to have a 48% knockdown of luciferase-expression, compared to a scramble siRNA (Figure 4.8). Clone 1 and Clone 3 show slightly improved knockdown efficiency to a scramble aptamer (40% knockdown) and greatly improved knockdown over siRNA alone (34% knockdown), likely due to the ability to bind to albumin and enter cells. These results indicate that Clone 1 and Clone 3 aptamer chimeras could be useful tools for performing *in vitro* knockdown assays without the use of transfection reagents.

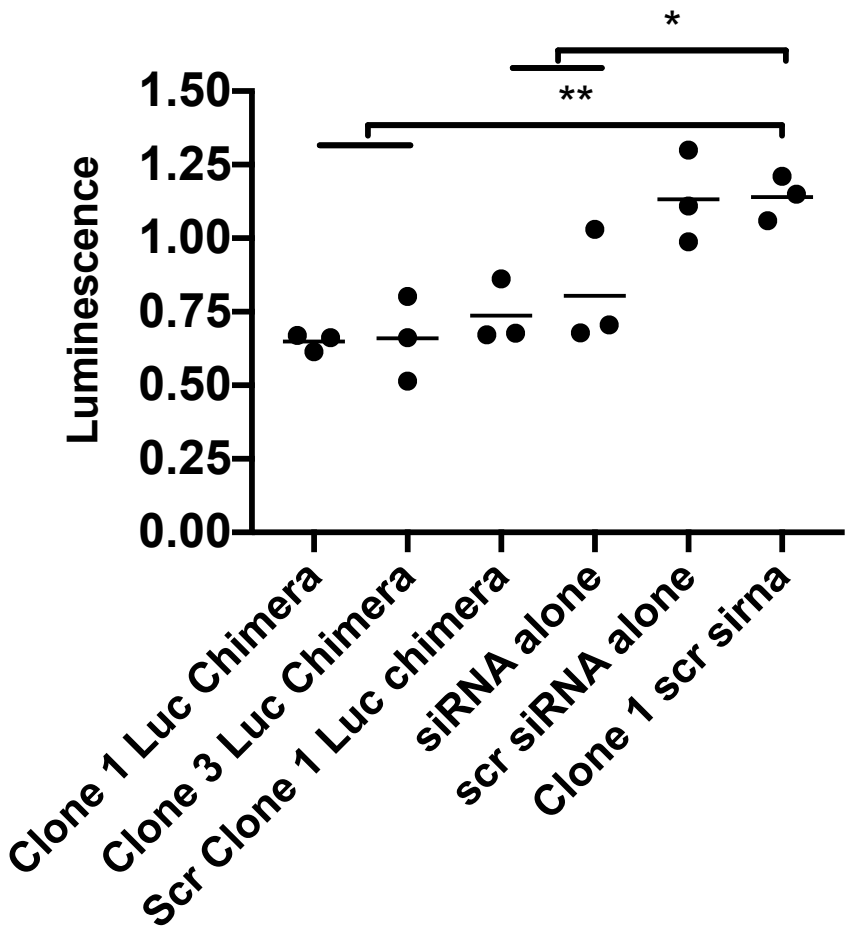

Figure 4.8 *in vitro* knockdown using carrier-free albumin aptamer chimeras. Luminescence knockdown was measured in luciferase-expressing MDA-MB-231 cells following incubation with 100 nM chimeras or siRNAs. Clone 1 and Clone 3 showed improved knockdown efficiency compared to scramble aptamer and siRNA alone. *, $p<0.05$, ** $p<0.01$. Luminescence values were normalized to cell count, data are presented as mean±SD from biological triplicates.

4.4.5 in vivo Characterization of Top Aptamers

To ensure correct annealing of the sense strand to the antisense strand, chimeras with Cy5-labeled sense strand were compared to unannealed sense strand on a 3% agarose gel, following gel electrophoresis (Figure A.4.2). Intravital microscopy was used to determine the half-life of the chimeras *in vivo* by observing Cy5 fluorescence decay in a mouse ear artery over time (Figure 4.9). Clone 1 is reported to have a 1.6-fold improvement (14.2 minutes) and Clone 3 is reported to

have an 2.6-fold improvement (23.2 minutes) in half-life circulation, compared to the scramble aptamer (9.0 minutes) used as a negative control. Interestingly, in one replicate IVM experiment, the Clone 1 chimera was not properly heat-prepared before systemic injection, meaning that the aptamer was not in its proper confirmation for binding (Figure 4.10 A), resulting in a half-life of 7.6 minutes. However, after ensuring proper heat preparation in the next replicate, meaning that the aptamer was in its proper confirmation for binding, the Clone 1 chimera displayed a half-life of 26.9 minutes, a 3-fold improvement over the scramble control aptamer (Figure 4.10 B).

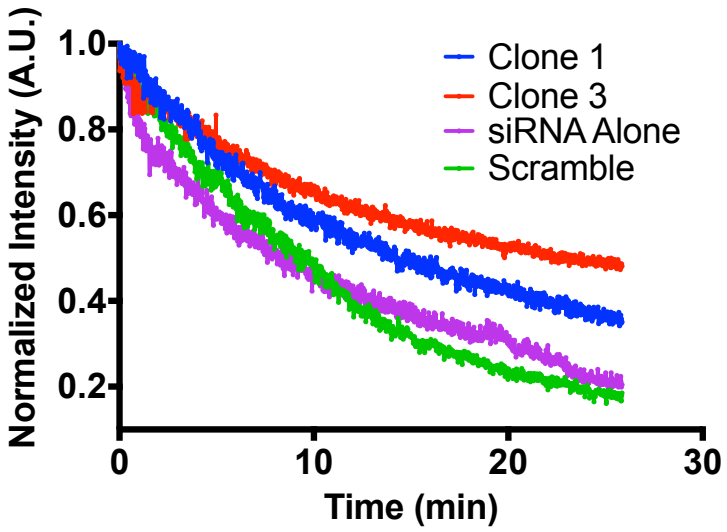

Figure 4.9 Measuring half-life of albumin chimeras. Intravital microscopy was used to determine the half-lives of Clone 1, Clone 3, and Scramble chimeras, compared to siRNA alone. The half-lives are reported as 14.2 min for Clone 1, 23.2 min for Clone 3, 9.0 min for scramble control aptamer, and 8.7 min for siRNA, n=1 (representative data).

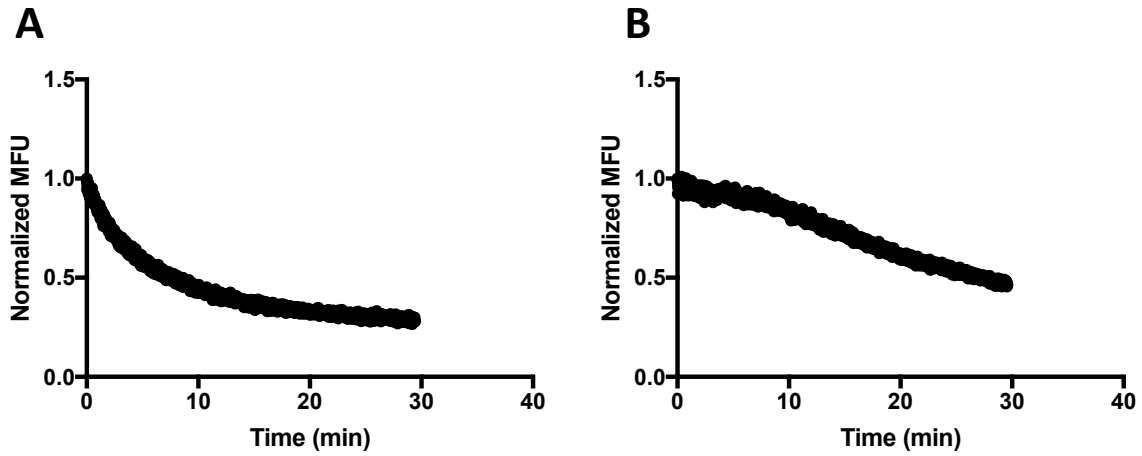

Figure 4.10 IVM before and after proper folding. Chimera binding to endogenous albumin is dependent on proper heat preparation and structural confirmation. Clone 1 without proper folding resulted in a reported half-life of 7.6 min (A), while Clone1 with proper aptamer folding resulted in a reported half-life of 26.9 min (B).

4.4.6 Truncating Aptamers

Future work is needed to confirm *in vivo* half-life results due to the low number of biological replicates. A major limitation of this system is the use of transcription reagents to generate large quantities of RNA antisense chimera strands. Low yields from each RNA transcription reaction hinder the ability to perform large-scale *in vivo* experiments. Synthesizing the full chimera antisense strand would be superior to transcription, as large-scale, pure product could be generated for use in *in vivo* experiments. However, the size of the chimera antisense strand, which includes the aptamer, spacer, and siRNA antisense strand (69-nt total), limits the efficiency of synthesis on a solid-state oligonucleotide synthesizer. Truncating the 40-nt aptamer region of the chimera antisense strand would improve the efficiency of oligo synthesis in an effort to generate large-scale batches of the chimera for *in vivo* studies.

The predicted structures of Clone 1 and Clone 3 aptamers were analyzed for their stem loops, which could be contributing to the binding affinity to albumin. Five truncated versions of

Clone 1 and four truncated versions of Clone 3 were designed and tested for their affinity to albumin (Table A.4.3) (Figure A.4.6). The truncated forms of each aptamer, along with the full length Clone 1 and Clone 3 chimeras, were screened for their binding to albumin-conjugated 96 well plates using a Cy5-labeled sense strand. None of the versions of the truncated aptamers retained their binding affinity to albumin, with no improvement in mean fluorescent intensity over the negative control aptamer (Figure 4.11). From these results, it appears that the full 40-nt length of each aptamer is required for proper aptamer confirmation and binding to albumin.

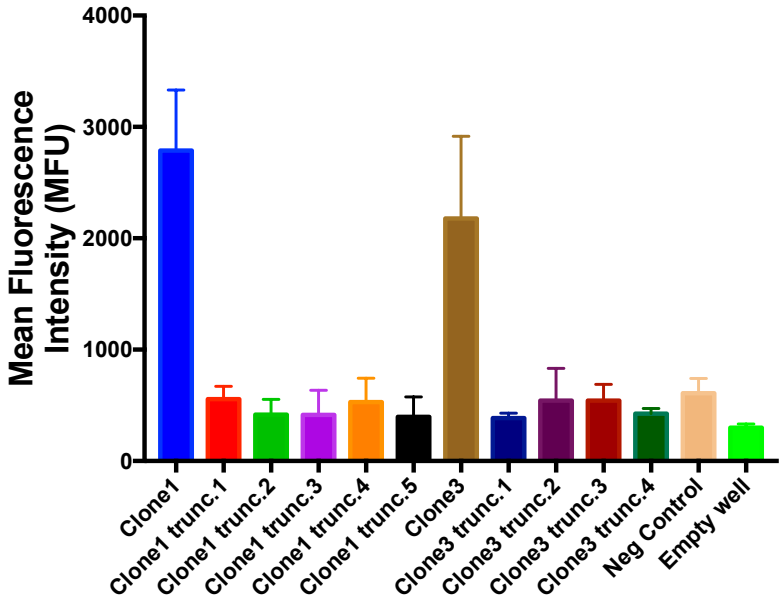

Figure 4.3 Truncating Clone1 and Clone 3 aptamers. Five truncated forms of Clone 1 and four truncated forms of Clone 3 were designed and screened in human albumin-conjugated plates to measure their relative binding, compared to full-length aptamers. None of the truncated forms of the aptamers retained their binding affinity to human albumin. Data are presented as mean±SD from biological triplicates.

4.5 Conclusions and Future Work

An RNA aptamer selection was performed using the dynamic flow system previously described. We report the isolation of the first modified-base RNA aptamers for serum albumin. Two aptamers, entitled Clone 1 and Clone 3, are reported to have nanomolar affinity to human and mouse albumin. Fusing these albumin-binding aptamers with therapeutic siRNA was shown to retain knockdown efficacy of a target gene and improve serum stability. Impressively, these chimeras improved the pharmacokinetic properties and circulation half-life of siRNA *in vivo*. The small size of these chimeras and improved bioavailability suggest potential for enhanced knockdown of *in vivo* genes. The modular design of these aptamer-siRNA chimeras allows for broad applications of gene-targeted therapeutics. Further experiments will focus on repeating *in vivo* half-life experiments with more biological replicates to confirm the results obtained and investigate *in vivo* knockdown efficacy. Additionally, further *in vitro* studies will be performed to investigate the pathway of uptake of these chimeras across multiple cell lines. Furthermore, specificity studies will be performed to investigate the ability of these aptamer chimeras to recognize albumin specifically, against other serum proteins.

4.6 Appendix

Table A.4.1 Primers used for aptamer chimera and siRNA PCR.

Primer Name	Primer Sequence
T7 FP	GTATAATACGACTCACTATAGGG
Luc Sense RP	GAGGAGTTCATTATCAGTGCAATTG
Luc Antisense RP	AACAATTGCACTGATAATGAACTCTC
Scr Sense RP	ATACGCGTATTATACGCGATTAACG
Scr Antisense RP	GTCGTTAATCGCGTATAATACGCGTAT

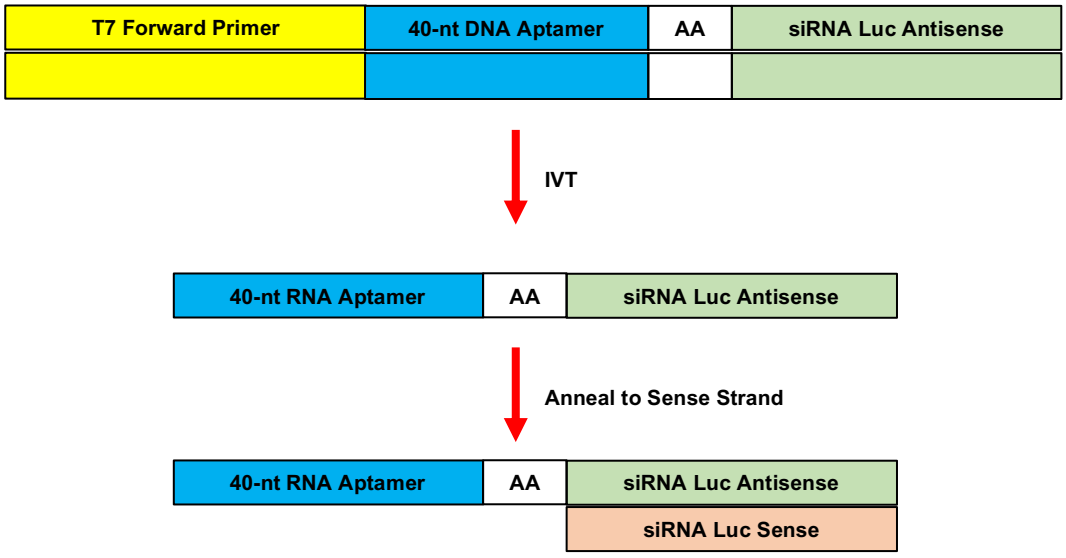

Figure A.4.1 Creating aptamer-siRNA chimeras. dsDNA with the T7 promoter region is *in vitro* transcribed into ssRNA. This ssRNA contains the aptamer and antisense strand of the siRNA. The chimeras can then be formed by annealing the sense strand to the full antisense strand.

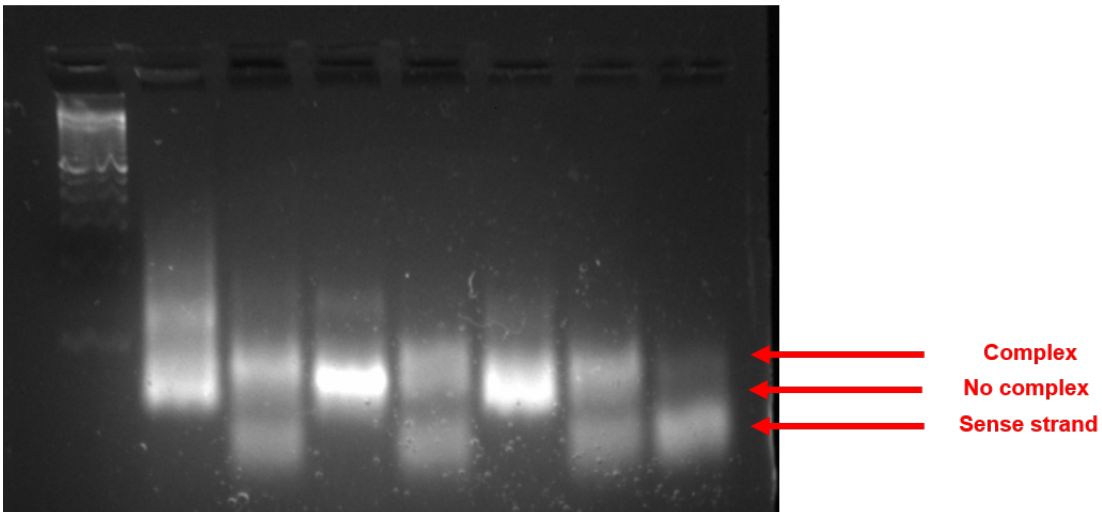

Figure A.4.2 Confirming annealing of antisense strand to sense strand. Clone 1, Clone 3, and scramble aptamer were annealed to sense strand and run on a 3% agarose gel to show electrophoretic shift between annealed and not annealed complexes. Lanes: (1) dsDNA ladder, (2) Clone 1 antisense alone, (3) annealed Clone 1 to sense strand, (4) Clone 3 antisense alone, (5) annealed Clone 3 to sense strand, (6) scramble aptamer antisense alone, (7) annealed scramble aptamer to sense strand, (8) sense strand alone.

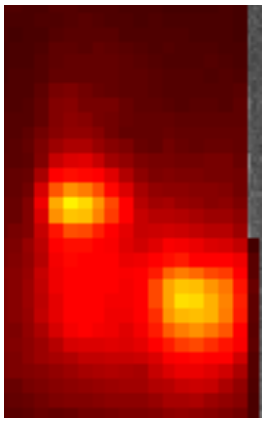

Figure A.4.3 Confirming annealing of aptamer chimera to Cy5-labeled sense strand. Clone 1 annealed to the Cy5-labeled sense strand and Cy5-labeled sense strand alone were run on a 3% agarose gel to confirm electrophoretic shift. IVIS was used to image the Cy5-labeled chimera and sense strand alone.

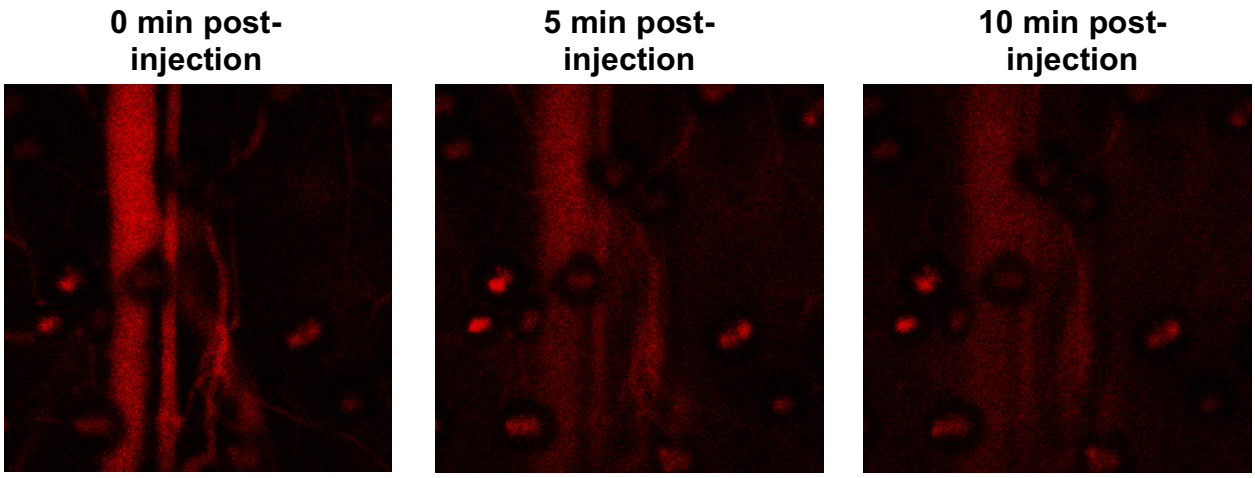

Figure A.4.4 Measuring half-life with intravital microscopy. Chimera half-life was measured with intravital microscopy. Cy5-labeled sense strands were annealed to antisense strands, and fluorescence decay was measured over 30 minutes. (Representative images)

Table A.4.2 Full list of aptamer chimeras and siRNAs used in *in vitro* and *in vivo* studies.

Name	Sequence	# of nt
Luc Sense	CAAUUGCACUGAUAAUGAACUCCTC	25
Luc Antisense	GAGGAGUUCAUUAUCAGUGCAAUUGUU	27
Scramble Sense	CGUUAAUCGCGUAUAAUACGCGUAU	25
Scramble Antisense	AUACGCGUAUUAUACGCGAUUAACGAC	27
Clone 1 Luc Antisense	GCGCCGCAACAGGUGUGACUGCCCUAGCCUCCGCUGUACCAAGAGGAGUUC AUUAUCAGUGCAAUUGUU	69
Clone 3 Luc Antisense	UGGUAACCCUUUCCGGCUACGGCUACUAAAGACUUUUAUGAAGAGGAGUUC AUUAUCAGUGCAAUUGUU	69
Negative Control Luc Antisense	GAUACUGAGCAUCGUACAUGAUCCCGCAACGGGCAGUAUUAAGAGGAGUUC AUUAUCAGUGCAAUUGU	69
Clone 1 Luc Scr Antisense	GCGCCGCAACAGGUGUGACUGCCCUAGCCUCCGCUGUACCAAAUACGCGUAU UAUACGCGAUUAACGAC	69
Clone 1 Luc Sense	GCGCCGCAACAGGUGUGACUGCCCUAGCCUCCGCUGUACCAACAAUUGCACU GAUAAUGAACUCCUC	67
Clone 3 Luc Sense	UGGUAACCCUUUCCGGCUACGGCUACUAAAGACUUUUAUGAACAAUUGCAC UGAUAAUGAACUCCUC	67
Negative Control Luc Sense	GAUACUGAGCAUCGUACAUGAUCCCGCAACGGGCAGUAUUAACAAUUGCAC UGAUAAUGAACUCUCUC	67
Clone 1 Scr Luc Sense	GCGCCGCAACAGGUGUGACUGCCCUAGCCUCCGCUGUACCAACGUUAAUCGC GUAUAAUACGCGUAU	67
Clone 3 Scr Luc Sense	UGGUAACCCUUUCCGGCUACGGCUACUAAAGACUUUUAUGAACGUUAAUCG CGUAUAAUACGCGUAU	67
Negative Control Scr Luc Sense	GAUACUGAGCAUCGUACAUGAUCCCGCAACGGGCAGUAUUAACGUUAAUCG CGUAUAAUACGCGUAU	67

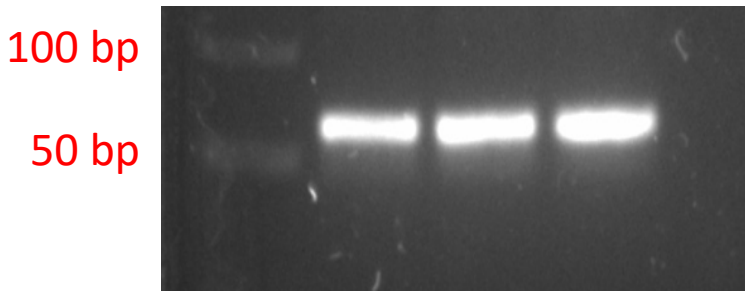

Figure A.4.5 Checking band size of albumin aptamers. Lanes: (1) dsDNA ladder, (2) starting RNA library, (3) Clone 1, (4) Clone 3.

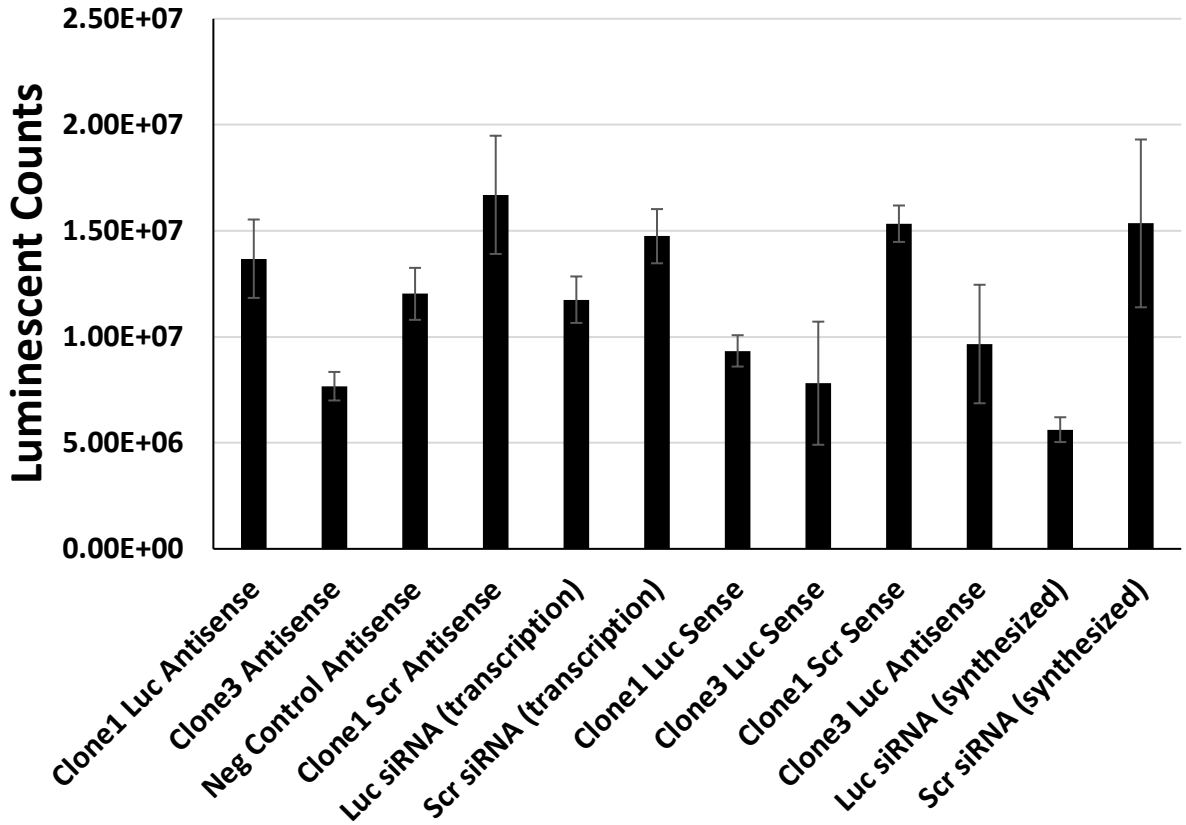

Figure A.4.6 Determining optimal confirmation of aptamer-siRNA chimeras. The antisense and sense strands were interchanged on the chimera to determine *in vitro* knockdown efficiency in luciferase-expressing MDA-MB-231 cells. Data are presented as mean±SD from biological triplicates.

Table A.4.3 List of truncated Clone 1 and Clone 3 albumin aptamers.

Aptamer Name	Aptamer Sequence	Number of nt
Full Clone 1	GCGCCGCAACAGGUGUGACUGCCCUAGCCUCCGCUGUACC	40
Truncate 1.1	GCGCCGCAACAGGUGUGACUGCCCUAGCCUCCGCU	35
Truncate 1.2	GCGCCGCAACAGGUGUGACUGC	22
Truncate 1.3	CGCAACAGGUGUG	13
Truncate 1.4	AGCCUCCGCU	10
Truncate 1.5	GCGCCGACUGCCCUAGCCUCCGCU	24
Full Clone 3	UGGUAACCCUUUCCGGCUACGGCUACUAAAGACUUUUAUG	40
Truncate 3.1	UGGUAACCCUUUCCGGCUACGGCUACUAAAG	31
Truncate 3.2	CUUUCCGGCUACGGCUACUAAAGACUUUUAUG	32
Truncate 3.3	CUUUCCGGCUACGGCUACUAAAG	23
Truncate 3.4	GGCUACGGCU	10

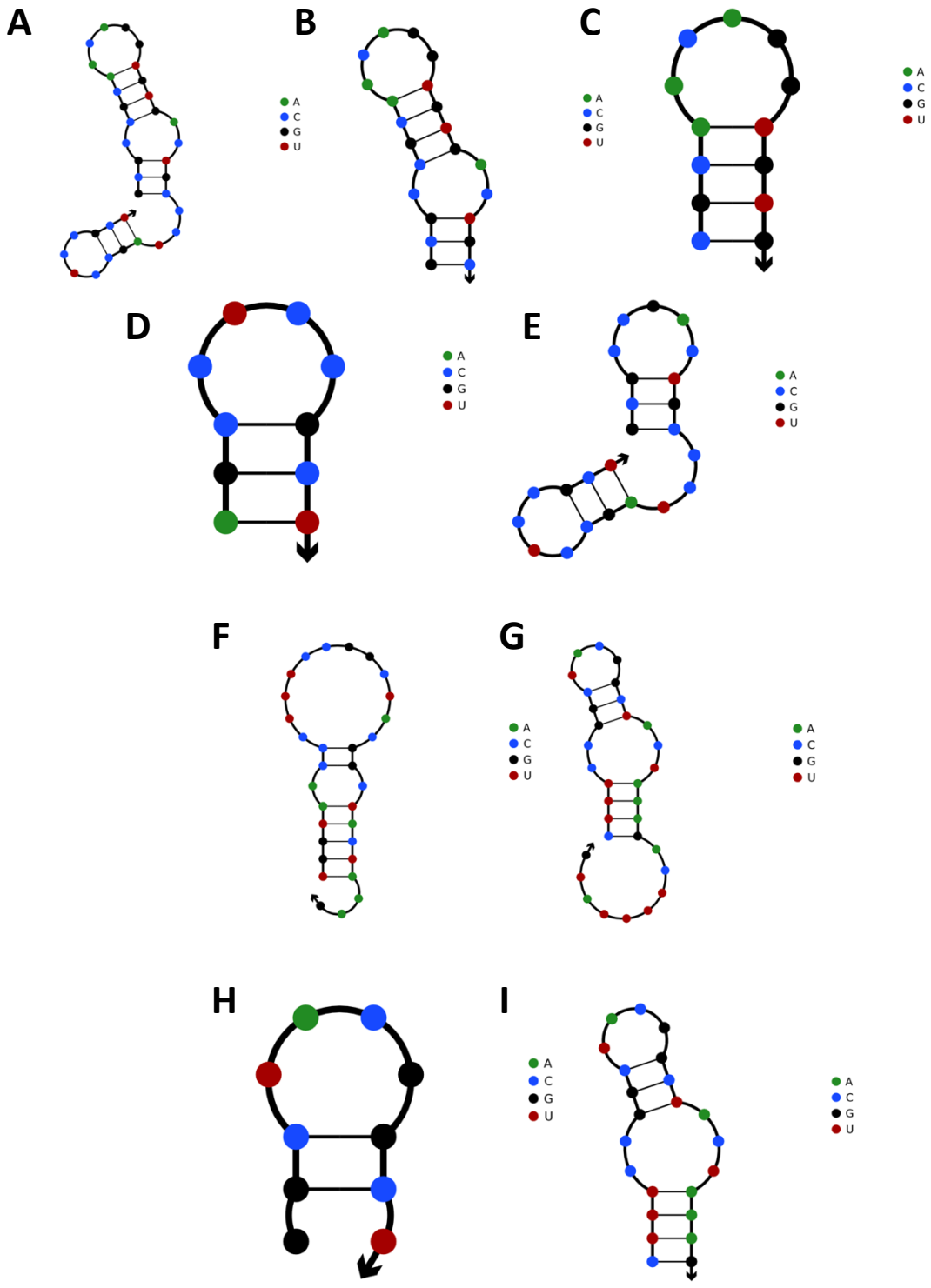

Figure A.4.7 Predicted structures of Clone 1 and Clone 3 truncated aptamers. Truncated versions of Clone 1 aptamer (A-E) and truncated version of Clone 3 aptamer (F-I)

Chapter 5

CRISPR-MEDIATED ISOGENIC CELL-SELEX APPROACH FOR GENERATING HIGHLY SPECIFIC APTAMERS AGAINST NATIVE MEMBRANE PROTEINS

Adopted from: Rosch JC, Neal EH, Balikov DA, Rahim M, & Lippmann ES. CRISPR-mediated isogenic cell-SELEX approach for generating highly specific aptamers against native membrane proteins. Cellular and Molecular Bioengineering, In Review, *with permission from Springer Publishing.*

5.1 Summary

The generation of affinity reagents that bind native membrane proteins with high specificity remains challenging. Most *in vitro* selection paradigms utilize different cell types for positive and negative rounds of selection (where the positive selection is against a cell that expresses the desired membrane protein and the negative selection is against a cell that lacks the protein). However, this strategy can yield affinity reagents that bind unintended membrane proteins on the target cells. To address this issue, we developed a systematic evolution of ligands by exponential enrichment (SELEX) scheme that utilizes isogenic pairs of cells generated via CRISPR techniques. Using a Caco-2 epithelial cell line with constitutive Cas9 expression, we knocked out the *SLC2A1* gene (encoding the GLUT1 glucose transporter) via lipofection with synthetic gRNAs. Cell-SELEX rounds were carried out against wild-type and GLUT1-null cells using a single-strand DNA library. Next-generation sequencing (NGS) was used to quantify enrichment of prospective binders to the wild-type cells. 10 rounds of cell-SELEX were conducted via simultaneous exposure of ssDNA pools to wild-type and GLUT1-null Caco-2 cells under continuous perfusion. The top binders identified from NGS were validated by flow cytometry and immunostaining for their specificity to the GLUT1 receptor. Our data indicate that highly specific aptamers can be isolated with a SELEX strategy that utilizes isogenic cell lines. This approach

may be broadly useful for generating affinity reagents that selectively bind to membrane proteins in their native conformations on the cell surface.

5.2 Introduction

To support basic research applications and clinical translation, there is an ever-increasing demand for the development of high-specificity affinity reagents for biological targets [1],[2]. While *in vitro* selection strategies have been used to develop many types of affinity reagents (including nucleic acid aptamers, peptides, and proteins) for a wide range of biological targets, the ability to generate highly specific binders to native membrane proteins remains challenging. Selection strategies for membrane proteins are often facilitated by the use of recombinant extracellular domains, but this approach has drawbacks because the recombinant domain may not properly fold due to the lack of a transmembrane anchor or include appropriate post-translational modifications; both of these issues can affect the ability of the binding reagent to selectively recognize the membrane protein when it is properly expressed in a cell lipid bilayer. Attempts to purify cell-surface targets into artificial support systems like nanodiscs can similarly lead to a loss of endogenous conformations and appropriate protein-protein interactions, while also imposing yield limitations. For these reasons, many selection strategies utilize whole cells to preserve membrane protein integrity. For example, nucleic acid libraries can be used to select aptamers against whole cells via standard SELEX approaches [121], whereas display techniques can be used to select peptide/protein-based affinity reagents against whole cells [122], [123]. These strategies have yielded binding reagents against various membrane proteins, including but not limited to, the glucagon receptor [124], EGFR [125], TGFBRIII [126], and PDGFRβ [127].

However, whole cell selections still have drawbacks. For example, most *in vitro* selections utilize different cell types for positive and negative rounds of selection. In this manner, the positive selection is performed on a cell type that expresses the desired membrane target and the negative selection is performed against a cell type that lacks the protein [128], [129]. This strategy can lead to the isolation of affinity reagents that bind unintended membrane proteins on the surface of cells. Attempts to use isogenic cells in the positive and negative selection steps have involved overexpressing the target of interest in a cell type and counterselecting with the parental cell line [130], [131], but this method can still lack sufficient counterselection stringency to yield aptamers with high specificity. Others have attempted sequential selections on recombinant, truncated extracellular motifs followed by whole cell biopanning [132], [133]. This approach has been shown to help improve specificity during the selection process but also reintroduces the cumbersome use of purified protein. Thus, there is substantial room for improvement in whole cell selection workflows for generating affinity reagents.

In this current study, we focus on the development of a novel SELEX approach that uses isogenic cell pairs to generate aptamers against membrane proteins. Aptamers are oligonucleotide-based affinity reagents that have been selected to bind to a variety of targets, including small molecules, proteins, and cell surface receptors. Properly selected aptamers are able to bind to their target with high affinity and specificity, with the added benefits of inexpensive and reproducible chemical synthesis, facile chemical modification, and low immunogenicity [134]. The selection of aptamers by SELEX is usually performed with isolated targets, with 71% of published targets for purified recombinant protein and 19% for synthesized small molecules [71]. In contrast, less than 10% of published aptamer papers have sought to identify aptamers for specific targets on the cell surface, likely due to the difficulties mentioned above. To overcome the previously mentioned

issues with whole cell-SELEX, we developed a strategy that utilizes isogenic pairs of cells generated with clustered regularly interspaced short palindromic repeats (CRISPR) techniques (Figure 5.1). In this approach, cell types are used in the positive and negative selection rounds that are prospectively identical except for the one cell surface protein of interest that has been knocked out, which we hypothesized would drive the specificity of the selection. The generation of knockouts with modern CRISPR technologies helps ensure a high specificity of indel formation in the desired gene of interest. For this proof-of-concept endeavor, we chose to generate aptamers against glucose transporter 1 (GLUT1) by knocking out the *SLC2A1* gene to engineer a null cell as an isogenic pair. GLUT1 is implicated in several diseases including Glucose Transporter Type 1 Deficiency Syndrome [135], Alzheimer's Disease [136], and brain microvasculature defects [137]. Several well-characterized antibodies exist for GLUT1, which is useful for direct comparisons to selected aptamers; however, very few of these antibodies target the extracellular domain of GLUT1, indicating that a high-fidelity aptamer would have utility for research applications. Additionally, GLUT1 is a member of 14 GLUT family members that are structurally similar, and GLUT1 is particularly homologous to GLUT2-4 [138]; likewise, GLUT1 has minimal extracellular exposure, with five short extracellular loops (<15 amino acids each) and one longer loop of 33 amino acids [139]. Thus, GLUT1 is an ideal test case for this study because: (1) it shares substantial structural homology with other transporters in the same family, permitting assessments of aptamer specificity after selection, and (2) its structure is relatively difficult to target extracellularly with an affinity reagent compared to other ligands such as single-pass transmembrane proteins that have a longer extracellular domain. This new selection strategy, deemed CRISPR-mediated isogenic cell-SELEX, successfully generated an aptamer that specifically binds to the GLUT1 transporter on multiple cell types and in human brain tissue. We

expect that this strategy will help researchers overcome many difficulties involved with cell-SELEX and identify improved affinity reagents with high specificity for cell membrane proteins.

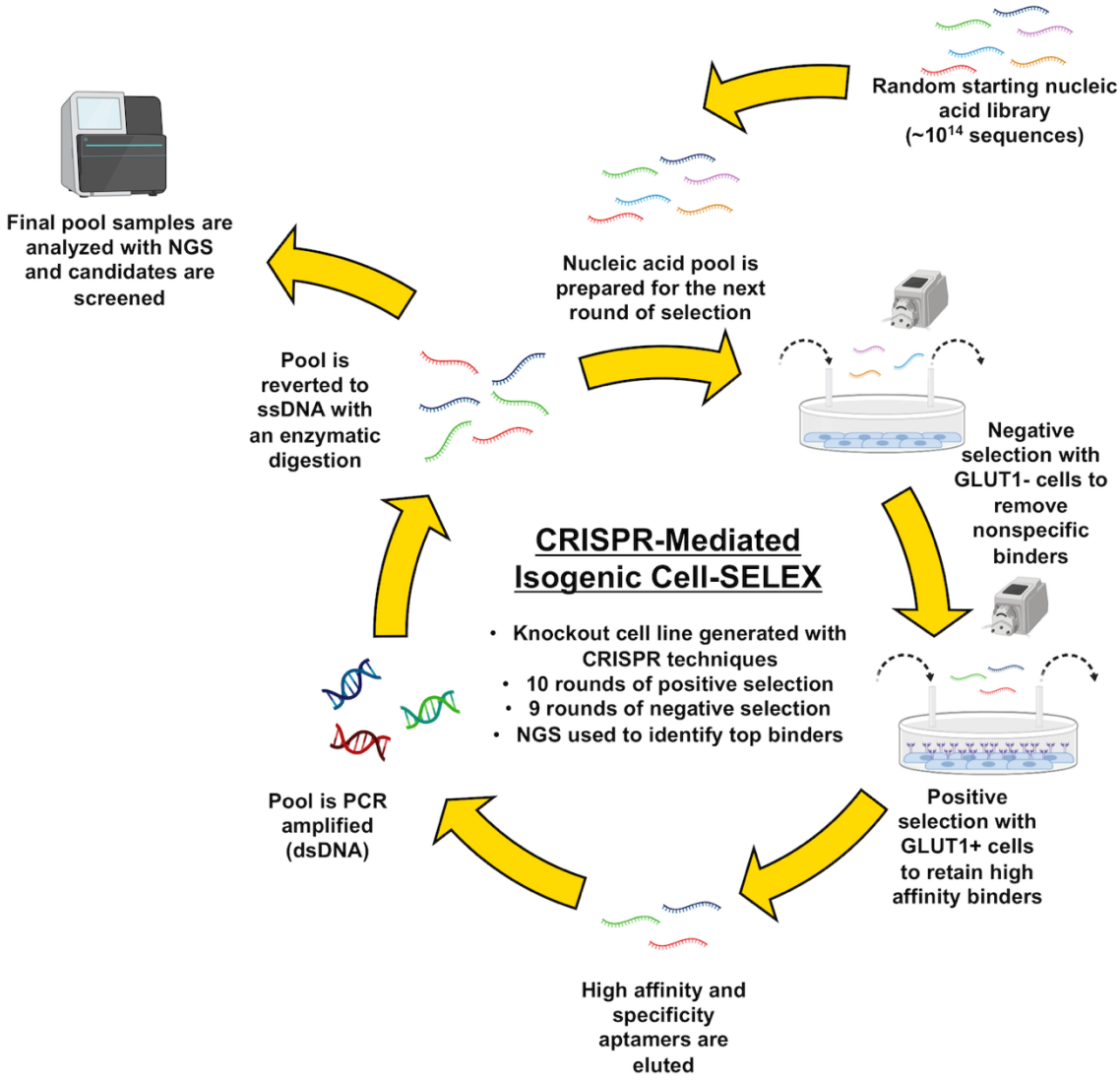

Figure 5.1 Overview of CRISPR-mediated isogenic cell-SELEX. A random ssDNA library is perfused over null cells, which do not express the protein of interest, as the negative selection. The library is simultaneously perfused over wild-type cells, which express the protein of interest, as the positive selection. Aptamers are eluted from the wild-type cells, PCR amplified, and regenerated to ssDNA by enzymatic digestion to be introduced into the next round of selection. For this study, ten rounds of selection were performed and analyzed with next generation sequencing.

5.3 Materials and Methods

5.3.1 Materials

All benchtop laboratory materials were purchased from Fisher Scientific and all chemicals were purchased from Sigma Aldrich, unless otherwise stated.

5.3.2 Cell lines and cell culture

Human Caco-2, MDA-MB-231, and HEK-293 cells were cultured in high glucose DMEM (Corning; 10-0130CV), with sodium pyruvate and L-glutamine, 10% heat inactivated fetal bovine serum (FBS) (Gibco, 26140079), 1X MEM non-essential amino acid solution (Sigma, M7145), and 1% penicillin-streptomycin (Gibco, P0781). FBS was heat-inactivated by heating at 56°C for 30 min followed by cooling on ice. Caco-2 cells were cultured on 0.1% gelatin (Sigma, G1890). Human brain microvascular endothelial cells were differentiated from induced pluripotent stem cells and purified according to previous protocols routinely used in our lab [140], [141]. All cells were cultured at 37°C in a 5% CO_2 humid atmosphere.

5.3.3 Strategy for Developing GLUT1-null Caco-2 Cells

To incorporate Cas9 expression into the Caco-2 cell line, cells were washed twice with DPBS, dissociated with TrypLE Select (Gibco, 1253029), and collected as a single-cell suspension. Based on cell density, this suspension was transduced with a multiplicity of infection (MOI) of 0.3 with Edit-R lentiviral mKate2-tagged, constitutively expressed Cas9 nuclease under the hEF1α promoter (Dharmacon, CAS11229) in transduction medium containing 5 μg/mL polybrene (EMD Millipore, TR-1003-G). Complete growth medium was added to the transduced

cells at a 3:1 dilution after 5 hours, and medium was changed every 48 hours prior to fluorescence activated cell sorting (FACS). Once ready for sorting, cells were dissociated and resuspended in phenol-red free DMEM medium (Gibco, 21063-029) supplemented with 10 μM Y27632 dihydrochloride (Tocris, 1254) and antibiotic-antimycotic (Gibco, 15240062). Cells were clonally sorted onto 96-well plates using a 5-laser FACS Aria III (BD Biosciences) with a 100 μm nozzle. Sorted cells were collected in sterile-filtered conditioned medium supplemented with 10 μM Y27632, 10 mM HEPES (Gibco, 15630080), and 1X penicillin-streptomycin. Clones were supplemented with an additional 100 μL of complete growth medium per well approximately 24 hours after sorting. Medium was changed with complete growth media every 48 hours after. Cas9 expression of the clones was validated with western blot and immunofluorescent imaging with a Cas9 antibody (Abcam, ab20444) and an occludin antibody (Thermo, 33-1500), similar to methods described below. Clone C6 was selected for further analysis and experimental use.

To generate knockouts, *SLC2A1* crRNA (CM-007509-01, CM-007509-02, CM-007509-03, CM-007509-04) and synthetic tracrRNA (U-002005-05) were ordered from Horizon Discovery and resuspended according to the company's instructions. Knockout rounds were performed by incubating precomplexed 25 nM crRNA, 25 nM tracrRNA, and Dharmafect 1 reagent (T-2001-01) with Caco-2 cells in antibiotic-free medium for 48 hours at 37°C. After 48 hours, the cells were switched to normal medium, allowed to become confluent, and then subjected to another round of gRNA delivery. After three transfections, the Caco-2 cells were re-seeded at a low density on a 150 mm dish (Fisher, FB0875714) and clonally expanded. 20 cell colonies were picked, expanded, and prospectively analyzed for GLUT1 expression by western blot. A single clone was then used for full validation of GLUT1 knockout.

5.3.4 Validating GLUT1 Knockout in Caco-2 Cell

GLUT1 knockout in the Caco-2 clonal cell line was determined with three analysis methods (western blot, immunofluorescent imaging, and Sanger sequencing followed by indel analysis).

For western blotting, total protein was collected from cell lysate in RIPA buffer (Sigma, R0278) containing 1% phosphatase inhibitor cocktail 3 (Sigma, P0044) and 1% protease inhibitor cocktail (Sigma, P8340), followed by incubation on ice for 30 minutes with occasional pipetting. The RIPA mixture was centrifuged at 12,000xg at 4°C for 15 minutes to isolate protein. Protein concentration was measured with a standard BCA assay (Thermo Fisher, 23225). 10 μg of protein for each condition was run on a 4-20% polyacrylamide gel (Bio-Rad, 5671094), transferred to nitrocellulose membranes (Thermo Fisher, IB23001) using the iBlot2 Gel Transfer Device (Thermo Fisher), blocked for 1 hour with Intercept TBS Blocking Buffer (Li-Cor, 927-600001), and incubated with primary antibodies overnight at 4°C (GLUT1: Abcam, 15309, 1:1000 dilution; GAPDH: CST, D16H11, 1:1000 dilution). Membranes were washed with TBS-T (TBS Buffer with 0.05% Tween-20), incubated with IRDye 800CW goat anti-rabbit secondary antibody (Li-Cor, 926-32211) for 1 hour, washed 3 times with TBS-T, and imaged on an Odyssey Fc Imager (Li-Cor).

For immunofluorescent imaging of cells, cells were washed twice with PBS and fixed in 4% paraformaldehyde (Thermo Fisher, J19942-K2) for 10 minutes. Fixed cells were washed three times, blocked with PBS containing 5% donkey serum and 0.3% Triton-X-100 for 1 hour, and incubated with primary GLUT1 antibody (Abcam, 15309, 0.5 μg/mL) overnight at 4°C. Cells were washed 5 times with PBS, incubated with Alexa Fluor 488 donkey anti-rabbit secondary antibody (Thermo Fisher, A-21206) in the dark for 1 hour, incubated with DAPI nuclear stain

(Thermo Fisher, D1306, 1:10000 dilution) for 10 minutes, washed 3 times, and imaged on a Leica DMi8 fluorescence microscope. Cell images were analyzed on FIJI.

For Tracking of Indels by Decomposition (TIDE) [142] analysis, genomic DNA primers flanking gRNA cute sites in the *SLC2A1* gene were designed using the NCBI Primer-BLAST website. The top primers for each cut site were ordered from Integrated DNA Technologies (IDT). Genomic DNA was extracted from wild-type and GLUT1-null Caco-2 cells with QuickExtract DNA Extraction Solution (Lucigen, SS000035-D2) and regions of interest were PCR amplified with the designed primers and Taq polymerase (NEB, M0273S). Amplified DNA was cleaned up with the Monarch DNA Gel Extraction Kit (NEB, T1020S) and samples were submitted to Genewiz for standard Sanger sequencing analysis. Sanger sequencing files for each cut site were analyzed on the TIDE online web tool to determine the indel formation percentage between the wild-type and GLUT1-null cell lines.

5.3.5 DNA Aptamer Library, Primers, and Buffers Used for SELEX

The ssDNA aptamer library was synthesized and HPLC-purified by IDT, with 40 nucleotide random bases flanked by 20 nucleotide primer ends required to perform PCR amplification (forward fixed region: TCGCACATTCCGCTTCTACC, reverse fixed region: CGTAAGTCCGTGTGTGCGAA). The starting library was designed with a A:C:G:T molar ratio of 3:3:2:2.4 to adjust for equimolar amounts of nucleotide incorporation. Primers used included: forward primer, TCGCACATTCCGCTTCTACC; 5'-biotinylated forward primer, /5bio/TCGCACATTCCGCTTCTACC; 5'-FAM-labeled forward primer, /5FAM/TCGCACATTCCGCTTCTACC; reverse primer, TTCGCACACACGGACTTACG; 5'-phosphorylated reverse primer, /5Phos/TTCGCACACACGGACTTACG. Wash buffer was

prepared with 5 mM $MgCl_2$ (Thermo Fisher, AM9530G) and 4.5 g/L glucose (RPI, G32040) in DPBS. Binding buffer was prepared with 100 mg/mL of yeast tRNA (Thermo Fisher, AM7119) and 1 mg/mL of bovine serum albumin (RPI, A30075).

5.3.6 Cell-SELEX Procedure

A recently published protocol for performing SELEX on isolated protein under dynamic flow conditions was used as a starting point for developing this CRISPR-mediated isogenic cell-SELEX protocol [143]. Four nanomoles of ssDNA aptamer library was diluted in binding buffer, heated at 95°C for 10 minutes, cooled on ice for 10 minutes, and then loaded into tubing of a peristaltic pump (Fisher Scientific, 13-310-661). For the first round of cell-SELEX, wild-type Caco-2 cells were seeded into a 0.1% gelatin coated 150 mm cell culture dish (Fisher Scientific, 12565100) and grown until just fully confluent. The initial ssDNA library was circulated over the wild-type Caco-2 cells for 1 hour at 4°C. After positive incubation, washing was conducted by pumping washing buffer over the cells for 15 minutes to remove weakly bound aptamers. After washing, bound aptamers were eluted by scraping the cells into ultrapure water and heating for 10 minutes at 95°C. The mixture was spun at 13,000xg for 5 minutes and the supernatant containing the unbound aptamers was collected.

The Round 1 eluted pool was PCR amplified for 10 cycles with GoTaq Hot Start Polymerase (Promega, M5001) (1X Colorless GoTaq Flexi Buffer, 0.2mM each dNTP, 0.2 uM forward and reverse primers, and 1.25 U Polymerase) [cycling conditions: 95°C for 2 minutes, 10 cycles of 95°C for 30 seconds, 56°C for 30 seconds, 72°C for 1 minutes]. A pilot PCR amplification was performed to determine the optimal PCR cycle conditions for scaleup by testing amplification cycles of 8, 10, 12, 14, and 16. The bands from this pilot test were checked on a 3%

agarose gel to ensure no smearing or higher molecular weight byproduct formation (data not shown). The optimized PCR was then performed with unlabeled forward primers and phosphate-labeled reverse primers. Double-stranded DNA (dsDNA) was reverted to ssDNA by incubating with 5U of λ-exonuclease (NEB, M0262S) at 37°C for 1 hour, followed by heat inactivation at 75°C for 10 minutes in a standard PCR thermocycler. The single-strand product was purified through phenol/chloroform/isomayl alcohol extraction (Thermo Fisher, P3803) and ethanol precipitated. ssDNA was resuspended in binding buffer before being used in the next round of selection.

After Round 1, a negative selection step was incorporated into the procedure. In Rounds 2-10, GLUT1-null Caco-2 cells were seeded into a 0.1% gelatin coated 35 mm cell culture treated dish (Fisher, 1256590) overnight and GLUT1-positive wild-type Caco-2 cells were seeded into a 0.1% gelatin coated 100 mm cell culture treated dish (Fisher, FB012924) overnight. The amplified Round 1 ssDNA pool was continuously recirculated over each cell type in series for 1 hour at 4°C, followed by washing with wash buffer for 15 minutes. Following the primary and negative selection step, bound ssDNA was again eluted, PCR-amplified to dsDNA and subsequently restored to ssDNA in a similar manner as described above. To increase selection pressure, the plate size of the negative cells was increased from 35 mm to 150 mm, the plate size of the wild-type cells was decreased from 150 mm to 100 mm (thus manipulating the ratio of positive to negative cells), and the time of washing increased from 15 minutes to 30 minutes by Round 6. For next-generation sequencing (NGS), dsDNA from wild-type cell samples was saved from Rounds 2, 4, 6, 8, and 10 and dsDNA from knockout-cell samples was saved from Rounds 6 and 10.

5.3.7 Pool Affinity Characterization

After six rounds of selection, a flow cytometry assay was used to qualitatively determine the affinity of the pool toward the wild-type and GLUT1-null Caco-2 cells. A Guava EasyCyte (Luminex) was used for all flow cytometry experiments. The Round 6 pool and starting library were PCR-amplified with FAM-labeled forward primer and phosphate-labeled reverse primer, followed by λ-exonuclease digestion. The Round 6 pool and the starting library were diluted to 200 nM in binding buffer, heated for 10 minutes at 95°C, cooled on ice for 10 minutes, and then mixed with $3x10^5$ wild-type or GLUT1-null Caco-2 cells. Cells were incubated for 60 minutes with rotation at 4°C, washed twice with cold washing buffer, and the mean fluorescence intensity of each sample was measured on the Guava over 10,000 gated events excluding dead cells. Flow cytometry data were analyzed and plotted with Flojo.

5.3.8 Next Generation Sequencing

The dsDNA from wild-type cell samples from Rounds 2, 4, 6, 8, and 10 and dsDNA from knockout-cell samples from Rounds 6 and 10 were sent to Vanderbilt Technologies for Advanced Genomics (VANTAGE) for NGS. 100 ng of gel-extracted dsDNA was sent for sequencing on an Illumina NovaSeq6000 PE150 Sequencer with an average of ~$3.9x10^7$ raw paired-end reads per sample. The NGS data was analyzed using AptaSUITE software [144] and only sequences with the correct 5' primer and 3' primer regions were counted toward the total accepted reads. The accepted reads were then sorted based on their overall abundance and enrichment in each sample.

5.3.9 Screening Top Aptamers From NGS

The top eight aptamers selected from NGS analysis were ordered from IDT with 5'-biotin labels. To screen these aptamers for their binding to the wild-type and GLUT1-null Caco-2 cells, the aptamer stocks were diluted to 200 nM in binding buffer, heated at 95°C for 10 minutes, cooled on ice, and mixed with $3x10^5$ cells. After 60 minutes of incubation with rotation at 4°C, the cells were washed twice with cold washing buffer. The cells were then resuspended in 1:200 dilution of streptavidin, Alexa Fluor 488 conjugate (Thermo Fisher, S11223) and incubated for 30 minutes at 4°C with rotation. The cells were washed a final two times and measured on the Guava flow cytometer for their mean fluorescence intensity over 10,000 gated events. Four aptamers from this flow cytometry screen were ordered from IDT with FAM fluorophore labels, along with an equilength FAM-labeled scrambled aptamer, and re-tested by flow cytometry. These aptamers were then further validated with live-cell imaging. $1x10^5$ wild-type and GLUT1-null Caco-2 cells were seeded into 24 well plates (Corning, 3526) and allowed to adhere overnight. The following day, cells were washed twice with wash buffer and blocked for 15 minutes with binding buffer at 4°C. Individual aptamers were diluted to 200 nM in binding buffer, heat prepped as described above, and incubated with cells at 4°C for 30 minutes. After incubation, the cells were incubated with the Cytopainter cell membrane stain (Abcam, ab219941), washed three times with washing buffer, and then imaged on a Leica DMi8 fluorescence microscope.

5.3.10 Generation of a Homogenous GLUT1 Expressing Caco-2 Cell Line

For affinity tests, a homogenous GLUT1+ Caco-2 cell line (termed high-expressing GLUT1 Caco-2) was generated by FACS with an Alexa Fluor 488 primary conjugated GLUT1 antibody (FAB1418G, 1:1000 dilution). Briefly, Caco-2 cells were washed twice with DPBS,

dissociated, and resuspended in phenol-free DMEM medium supplemented with 10 μM Y27632 and 1X antibiotic-antimycotic. Fluorescent cells were sorted into 12 well plates using the 5-laser FACS Aria III with a 100 μm nozzle. Sorted cells were supplemented with complete growth medium 24 hours after sort and medium was changed with complete growth medium every 48 hours afterwards. Despite some controversy as to whether this antibody recognizes an extracellular epitope on GLUT1 [145], [146], we verified homogenous GLUT1 expression in the sorted cells using western blot analysis, immunofluorescent imaging, and flow cytometry.

5.3.11 Flow Cytometry Analysis of Top Binding Aptamer

The affinity and specificity of aptamer A5 were measured by flow cytometry. To determine the affinity of the A5 aptamer and scrambled aptamer control for high-expressing and GLUT1-null Caco-2 cells, the aptamers were serially diluted from 500 nM to 0 nM in binding buffer. Cells were washed twice and dissociated with 0.02% EDTA. $3x10^5$ cells were incubated in each aptamer dilution for 1 hour at 4°C and measured for their mean fluorescence intensity on the Guava flow cytometer. Graphpad Prism was used to determine the apparent dissociation constant (K_d) of the aptamer binding by fitting the data to a standard one-site, specific binding model. The specificity of aptamer A5 was determined by performing qualitative flow cytometry binding experiments using HEK-293 cells, MDA-MB-231 cells, and iPSC-BMECs. In these experiments, $3x10^5$ cells were incubated with 200 nM aptamer A5 in binding buffer at 4°C for 1 hour, washed twice, and measured for their mean fluorescence intensity on the Guava flow cytometer. Mean fluorescent binding values of aptamers were compared to values obtained for a GLUT1 antibody targeting an intracellular epitope (Abcam, ab15309, 1:1000 dilution). For this comparison, cells were fixed in 4% PFA for 20 minutes, blocked with PBS containing 5% donkey

serum and 0.3% Triton-X-100 for 1 hour, and incubated with the primary GLUT1 antibody overnight at 4°C. The following day, cells were incubated with Alexa 488 donkey anti-rabbit secondary for 1 hour, washed three times, and analyzed for mean fluorescence intensity in the same manner.

5.3.12 Tissue Imaging

De-identified human brain tissue samples were provided by the Cooperative Human Tissue Network Western Division run by Vanderbilt University Medical Center. Tissue blocks were embedded in optimal cutting temperature compound (Fisher, 23730571), sliced into 10 μm sections, mounted on charged glass slides, and stored at -80°C. For imaging, the tissue sections were warmed to room temperature and blocked with binding buffer containing 20% FBS and 1 mg/ml yeast tRNA for 60 minutes. Following blocking, the tissue sections were incubated with 200 μL of 250 nM FAM-labeled aptamers in binding buffer or 200 μL of GLUT1 antibody (Abcam, ab15309, 1:1000 dilution) in PBS with 2% FBS for 1 hour on ice in the dark. For tissue sections incubated with antibody, Alexa Fluor 488 conjugated donkey anti-rabbit secondary was incubated for 1 hour following primary incubation. Tissue sections were then washed three times with washing buffer and co-stained with DAPI in PBS for 10 minutes. Tissue sections were then mounted with anti-fade reagent (Thermo Fisher, P10144) and imaged using a Leica DMi8 fluorescence microscope. For dual imaging, tissue sections were incubated with 200 μL of 250 nM Alexa Fluor 647-labeled aptamers in binding buffer or GLUT1 antibody in PBS with 2% FBS for 1 hour on ice in the dark. Antibody-incubated tissue sections were followed by treatment with Alexa Fluor 647 conjugated donkey anti-mouse secondary (Thermo Fisher, A-31573) for 1 hour. Tissue sections were then incubated with DyLight 488 labeled lycopersicon esculentum lectin

(Vector Laboratories, DL-1174 1:100 dilution) in PBS for 30 minutes, followed by DAPI for 10 minutes. Tissue sections were then mounted and imaged.

5.3.13 Measurements of Aptamer Serum Stability

To determine the serum stability of aptamer A5, 1 μg of aptamer was incubated with 50% FBS at 37°C for the following time points: 0, 0.25, 0.5, 1, 2, 4, 8, 12, 24, and 30 hours. Following the incubation, the DNA was run on a 3% agarose gel and visualized using an Odyssey Fc Imager.

5.3.14 Measurments of Glucose Uptake into Cells

$2x10^4$ wild-type Caco-2 cells were seeded into each well of a 96 well plate and allowed to adhere overnight. The following day, glucose uptake was measured using the Glucose Uptake-Glo Assay (Promega, J1341). Prior to performing the experiment, cells were incubated with 50 μM of a single aptamer (A1-A8) for 30 min, 50 μM of cytochalasin B (Sigma C6762) for 5 minutes, or left untreated. Cells were then washed to remove any glucose, incubated with 50 μL of 2-Deoxy-D-glucose (2-DG), and incubated with stop and neutralization buffers according to the manufacturer's instructions. 100 μL of glucose-6-phosphate dehydrogenase (G6PDH) were added to each well, incubated for 2 hours, and then luminescence was measured on a Tecan Infinite M1000 Pro. Glucose uptake inhibition by aptamers A1-A8 was compared to inhibition by cytochalasin B, cells that did not receive 2-DG, and untreated cells.

5.4 Results and Discussion

5.4.1 Generation of GLUT1-null Caco-2 Cells

To select aptamers against the GLUT1 transporter, we first sought to engineer a GLUT1-null cell line by using CRISPR techniques to knock out the *SLC2A1* gene, which encodes the GLUT1 glucose transporter. This GLUT1-null cell line was intended for use in the negative selection step as the isogenic pair to remove any aptamers from the selection process that were not specific to the GLUT1 transporter. Wild-type cells would then be used in the positive selection step as they express GLUT1 as the primary target. The Caco-2 epithelial cell line was chosen for this aptamer selection due to its high predicted expression of GLUT1 by the Human Protein Atlas [147]. To facilitate the gene editing process, we engineered a Caco-2 line with constitutive Cas9 expression using lentiviral transduction and clonal sorting (Figure 5.2 A,B). Immunofluorescent imaging (Figure 5.2 C) and flow cytometry analysis (Figure A.5.1) were initially used to demonstrate that the GLUT1 transporter was expressed in the Cas9-expressing Caco-2 cells, albeit heterogeneously. To generate the *SLC2A1* knockout, synthetic gRNAs were delivered to the Caco-2 cells using lipofection, and after three rounds of gRNA treatment, single clones were picked for expansion and initial analysis by western blot (Figure A.5.2)**.** One clone was chosen for full analysis, and GLUT1 knockout in this clone was validated with immunofluorescent imaging (Figure 5.2 C) and western blot (Figure 5.2D). Additionally, the online Tracking of Indels by DEcomposition (TIDE) [129] genomic assessment tool was used to quantify the percent knockout. By computational assessment of Sanger-sequenced genomic DNA (Figure A.5.3), two of the four cut sites were predicted to have indel formations of at least 94% (Figure 5.2 E and Figure A.5.4)**,** which is highly indicative of a knockout. Collectively, these results demonstrate the engineered

Caco-2 cell line has complete knockout of the GLUT1 protein and was therefore suitable for use in our aptamer selection.

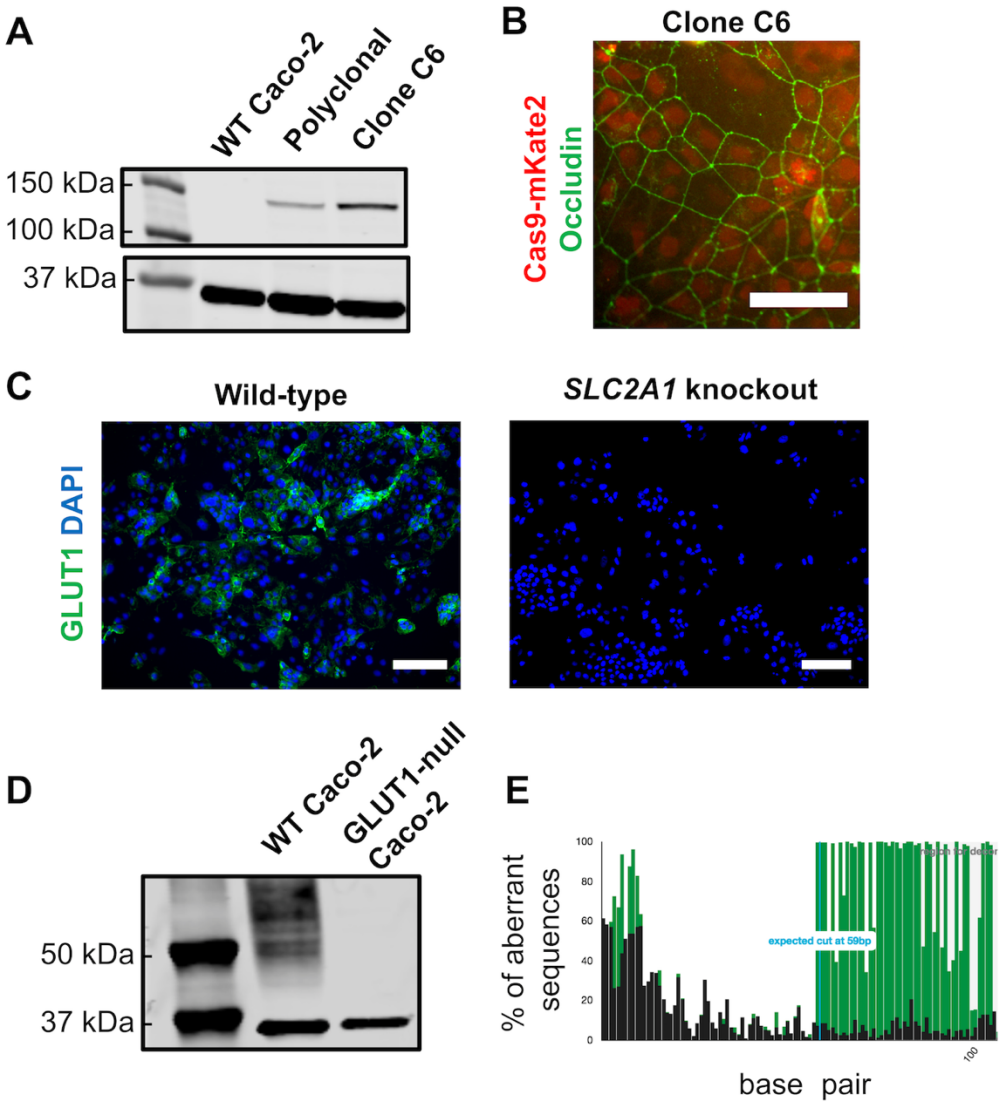

Figure 5.2 Generation of GLUT1-null Caco-2 cells. (A) Cas9-expressing Caco-2 cells were created by transduction with lentivirus and clonal isolation. Western blot analysis was used to confirm Cas9 expression in the polyclonal line and the final selected clone C6, with GAPDH as the housekeeping protein. (B) Immunofluorescent image showing Cas9 expression in clone C6, with Cas9 fused to mKate2 (red) and occludin (green) marking the cell borders (scale bar: 100 μm). (C) Immunofluorescent staining of GLUT1 in wild-type versus *SLC2A1* knockout Caco-2 cells (referred to as GLUT1-null Caco-2) (scale bar: 200 μm). (D) Western blot image of GLUT1 protein expression (expected band size of 55 kDa) in wild-type (WT) versus GLUT1-null Caco-2 cells. GAPDH was used as the housekeeping protein, with bands visible at correct band size of 37

kDa for both cell lines. (E) Example TIDE genomic assessment data for one of the four expected gRNA cut sites. The black sequence is the control sample (wild-type Caco-2 cells) and the green sequence is the test sample (*SLC2A1* knockout). The TIDE web tool predicts an indel formation of 96.1% for this particular cut site. Full Sanger sequencing and TIDE results are shown in Figure A.5.3 and A.5.4.

5.4.2 Selection of DNA Aptamers Against GLUT1

Wild-type and GLUT1-null Caco-2 cells were used for the positive and negative selection steps of CRISPR-mediated isogenic cell-SELEX, respectively. The selection process is summarized in Figure 5.1, building upon established protocols [121], [124]. In the first round of this selection process, a random 40-mer DNA library was perfused over the wild-type Caco-2 cells to enrich the library for binding to the wild-type GLUT1+ cells. Following the first round, a negative selection step was added to the positive selection step, by perfusing the pool over the GLUT1-null cells followed by the wild-type cells. In this process, the pool is continuously circulated over both cell types for a fixed amount of time, in an effort to allow the nucleic acid pool to interact with both cell types in a single round of selection; we recently used this strategy for isolating aptamers against recombinant protein targets [143]. Following this simultaneous positive and negative selection, cells were washed and aptamers were eluted from each Caco-2 population. ssDNA was PCR amplified and the resultant dsDNA was restored to single-strand form with enzyme digestion to be introduced into the next round of selection.

After Round 6 of selection, the pool affinity was tracked with a flow cytometry binding assay. The Round 6 pool was amplified with FAM-labeled forward primer and showed preferential binding to the wild-type Caco-2 cells compared to the fluorescently-labeled starting library (Figure 5.3 A). Additionally, the Round 6 pool showed negligible binding as to the GLUT1-null Caco-2 cells, similar to the starting library (Figure 5.3 B). Thus, through six rounds,

it appeared that the nucleic acid pool was enriching to bind the wild-type cells and not the GLUT1-null cells. Four more rounds of selection were completed to further enrich the pools. In total, ten rounds of selection were performed, with ten positive selection steps and nine negative selection steps. After completion of the selection, samples of the pools from Rounds 2, 4, 6, 8, and 10, along with samples from the negative selection from Rounds 6 and 10, were subjected to NGS analysis. Sequencing data were then analyzed with AptaSUITE bioinformatics software [144]. Only sequences with the correct 5' primer and 3' primer regions were accepted (Table A.5.1), and the number of unique sequences was tracked in each sample, with a sharp convergence after round 6 (Figure 5.4 and Table A.5.2). Sequences were ranked in each sample based on their overall abundance (the overall number the sequence appeared in the pool) and enrichment (fold-change in any particular sequence between two rounds), similarly to previous reports [148], [149]. Based on this analysis, eight prospective aptamers were selected from the NGS data (Table 5.1), including the three most abundant sequences from Round 10 (A1-A3), the top enriched sequence from Round 10 (A4), the top enriched sequence from Round 6 (A5), the second most abundant sequence in Round 6 (A6), the fourth most abundant sequence from Round 6 (A7), and the top enriched aptamer from Round 4 (A8). These sequences were cross-compared with the NGS data from the negative selection rounds to make sure they were not also enriched in the GLUT1-null cells (data not shown), in an effort to avoid sequences that may have been amplified by PCR bias.

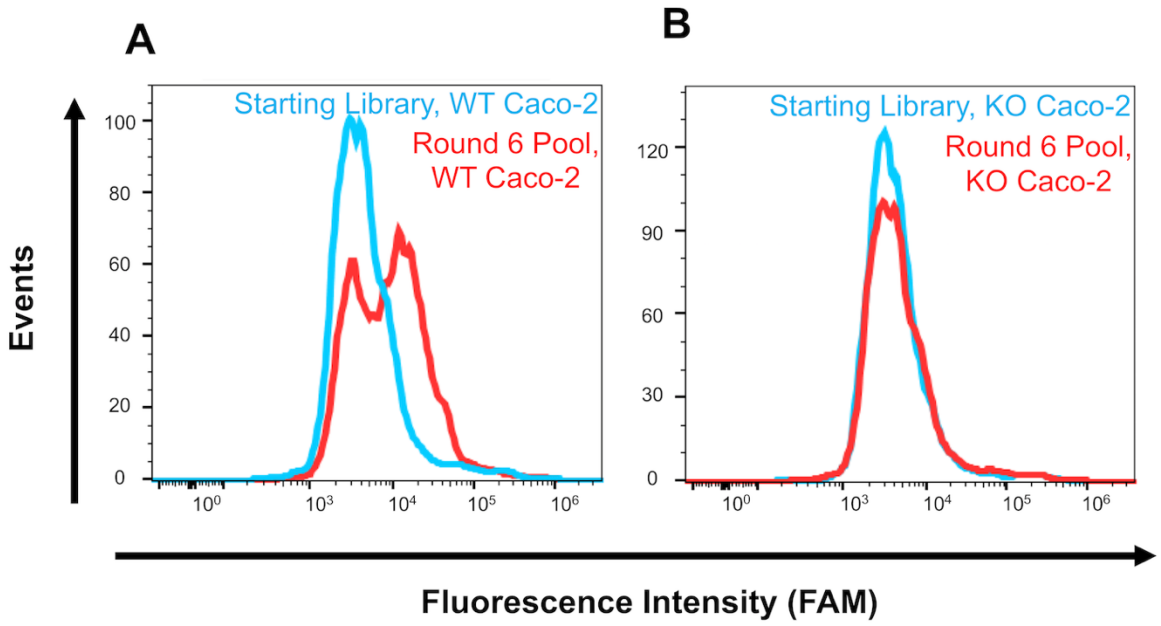

Figure 5.3 Pool affinity measurements. Affinity was measured by flow cytometry after PCR amplification of each bulk pool with FAM-labeled primers. The apparent binding of the Round 6 pool and the starting library were measured by incubating each ssDNA sample with either wild-type or GLUT1-null Caco-2 cells. (A) Histograms for binding of the Round 6 pool to the wild-type Caco-2 cells compared to the starting library. (B) Histograms for binding of the Round 6 pool to the GLUT1-null Caco-2 cells compared to the starting library. Each flow cytometry assay for the starting library and Round 6 pool was performed in duplicate against each cell type.

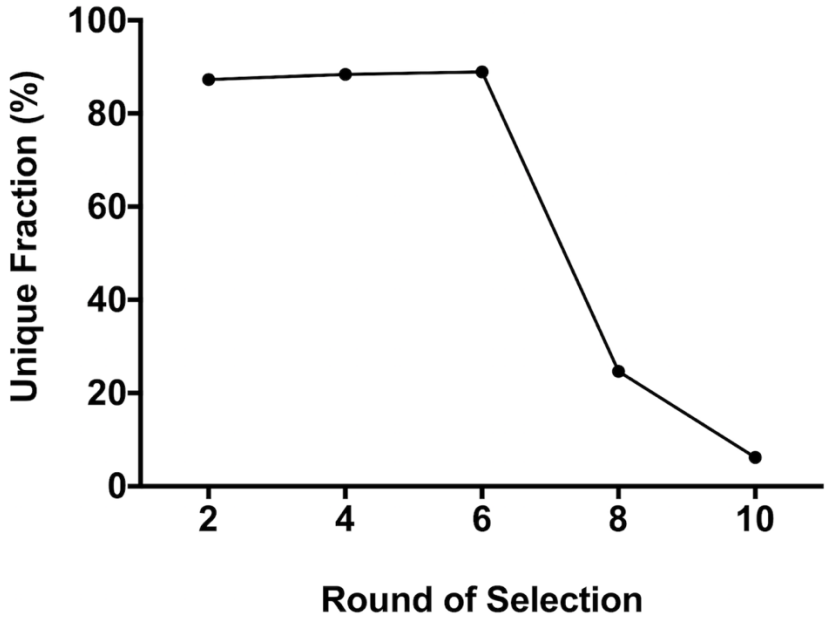

Figure 5.4 NGS analysis. NGS data was analyzed with the AptaSUITE web tool. The percent of unique sequences was quantified for each of the sequenced rounds. After Round 6, the percent of unique sequences still present in the pool sharply decreases and continues to decrease through Round 10. More information on NGS data are found in Table A.5.1 and Table A.5.2.

Table 5.1 Aptamer sequences identified by NGS. Sequences for the eight aptamers chosen for further characterization based on enrichment profiles as described in the main text. The sequence for the scrambled negative control aptamer is also provided.

Aptamer	Sequence
A1	AAGCAGCGGGAGGACCTTAATGGTTTCGAATTGAGCCTGC
A2	GTGCCTCAGCAGTAACGTGGAATTTTTGACCCCGCAATAC
A3	GGACGCAGAGACAATTTCTACAGTTTTCTGCAATCGTCTC
A4	CTACCACTGTCCAGGTTGAAATTAGTTCGCTTCTGGGGAC
A5	CATGGCTAGGTGTTTATTAATCCTGTAGGATTTGCGGAAT
A6	CCAGTAGCAATATAAATGGCAACCGGGCATTCTTTATCGC
A7	CCAGTAGCCATTTTAATGGACATAATAGCGTATTAAAATC
A8	CACGCGGAGTTATAAATCAACGCCGTAATTTATAGGATAC
ScrA	ATTGCATTCCTGCCGCTACGTAGCTAAGCTAGGCTAATAG

5.4.3 Identification of GLUT1-binding Aptamer Candidates

The top eight sequences from the NGS data were screened for their binding to the wild-type and GLUT1-null Caco-2 cell lines using a flow cytometry assay. Aptamers A1-A8 were synthesized with biotin labels, incubated with wild-type Caco-2 cells, and mixed with streptavidin Alexa Fluor 488 conjugate, where mean fluorescence intensity was compared to a scrambled aptamer and unlabeled cells. All of the aptamers showed binding to the wild-type Caco-2 cells, compared to the controls, with several of the aptamers showing prospectively higher binding (Figure A.5.5 A). The mean fluorescence intensity of the aptamers was also measured for binding to the GLUT1-null Caco-2 cells, with none of the aptamers showing a strong difference in binding compared to the controls (Figure A.5.5 B)**.** Owing to the potential for human error imparted by separate primary and secondary binding events, we next re-tested aptamers A1, A2, A5, and A7 with primary conjugated FAM labels (Figure 5.5 A). All aptamers showed strong binding to the wild-type Caco-2 cells, but only aptamer A1 and A5 showed negligible binding to GLUT1-null Caco-2 cells compared to the scrambled aptamer. Because this bulk fluorescence analysis was potentially complicated by heterogeneous GLUT1 expression in the wild-type Caco-2 cells, these aptamers were characterized further with immunofluorescent imaging. FAM-labeled aptamers were incubated with both cell lines, and live-cell images were taken and compared to the scrambled aptamer. Again, all of the aptamers demonstrated binding to the wild-type Caco-2 cells relative to the scrambled aptamer (Figure 5.5 B). Aptamers A1, A2, and A7 showed variable adhesion to the GLUT1-null cells, likely indicating some off-target binding. However, aptamer A5 showed no apparent binding to the GLUT1-null cell line. Based on the flow cytometry and imaging data, aptamer A5 was chosen for further characterization due to its strong apparent specificity for the GLUT1 transporter. For reference, the secondary structure of aptamer A5 was predicted with

NUPAC software [150] (Figure A.5.6) and it remains stable in 50% serum for up to 12 hours (Figure A.5.7), indicating its potential suitability for long-term imaging applications.

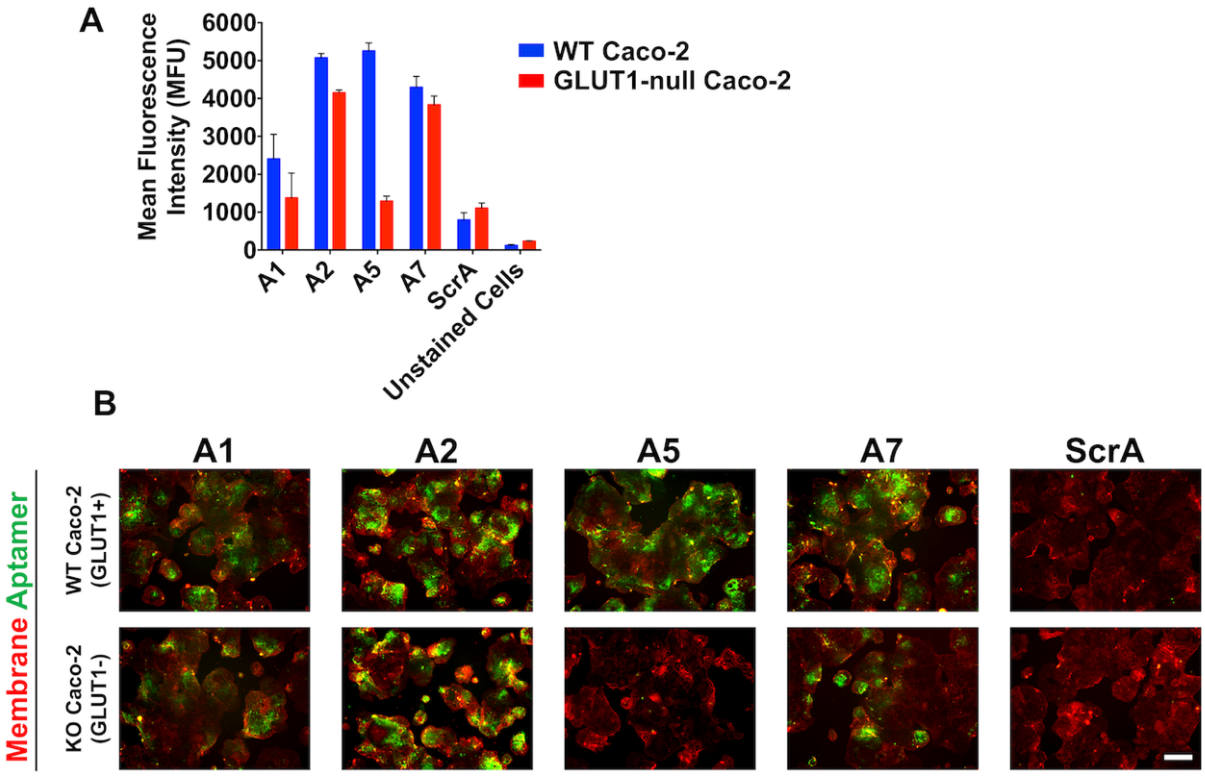

Figure 5.5 Prospective assessment of the affinity and specificity of selected aptamers. (A) FAM-labeled aptamer binding to wild-type and GLUT1-null Caco-2 cells was characterized by flow cytometry. Data are presented as mean ± SD from biological triplicates. (B) FAM-labeled aptamers were characterized by incubation with wild-type and GLUT1-null Caco-2 cells, followed by immunofluorescent imaging, where red indicates the cell membrane stain and green indicates the bound aptamer (scale bar: 200 μm). Images are representative of two biological replicates.

5.4.4 Characterization of Aptamer A5 Affinity and Specificity

First, to alleviate the issues encountered in Figure 5.5 with a heterogeneously expressing GLUT1 population (since the presence of GLUT1- cells could skew affinity determinations), we

used fluorescence-activated cell sorting (FACS) with a GLUT1-specific antibody to generate a culture of uniformly GLUT1+ Caco-2 cells (termed "high-expressing GLUT1" Caco-2 cells). This high-expressing GLUT1 Caco-2 cell line was validated by western blot, flow cytometry analysis, and immunocytochemistry (Figure A.5.8). Flow cytometry was then used to determine the affinity of aptamer A5 to these high-expressing GLUT1 Caco-2 cells, which was measured at 160±49 nM (Figure 5.6). This result was compared to several negative controls, including a scramble aptamer incubated with the high-expressing GLUT1 Caco-2 cells and aptamer A5 incubated with the GLUT1-null Caco-2 cells (Figure 5.6). Aptamer A5 shows good selectivity as demonstrated by lower binding to the GLUT1-null Caco-2 cells (860±53 nM). The scrambled aptamer exhibits negligible binding to the high-expressing GLUT1 Caco-2 cells (e.g. binding is too low to calculate an affinity), demonstrating that these measurements are not being predominantly influenced by nonspecific interactions.

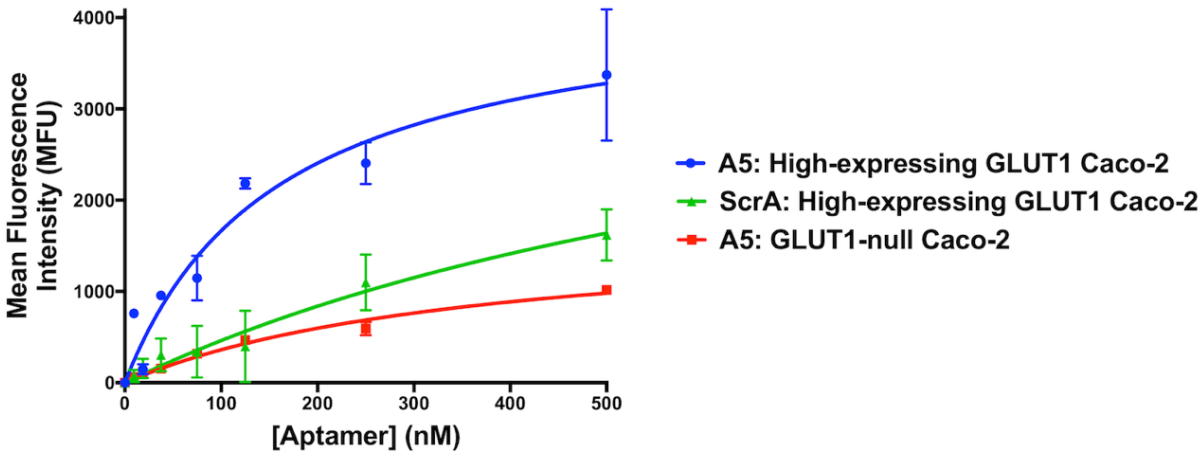

Figure 5.6 Aptamer A5 affinity analysis. Flow cytometry measurements of serially diluted (0 nM-500 nM) FAM-labeled aptamer A5 binding to high-expressing GLUT1 or GLUT1-null Caco-2 cells. The FAM-labeled scrambled aptamer was used as a negative control with the high-expressing GLUT1 Caco-2 cells. Measurements were performed in duplicate with error bars representing mean ± SD.

Beyond the quantitative comparison of binding to the GLUT1+ and GLUT1- cells, the specificity of aptamer A5 to the GLUT1 transporter was next determined by screening the aptamer against several cell lines that exhibit varying degrees of GLUT1 protein expression. The Human Protein Atlas predicts low to moderate expression of GLUT1 in HEK-293 cells and MDA-MB-231 breast cancer cells. We also routinely differentiate human induced pluripotent stem cells to brain microvascular endothelial cells (iPSC-BMECs) [140], [141], which express high levels of GLUT1. Western blot analysis was used to confirm these trends (low endogenous expression of GLUT1 in HEK-293 cells, high expression in iPSC-BMECs, and moderate expression in MDA-MB-231 cells), which were compared directly to wild-type and GLUT1-null Caco-2 cells (Figure 5.7 A). Flow cytometry was then used to determine the binding of aptamer A5 to each of these cell types (Figure 5.7 B). Binding patterns correlated to protein expression levels for each of the three cells types, with low binding to the HEK-293 cells, strong binding to the iPSC-BMECs, and moderate binding to the MDA-MB-231 cells. These affinity and specificity data across multiple cell types further verified the binding of aptamer A5 to the GLUT1 transporter. Additionally, the other selected aptamers GLUT1 showed similar binding patterns to aptamer A5, suggesting that while these aptamers may target other proteins, they retain some specificity for the GLUT1 transporter (Figure A.5.9).

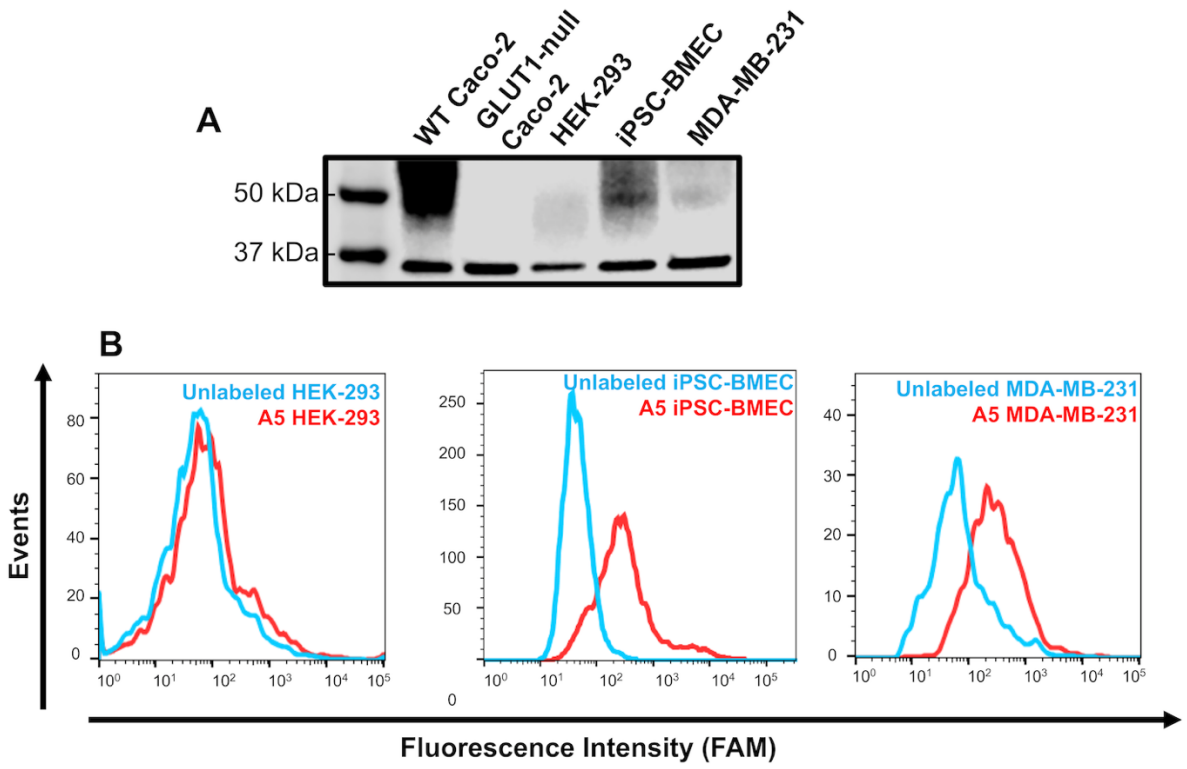

Figure 5.7 Specificity of aptamer A5 to multiple cell types. (A) Western blot showing GLUT1 expression in various cell types. GAPDH was used as the loading control. (B) Representative flow cytometry histograms for binding of FAM-labeled aptamer A5 to HEK-293 cells, iPSC-BMECs, and MDA-MB-231 cells. Binding is compared to unlabeled cells. Flow cytometry binding specificity experiments were performed in triplicate to verify trends.

Last, to confirm that aptamer A5 specificity was not influenced by potential off-target edits in the particular GLUT1-null Caco-2 clone that was utilized for SELEX, we tested the binding of aptamer A5 to other clones described in Figure A.5.2. As shown by flow cytometry, aptamer A5 robust binds to wild-type Caco-2 cells and Caco-2 cells from the bulk pool that received three rounds of gRNA delivery (where many of the cells likely retain GLUT1 expression) (Figure A.5.10). In contrast, aptamer A5 binding against each of the tested clones was reduced (Figure A.5.10). Thus, even if other genes besides *SLC2A1* were unexpectedly edited in these clones, the

shared reduction in aptamer A5 binding strongly suggests that the aptamer is specifically recognizing GLUT1.

5.4.5 Imaging Brain Cortex Tissue with Aptamer A5

We next validated aptamer A5 using primary tissue. GLUT1 is highly expressed in brain vasculature but not in other resident neural cell types [151]. The same GLUT1 antibody used for flow cytometry analysis of cell lines showed binding to the vasculature in frozen human brain cortical tissue (Figure 5.8 A), with minimal binding to other cell types. FAM-labeled aptamer A5 showed a similar binding pattern as the antibody, with minimal background and binding to other cell types (Figure 5.8 A). In comparison, a FAM-labeled scrambled aptamer did not show strong binding to any cell types in the brain tissue. To further confirm the binding patterns of the aptamer to brain vasculature, the GLUT1 antibody was used in combination with a lectin dye to highlight brain vasculature (Figure 5.8 B). The lectin and antibody showed similar fluorescent overlap, indicating similar binding areas. When the lectin was used in combination with an Alexa Fluor 647-conjugated aptamer A5, similar binding patterns were also observed (Figure 5.8 C). These results further suggest that aptamer A5 can selectively bind the GLUT1 transporter in its native conformation.

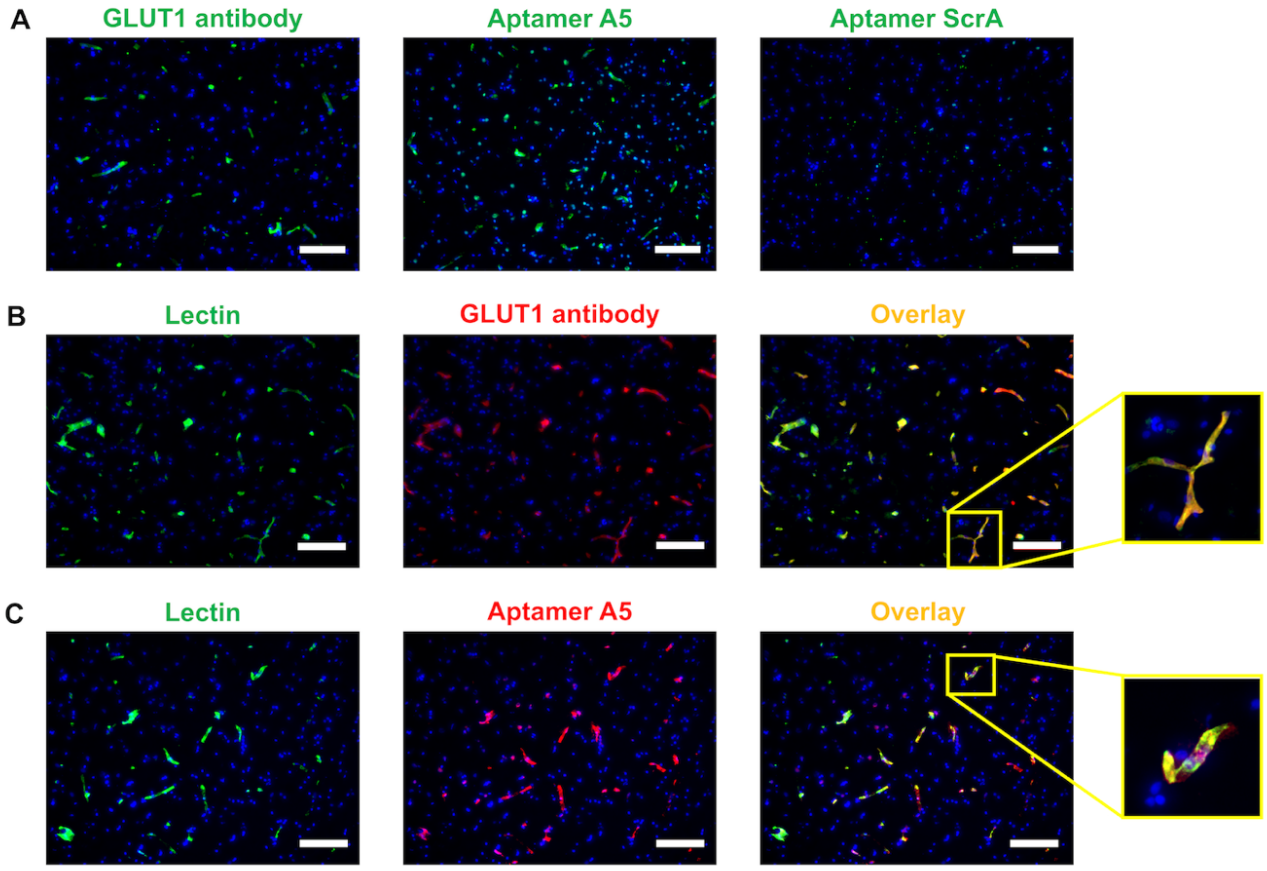

Figure 5.8 Specific binding of aptamer A5 to GLUT1 in human tissue. (A) Human brain cortical tissue was labeled with a GLUT1 Alexa Fluor 488-conjugated antibody, FAM-labeled aptamer A5, or FAM-labeled scrambled aptamer. (B) Human tissue was co-labeled with lectin and the GLUT1 antibody. (C) Human tissue was co-labeled with lectin and the Alexa Fluor 647-labeled aptamer A5. All immunolabeling was performed with two separate tissue samples, with three images taken from each tissue section to validate expression patterns. The representative images are provided with DAPI co-labeling (blue) (scale bar: 200 μm).

5.4.6 Inhibiting Glucose Uptake with Selected Aptamers

Data from Figure 5.5 and Figure A.5.5 indicate that other selected aptamers bind GLUT1 but lack specificity (i.e. they exhibit binding to the GLUT1-null Caco-2 cells). The Human Protein Atlas suggests that Caco-2 cells express GLUT2 and GLUT3 in addition to GLUT1, which led us to question if these nonspecific aptamers were recognizing other glucose transporters (and were

thereby specific to the GLUT family, just not GLUT1 individually). As such, to further characterize these aptamers, a glucose uptake assay was performed to see if any of the eight aptamers identified with NGS could inhibit glucose entry into Caco-2 cells. Indeed, three of the aptamers (A1, A2, and A7), which also demonstrated prospective GLUT1 binding (Figure A.5.9), yielded a significant decrease in glucose uptake that was indistinguishable from cytochalasin B, a well-characterized inhibitor of glucose transport (Figure A.5.11). These data suggest that these aptamers might be binding to a shared epitope between GLUT transporters, without being exclusive to GLUT1. Explicit testing of GLUT2/3 knockouts would be necessary to fully validate these findings, and these experiments are being planned in the future to further qualify our cell-SELEX approach.

5.5 Conclusion and Future Work

To improve the generation of affinity reagents that bind to native cell membrane proteins with high specificity, a novel SELEX strategy was developed that utilizes isogenic cell lines. In an effort to identify aptamers specific to the GLUT1 transporter, CRISPR techniques were used to knock out the *SLC2A1* gene in Caco-2 epithelial cells to create a GLUT1-null cell line. Wild-type Caco-2 cells expressing GLUT1 were used in the positive selection step and the GLUT1-null Caco-2 cells were used in the negative selection step. Ten rounds of selection were performed, and candidate aptamer sequences were identified with NGS. Most of the aptamers bound strongly to the surface of Caco-2 cells, and one of the aptamers (A5) was highly specific to the GLUT1 transporter, as demonstrated by low nanomolar affinity for wild-type but not GLUT1-null Caco-2 cells, representative binding to other cell types with varying degrees of GLUT1 expression, and selective binding to vasculature in human brain cortical tissue.

A possible limitation of this approach is that the presence of off-target CRISPR edits was not examined, so the explicit method we used to create the knockout cells could also have affected the expression of other proteins. Although we did show that knockout clonality did not influence the performance of the most specific aptamer identified in this study, it may have influenced the SELEX procedure in unintended ways that limited the efficiency of the selection (as seen by only one of the eight identified aptamers being highly specific for GLUT1). Furthermore, although efforts were made to control parameters such as density, which can influence receptor expression levels [152], [153], fluctuations may have occurred between selection rounds to influence the final outcomes. In addition, despite the clonal selection of the original Cas9-expressing Caco-2 cells, mutations may have arisen throughout the SELEX process as the cells were continuously propagated, which could reimpose some heterogeneity outside of the GLUT1 knockout. Last, while this cell-SELEX approach can be definitively used to obtain highly specific aptamers, more in-depth cell engineering to remove homologous family members may be necessary to improve the hit rate of selected aptamers. Other users should be mindful of these variables when utilizing this cell-SELEX approach.

Overall, our data indicate that highly specific aptamers can be efficiently isolated against native membrane proteins with our SELEX strategy that uses CRISPR-engineered isogenic cell lines. With further improvements, this approach may be broadly useful for generating affinity reagents that bind to diverse classes of membrane proteins with high specificity. We also expect that isogenic whole cell selection methods could be extended to other classes of amino acid-based affinity reagents with similar success. Future efforts will focus on strategies for improving the affinity of selected aptamers through random or site-directed mutagenesis.

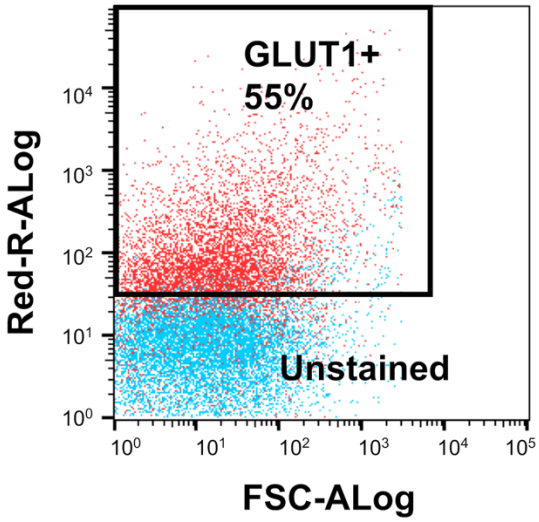

Figure A.5.1 Flow cytometry dot plot showing relative expression of GLUT1 in wild-type Caco-2 cells using a GLUT1 antibody conjugated with Alexa Fluor 647. Caco-2 cells heterogeneously express GLUT1 (~55% of the total population) under the conditions used for SELEX.

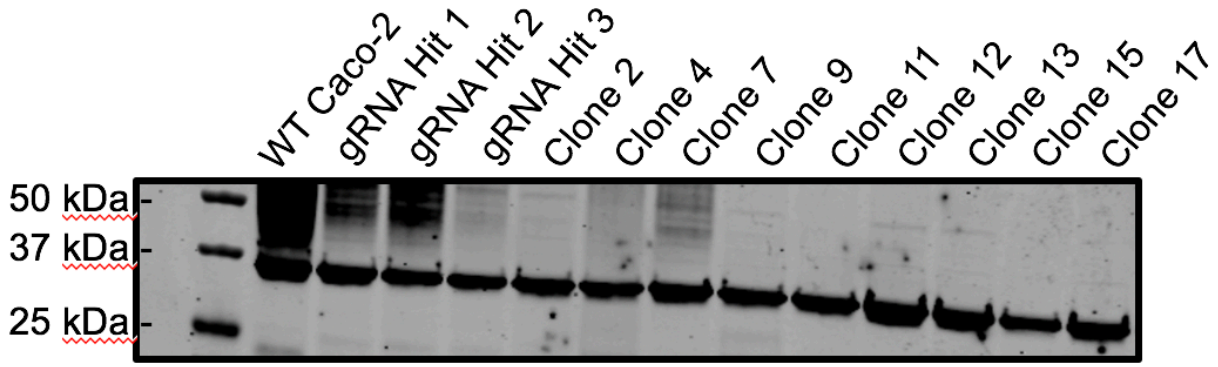

Figure A.5.2 Screening individual Caco-2 clones for GLUT1 expression. Western blot of GLUT1 protein expression for wild-type Caco-2 cells, bulk pools from the three rounds of gRNA delivery, and nine individually picked Caco-2 clones. The band at ~37 kDa is the GAPDH loading control. Clone 15 was chosen for further verification of GLUT1 knockout and use in the aptamer selection workflow.

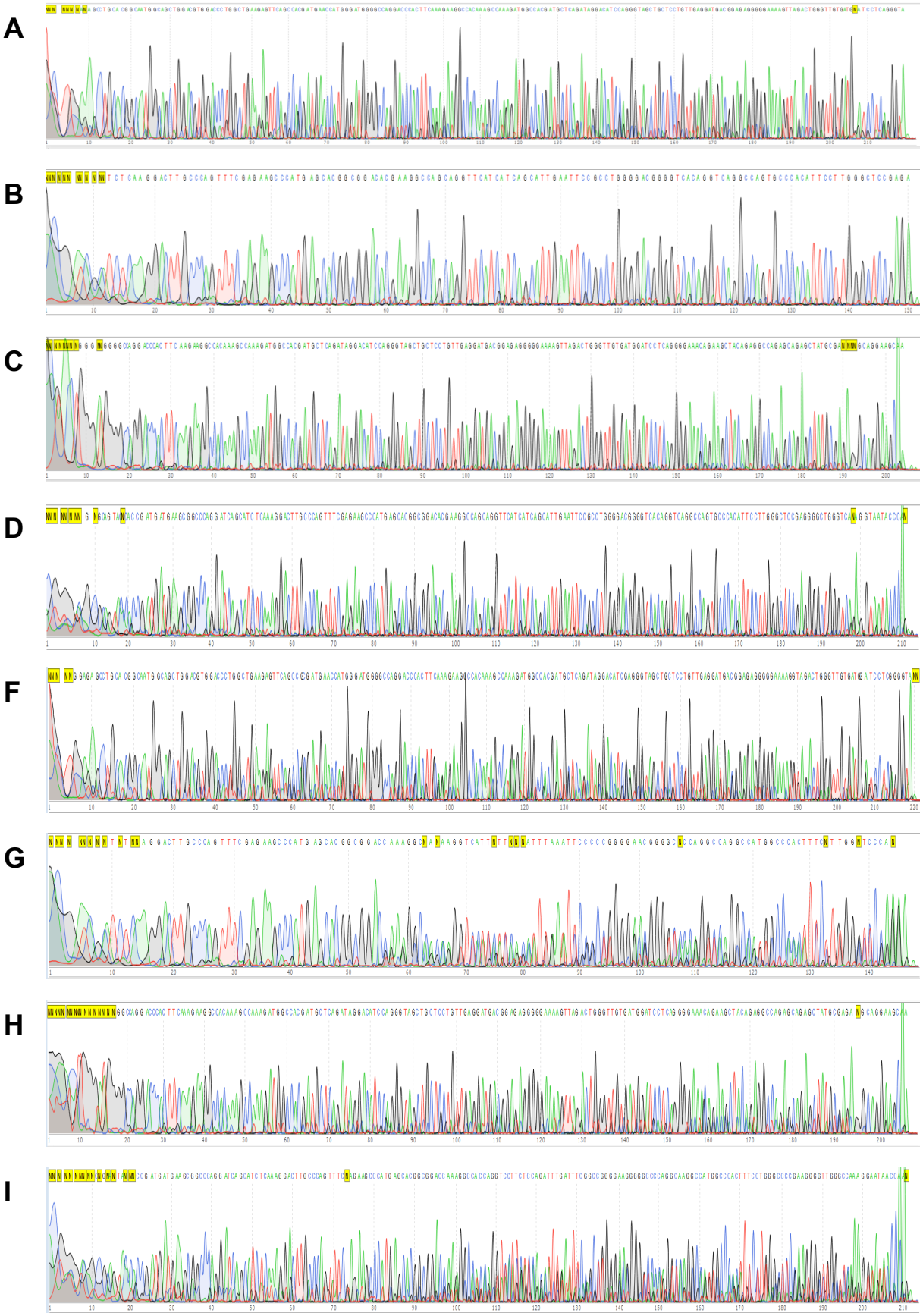
A
B
C
D
F
G
H
I

Figure A.5.3 Sanger sequencing files for wild-type and Clone15 Caco-2 cells. (A-D) Sanger sequencing files for the four cut sites from the four gRNAs for the control, wild-type Caco-2 cells. (F-I) Sanger sequencing files for the four cut sites from the four gRNA for the Clone15 GLUT1-null Caco-2 cells.

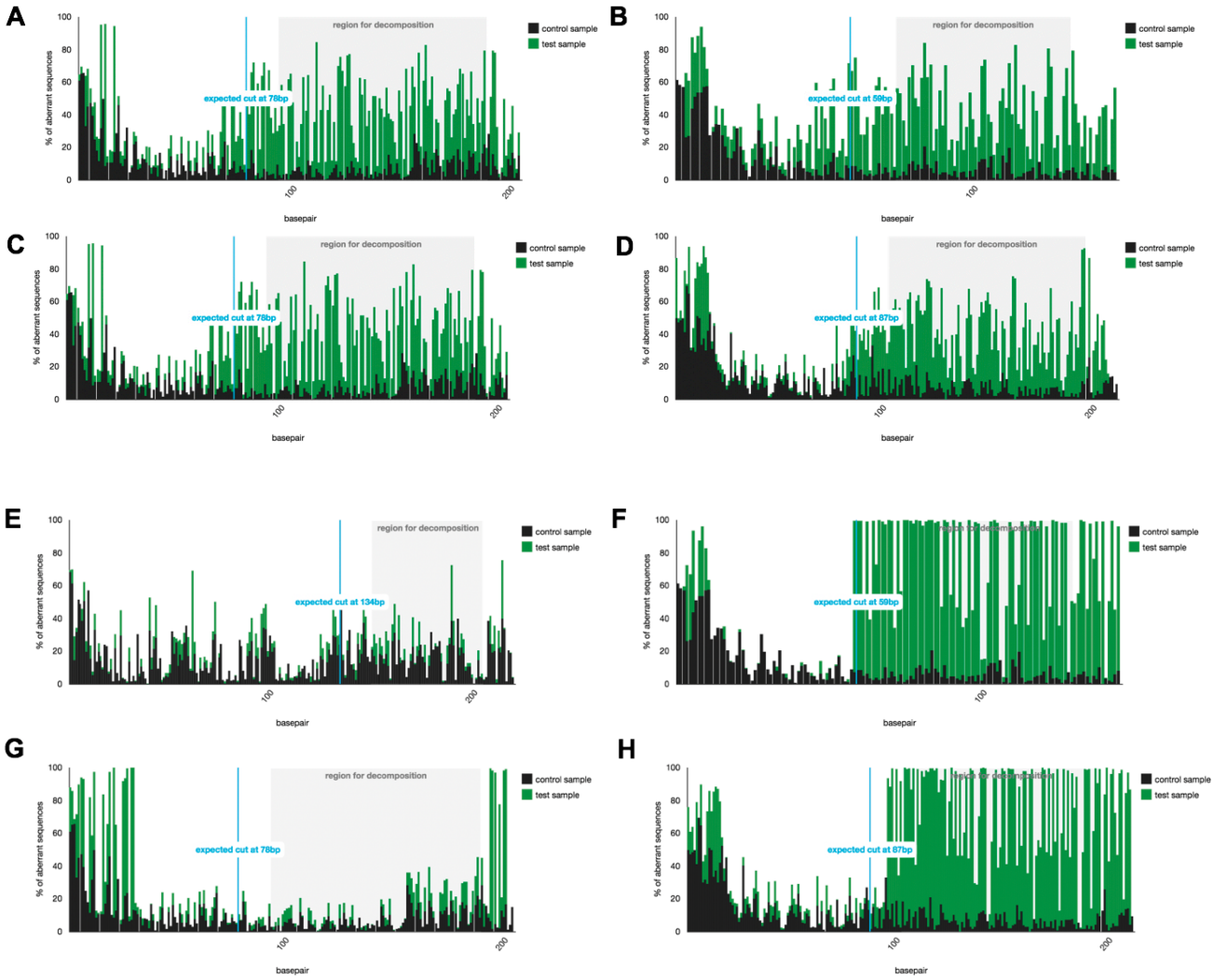

Figure A.5.4 TIDE results for gRNA Hit 3 Pool and Clone15 Caco-2 cells. (A-D) TIDE files for the four cut sites from the four gRNAs for the Hit 3 Pool, compared to the control, wild-type Caco-2 cells. (cutting efficiencies: 47.6%, 35.7%, 47.7%, 36.6%, respectively). (E-H) TIDE files for the four cut sites from the four gRNAs for Clone15, compared to the control, wild-type Caco-2 cells. (cutting efficiencies: 11.0%, 96.1%, 7.1%, 93.4%, respectively).

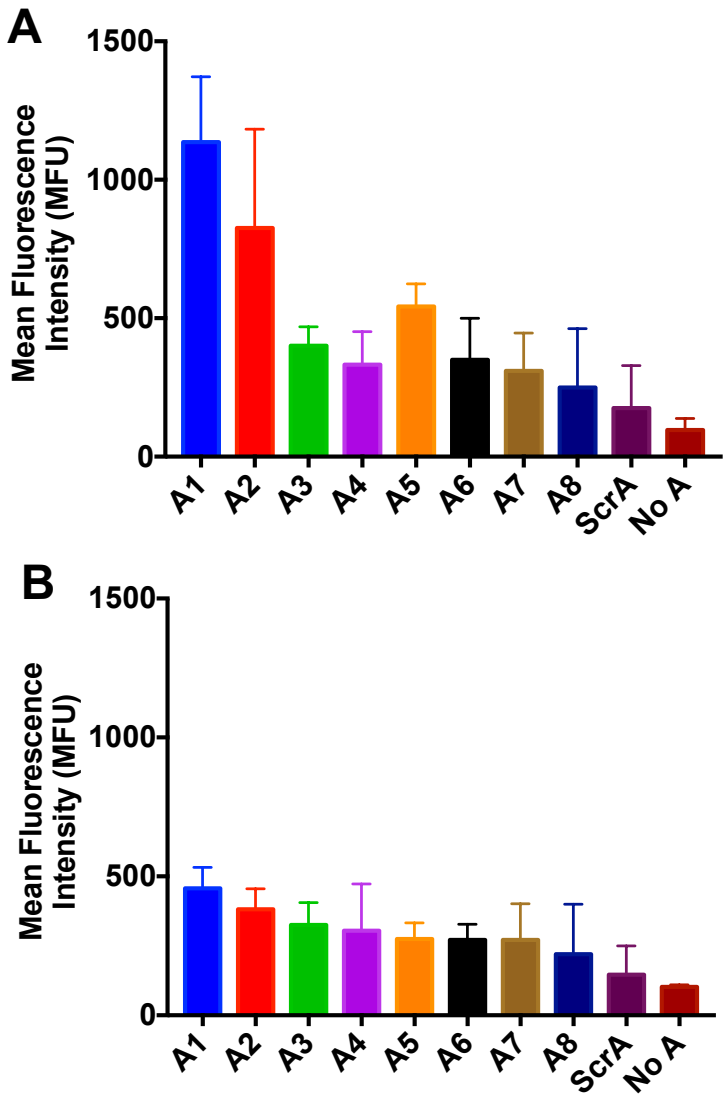

Figure A.5.5 Preliminary analysis of aptamer specificity using biotin/streptavidin labeling. Flow cytometry measurements of aptamer binding to wild-type Caco-2 cells (panel A) and GLUT1-null Caco-2 cells (panel B). In both cases, binding is compared to a scrambled control aptamer and unlabeled cells. Aptamers were biotin-labeled and after incubation with cells, Alexa Fluor 488-conjugated streptavidin was used for detection. Data are presented as mean ± SD from biological triplicates.

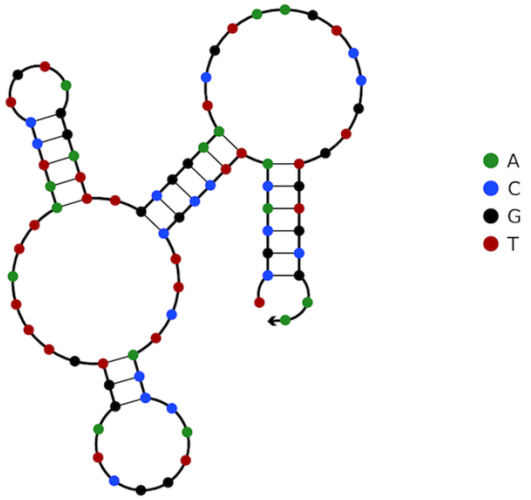

Figure A.5.6 Aptamer A5 structure. NUPACK nucleic acid software was used to predict the structure of aptamer A5 [150].

Figure A.5.7 Serum stability of aptamer A5. The serum stability of aptamer A5 was tested by incubation with 50% serum for various time points from 0 to 30 hours. DNA samples were visualized in a 3% agarose gel.

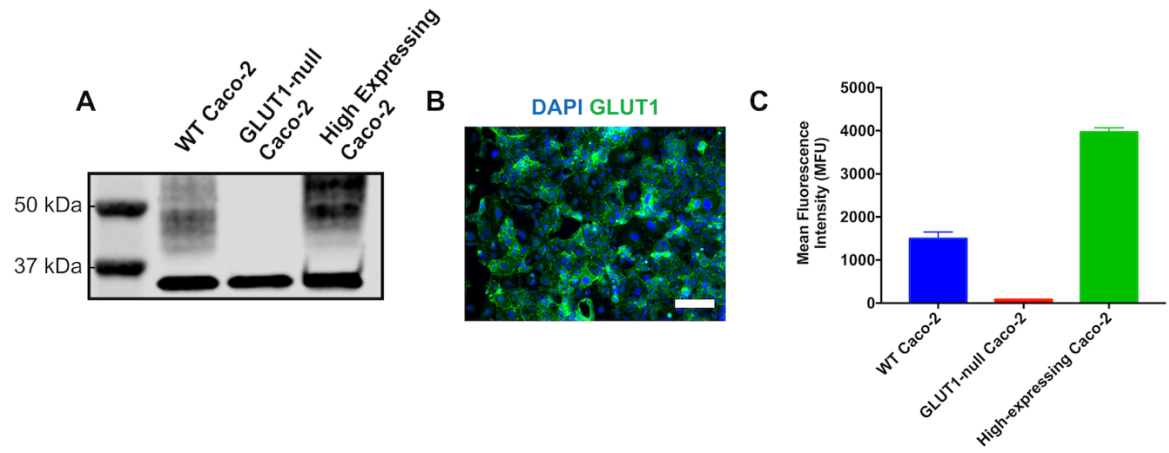

Figure A.5.8 Validation of FACS-sorted high-expressing Caco-2 cells used for affinity measurements. Caco-2 cells were FACS-enriched with an Alexa Fluor 488-conjugated GLUT1 antibody and assessed for GLUT1 expression. (A) Western blot for GLUT1 expression. (B) Immunofluorescent imaging demonstrates relatively homogenous expression of GLUT1 (scale bar: 200 μm). (C) Flow cytometry measurements of GLUT1 antibody binding to wild-type Caco-2 cells, GLUT1-null Caco-2 cells, and high-expressing GLUT1 Caco-2 cells. Flow cytometry binding experiments performed in duplicate with error bars representing mean ± SD.

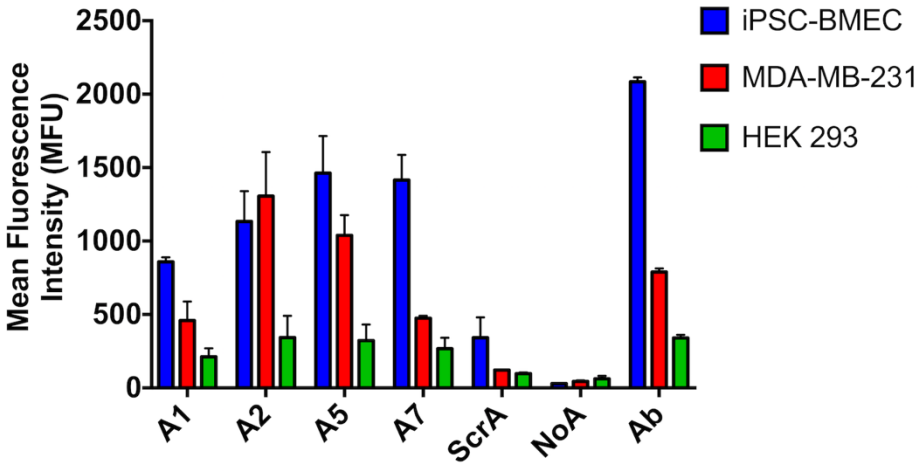

Figure A.5.9 Aptamer specificity against multiple cell types. Aptamers A1, A2, A5, and A7 were screened against three cell types expressing different levels of GLUT1 (iPSC-BMEC, MDA-MB-231, and HEK-293). Mean aptamer fluorescence intensity was compared to a scrambled aptamer, unstained cells (NoA), and a GLUT1 antibody. Flow cytometry binding experiments were performed in triplicate with error bars representing mean ± SD.

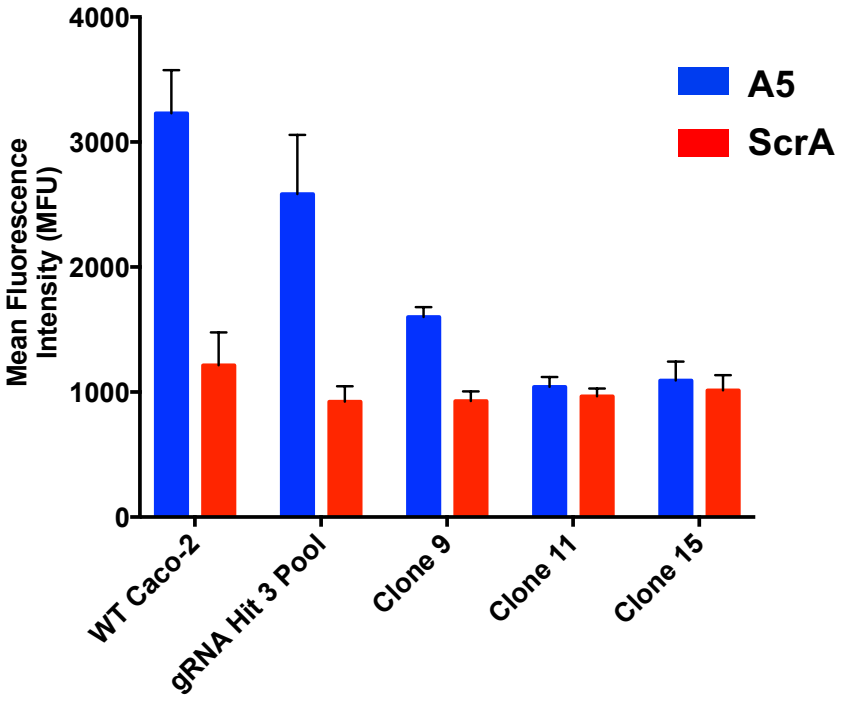

Figure A.5.10 Aptamer A5 specificity against multiple Caco-2 GLUT1 knockout clones described in SI Figure 2. Flow cytometry was used to measure the binding of aptamer A5 and the scrambled control for wild-type Caco-2 cells, the bulk Caco-2 population after three rounds of gRNA delivery ("gRNA Hit 3 Pool"), and three of the GLUT1 knockout clones (Clone 9, 11, and 15). Flow cytometry binding experiments were performed in duplicate with error bars representing mean ± SD.

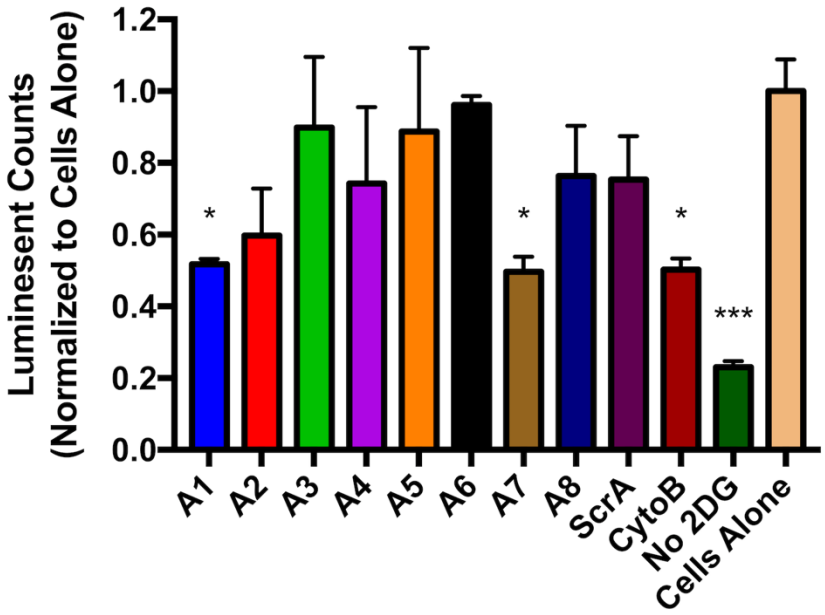

Figure A.5.11 Glucose uptake assay. Glucose uptake was measured via 2-deoxy-D-glucose (2-DG) uptake using the Uptake-Glo assay. Glucose uptake was compared between Caco-2 cells incubated with aptamers A1-A8, the scrambled aptamer, cytochalasin B, cells that did not receive any treatment, and cells that did not receive any 2-DG. Luminescent counts were normalized to cells that did not receive any treatment. The assay was performed once with duplicate wells for each condition with error bars representing mean ± SD. Significance was determined with an ordinary one-way ANOVA in Graphpad (*$p<0.05$, ***$p<0.001$).

Table A.5.1 Overall summary of NGS reads analyzed with AptaSUITE. Only the sequences with the correct 5'- and 3'-primer regions were categorized as accepted reads.

Total Processed Reads	286,241,565
Total Accepted Reads	120,218,826
Invalid Alphabet	265,435
5' Primer Error	161,332,861
3' Primer Error	4,272,953
Total Primer Overlaps	414,429

Table A.5.2 Round-specific summary of NGS reads.

Round Number	Pool Size	Number of Unique Sequences	Unique Fraction Percent
Round 2	14,292,584	12,495,271	87.42
Round 4	18,764,100	16,611,552	88.52
Round 6	18,547,733	16,492,772	88.92
Round 8	13,036,315	3,435,766	26.36
Round 10	26,203,634	1,999,360	7.63

Chapter 6

CONCLUSIONS AND FUTURE OUTLOOK

In this dissertation, I have discussed our work to address certain aspects of the conventional aptamer selection workflow in an effort to improve aptamer affinity and specificity. As discussed in the introduction chapter, aptamers have lagged behind other affinity reagents in therapeutic applications, with only one aptamer having FDA approval [13]. There are numerous issues involved with isolating aptamers and applying them as therapeutics, some of which have been addressed in the past three decades. This dissertation aimed to develop a new selection strategy that included improvements from the literature, as well introduce new concepts to improve upon other selections. A common lab peristaltic pump was used to introduce flow mechanics into the aptamer selection, thereby increasing the stringency of washing and allowing for recirculation of the aptamer pools introduced. In the purified-target selections, soluble off-targets were introduced into the negative selection step using the flow-based system. In this dynamic flow system, aptamers are introduced to the primary target and off-targets simultaneously, in an effort to improve the affinity and specificity of aptamers that can be isolated.

The first selection used the dynamic flow system to isolate high affinity DNA aptamers for PDGF-BB, with specificity against the other PDGF homodimers, -AA, -CC, and -DD. In this selection, complementary blocking regions, emulsion PCR, and λ-exonuclease were used in the workflow to improve certain aspects of the selection workflow. Flow was used to circulate the starting library and aptamer pools over the immobilized primary target, PDGF-BB. The aptamers bound to PDGF-BB were then washed with the flow system and soluble off-targets were introduced to remove low affinity and specificity binders. At the end of the selection, next

generation sequencing was used to identify prospective aptamers for further characterization. Several high-affinity binders were identified with this selection workflow, with variable specificity against the off-targets, similar to other aptamers reported in the literature. Future work will focus on reperforming this selection with different parameters in an effort to improve the specificity of the aptamers isolated against all of the homodimers and heterodimer in the PDGF family of proteins. Additionally, a more elaborate pumping system will be used with multiple lines to introduce a starting nucleic acid library to multiple primary targets simultaneously. In this workflow, DNA aptamers will be isolated for all of the members of the PDGF family, in an effort to improve throughput for selecting aptamers with specificity against structurally similar targets. We aim to expand this dynamic flow system to develop aptamers for multiple primary targets simultaneously, using the same strategies discussed in Chapter 2.

The next selection applied the dynamic flow system to a peptide target. RNA aptamers were isolated for the kinesin-12 coverstrand peptide, in an effort to develop antimitotic reagents to specifically halt the movement of kinesin on microtubules. Two RNA aptamers were isolated with micromolar affinity against the kinesin-12 coverstrand peptide, with one aptamer having moderate specificity against a similar target, the kinesin-1 coverstrand peptide. Future work will test these aptamers *in vitro* for their inhibitory effect by binding to the kinesin-12 coverstrand and halting movement on microtubules. Ultimately, these aptamers could be used to specifically target individual kinesin molecules and systematically halt different kinesins' function for cancer applications.

The third selection discussed in this thesis applied the dynamic flow system to another protein target, serum albumin. 2'-fluorine modified RNA aptamers were isolated for albumin with nanomolar affinity. These aptamers were fused with siRNAs, to form chimeras, for *in vitro* and

in vivo applications. These chimeras were able to retain silencing efficacy *in vitro* and were able to knockdown a gene of interest without the use a transfection reagent. Additionally, these aptamer chimeras improved the half-life and bioavailability of siRNA *in vivo*. These studies were limited by the amount of RNA able to be generated due to the overall size of the aptamer-siRNA chimeras. This study was also hindered by the failure to successfully truncate the aptamers into smaller sizes in an attempt to synthesize the chimeras on a solid-state oligosynthesizer. A future selection will focus on repeating the work in this chapter with a smaller starting library to decrease the overall size of the chimera. Using a 20 nt starting library would reduce the overall length of the chimera from 69 nt to 49 nt, improving the yield with an oligosynthesizer and allowing for further *in vivo* studies. Future *in vivo* studies will include repeating half-life studies with more replicates and investigating gene silencing efficacy. Furthermore, these albumin-binding aptamer-siRNA chimeras will be used in studying caveolae-mediated transport at the blood-brain barrier during injury.

The final selection performed for this dissertation developed a novel selection methodology for isolating DNA aptamers for proteins on the surface of whole cells. A custom GLUT1-null Caco-2 cell line was generated using CRISPR techniques to be used in the negative selection, with the wild-type Caco-2 cell line used in the positive selection. DNA aptamers were isolated that bind to the wild-type cell lines, with one aptamer showing specificity against the GLUT1-null cell line. Further characterization revealed that this aptamer was more than likely binding to the GLUT1 transporter specifically. Future studies will aim to use this aptamer for GLUT1 binding assays in our BMEC filter assays. Additionally, this aptamer will be used in our lab's arrayed high-throughput CRISPR screen investigating GLUT1 regulation at the blood brain barrier. The screen will identify genes with blood-brain barrier relevance, with applications in

neurodegenerative diseases, such as Alzheimer's Disease. Furthermore, this whole-cell aptamer selection methodology will be applied to new cell surface protein targets. For example, custom TGFβRI-, BMPR1A-, and BMPR2-null cell lines will be generated with similar CRISPR techniques. Aptamers will be isolated to bind to these cell lines with high affinity and specificity. Multivalent aptamers with Type I and Type II TGF/BMP binding ability will be tested for their ability to create receptor tetramers and control cellular phosphorylation cascades [154], [155].

Overall, this dissertation described a new novel SELEX workflow for isolating high affinity and specificity aptamers for four targets. The methods described in this dissertation could be useful for other researchers in developing aptamers for their targets of interest. Additionally, the aptamers isolated have applications in cancer and studying the BBB. Future work will focus on applying these purified-target and whole-cell selections to new targets aimed at developing therapeutic aptamers. Furthermore, the selection workflow can be further optimized in an effort to improve the specificity of aptamers that can be isolated. These efforts will include adjusting selection platforms, such as drastically altering the ratio of primary target to off-targets by reducing the amount of primary target and increasing the off-targets over iterative rounds. Multiplexing the selection will also be incorporated by introducing multiple primary targets and increasing the number of off-targets to introduce prospective aptamers to more structurally similar targets, in an effort to increase the selectivity of the workflow. An array-based system would also improve the throughput of the aptamers selected from this workflow. Overall, this selection workflow can be further optimized to improve specificity and throughput aimed at developing aptamers for a wide range of therapeutic targets.

Chapter 7

REFERENCES

[1] M. R. Dunn, R. M. Jimenez, and J. C. Chaput, “Analysis of aptamer discovery and technology,” *Nat. Rev. Chem.*, vol. 1, no. 10, p. 76, Oct. 2017, doi: 10.1038/s41570-017-0076.

[2] H. Sun, X. Zhu, P. Y. Lu, R. R. Rosato, W. Tan, and Y. Zu, “Oligonucleotide Aptamers: New Tools for Targeted Cancer Therapy,” *Mol. Ther. Nucleic Acids*, vol. 3, no. 8, p. e182, Aug. 2014, doi: 10.1038/mtna.2014.32.

[3] A. Ozer, J. M. Pagano, and J. T. Lis, “New Technologies Provide Quantum Changes in the Scale, Speed, and Success of SELEX Methods and Aptamer Characterization,” *Mol. Ther. Nucleic Acids*, vol. 3, no. 8, p. e183, Aug. 2014, doi: 10.1038/mtna.2014.34.

[4] A. D. Ellington and J. W. Szostak, “In vitro selection of RNA molecules that bind specific ligands,” *Nature*, vol. 346, no. 6287, pp. 818–822, Aug. 1990, doi: 10.1038/346818a0.

[5] C. Tuerk and L. Gold, “Systematic evolution of ligands by exponential enrichment: RNA ligands to bacteriophage T4 DNA polymerase,” *Science*, vol. 249, no. 4968, pp. 505–510, Aug. 1990.

[6] R. Stoltenburg, C. Reinemann, and B. Strehlitz, “SELEX--a (r)evolutionary method to generate high-affinity nucleic acid ligands,” *Biomol. Eng.*, vol. 24, no. 4, pp. 381–403, Oct. 2007, doi: 10.1016/j.bioeng.2007.06.001.

[7] M. Cho *et al.*, “Quantitative selection of DNA aptamers through microfluidic selection and high-throughput sequencing,” *Proc. Natl. Acad. Sci.*, vol. 107, no. 35, pp. 15373–15378, Aug. 2010, doi: 10.1073/pnas.1009331107.

[8] A. Geiger, P. Burgstaller, H. von der Eltz, A. Roeder, and M. Famulok, “RNA Aptamers That Bind l-Arginine with Sub-Micromolar Dissociation Constants and High Enantioselectivity,” *Nucleic Acids Res.*, vol. 24, no. 6, pp. 1029–1036, Mar. 1996, doi: 10.1093/nar/24.6.1029.

[9] R. D. Jenison, S. C. Gill, A. Pardi, and B. Polisky, “High-resolution molecular discrimination by RNA,” *Science*, vol. 263, no. 5152, pp. 1425–1429, Mar. 1994, doi: 10.1126/science.7510417.

[10] L. Chen *et al.*, “The isolation of an RNA aptamer targeting to p53 protein with single amino acid mutation,” *Proc. Natl. Acad. Sci.*, vol. 112, no. 32, pp. 10002–10007, Aug. 2015, doi: 10.1073/pnas.1502159112.

[11] H. Sun and Y. Zu, “A Highlight of Recent Advances in Aptamer Technology and Its Application,” *Molecules*, vol. 20, no. 7, pp. 11959–11980, Jun. 2015, doi: 10.3390/molecules200711959.

[12] A. D. Keefe, S. Pai, and A. Ellington, “Aptamers as therapeutics,” *Nat. Rev. Drug Discov.*, vol. 9, no. 7, p. 537, Jul. 2010, doi: 10.1038/nrd3141.

[13] J. Zhou and J. Rossi, “Aptamers as targeted therapeutics: current potential and challenges,” *Nat. Rev. Drug Discov.*, vol. 16, no. 3, pp. 181–202, Mar. 2017, doi: 10.1038/nrd.2016.199.

[14] V. Thiviyanathan and D. G. Gorenstein, “Aptamers and the Next Generation of Diagnostic Reagents,” *Proteomics Clin. Appl.*, vol. 6, no. 0, pp. 563–573, Dec. 2012, doi: 10.1002/prca.201200042.

[15] Z. Zhang, O. Oni, and J. Liu, “New insights into a classic aptamer: binding sites, cooperativity and more sensitive adenosine detection,” *Nucleic Acids Res.*, vol. 45, no. 13, pp. 7593–7601, Jul. 2017, doi: 10.1093/nar/gkx517.
[16] S. M. Nimjee, C. P. Rusconi, and B. A. Sullenger, “Aptamers: An Emerging Class of Therapeutics,” *Annu. Rev. Med.*, vol. 56, no. 1, pp. 555–583, 2005, doi: 10.1146/annurev.med.56.062904.144915.
[17] H. Shi, B. E. Hoffman, and J. T. Lis, “RNA aptamers as effective protein antagonists in a multicellular organism,” *Proc. Natl. Acad. Sci.*, vol. 96, no. 18, pp. 10033–10038, Aug. 1999, doi: 10.1073/pnas.96.18.10033.
[18] D. G. NICKENS, J. T. PATTERSON, and D. H. BURKE, “Inhibition of HIV-1 reverse transcriptase by RNA aptamers in Escherichia coli,” *RNA*, vol. 9, no. 9, pp. 1029–1033, Sep. 2003, doi: 10.1261/rna.5550103.
[19] K. Wakui *et al.*, “Rapidly Neutralizable and Highly Anticoagulant Thrombin-Binding DNA Aptamer Discovered by MACE SELEX,” *Mol. Ther. Nucleic Acids*, vol. 16, pp. 348–359, Mar. 2019, doi: 10.1016/j.omtn.2019.03.002.
[20] R. Cp, Y. A, L. Hk, L. Jh, and S. Ba, “Blocking the initiation of coagulation by RNA aptamers to factor VIIa.,” *Thromb. Haemost.*, vol. 84, no. 5, pp. 841–848, Nov. 2000.
[21] E. W. M. Ng, D. T. Shima, P. Calias, E. T. Cunningham, D. R. Guyer, and A. P. Adamis, “Pegaptanib, a targeted anti-VEGF aptamer for ocular vascular disease,” *Nat. Rev. Drug Discov.*, vol. 5, no. 2, pp. 123–132, Feb. 2006, doi: 10.1038/nrd1955.
[22] J. Charlton, G. P. Kirschenheuter, and D. Smith, “Highly Potent Irreversible Inhibitors of Neutrophil Elastase Generated by Selection from a Randomized DNA−Valine Phosphonate Library,” *Biochemistry (Mosc.)*, vol. 36, no. 10, pp. 3018–3026, Mar. 1997, doi: 10.1021/bi962669h.
[23] C. Q. Vu, P. Rotkrua, B. Soontornworajit, and Y. Tantirungrotechai, “Effect of PDGF-B aptamer on PDGFRβ/PDGF-B interaction: Molecular dynamics study,” *J. Mol. Graph. Model.*, vol. 82, pp. 145–156, Jun. 2018, doi: 10.1016/j.jmgm.2018.04.012.
[24] J. P. Dassie *et al.*, “Targeted Inhibition of Prostate Cancer Metastases with an RNA Aptamer to Prostate-specific Membrane Antigen,” *Mol. Ther.*, vol. 22, no. 11, pp. 1910–1922, Nov. 2014, doi: 10.1038/mt.2014.117.
[25] H. Ulrich *et al.*, “In vitro selection of RNA molecules that displace cocaine from the membrane-bound nicotinic acetylcholine receptor,” *Proc. Natl. Acad. Sci. U. S. A.*, vol. 95, no. 24, pp. 14051–14056, Nov. 1998.
[26] B. Cao, Y. Hu, J. Duan, J. Ma, D. Xu, and X.-D. Yang, “Selection of a Novel DNA Aptamer for Assay of Intracellular Interferon-Gamma,” *PLOS ONE*, vol. 9, no. 5, p. e98214, May 2014, doi: 10.1371/journal.pone.0098214.
[27] X. Yu *et al.*, “Targeting EGFR/HER2/HER3 with a Three-in-One Aptamer-siRNA Chimera Confers Superior Activity against HER2+ Breast Cancer,” *Mol. Ther. Nucleic Acids*, vol. 10, pp. 317–330, Dec. 2017, doi: 10.1016/j.omtn.2017.12.015.
[28] E. D. Pratico, B. A. Sullenger, and S. K. Nair, “Identification and Characterization of an Agonistic Aptamer Against the T Cell Costimulatory Receptor, OX40,” *Nucleic Acid Ther.*, vol. 23, no. 1, pp. 35–43, Feb. 2013, doi: 10.1089/nat.2012.0388.
[29] M. M. Soldevilla, H. Villanueva, M. Bendandi, S. Inoges, A. López-Díaz de Cerio, and F. Pastor, “2-fluoro-RNA oligonucleotide CD40 targeted aptamers for the control of B lymphoma and bone-marrow aplasia,” *Biomaterials*, vol. 67, pp. 274–285, Oct. 2015, doi: 10.1016/j.biomaterials.2015.07.020.

[30] F. Pastor *et al.*, "CD28 Aptamers as Powerful Immune Response Modulators," *Mol. Ther. Nucleic Acids*, vol. 2, no. 6, p. e98, Jun. 2013, doi: 10.1038/mtna.2013.26.
[31] S. Kruspe, F. Mittelberger, K. Szameit, and U. Hahn, "Aptamers as Drug Delivery Vehicles," *ChemMedChem*, vol. 9, no. 9, pp. 1998–2011, Sep. 2014, doi: 10.1002/cmdc.201402163.
[32] A. P. Dinis Ano Bom, P. C. da Costa Neves, C. E. Bonacossa de Almeida, D. Silva, and S. Missailidis, "Aptamers as Delivery Agents of siRNA and Chimeric Formulations for the Treatment of Cancer," *Pharmaceutics*, vol. 11, no. 12, Dec. 2019, doi: 10.3390/pharmaceutics11120684.
[33] M. Iaboni *et al.*, "Aptamer-miRNA-212 Conjugate Sensitizes NSCLC Cells to TRAIL," *Mol. Ther. Nucleic Acids*, vol. 5, no. 3, p. e289, Mar. 2016, doi: 10.1038/mtna.2016.5.
[34] G. Yu, H. Li, S. Yang, J. Wen, J. Niu, and Y. Zu, "ssDNA Aptamer Specifically Targets and Selectively Delivers Cytotoxic Drug Doxorubicin to HepG2 Cells," *PLOS ONE*, vol. 11, no. 1, p. e0147674, Jan. 2016, doi: 10.1371/journal.pone.0147674.
[35] J. Zhu, H. Huang, S. Dong, L. Ge, and Y. Zhang, "Progress in Aptamer-Mediated Drug Delivery Vehicles for Cancer Targeting and Its Implications in Addressing Chemotherapeutic Challenges," *Theranostics*, vol. 4, no. 9, pp. 931–944, Jul. 2014, doi: 10.7150/thno.9663.
[36] N. Alizadeh, M. Y. Memar, B. Mehramuz, S. S. Abibiglou, F. Hemmati, and H. S. Kafil, "Current advances in aptamer-assisted technologies for detecting bacterial and fungal toxins," *J. Appl. Microbiol.*, vol. 124, no. 3, pp. 644–651, 2018, doi: 10.1111/jam.13650.
[37] V. C. Ozalp, F. Eyidogan, and H. A. Oktem, "Aptamer-Gated Nanoparticles for Smart Drug Delivery," *Pharmaceuticals*, vol. 4, no. 8, pp. 1137–1157, Aug. 2011, doi: 10.3390/ph4081137.
[38] J. Zhou and J. J. Rossi, "Cell-Specific Aptamer-Mediated Targeted Drug Delivery," *Oligonucleotides*, vol. 21, no. 1, pp. 1–10, Feb. 2011, doi: 10.1089/oli.2010.0264.
[39] M. S. Spitzer *et al.*, "Comparative antiproliferative and cytotoxic profile of bevacizumab (Avastin), pegaptanib (Macugen) and ranibizumab (Lucentis) on different ocular cells," *Graefes Arch. Clin. Exp. Ophthalmol.*, vol. 245, no. 12, pp. 1837–1842, Dec. 2007, doi: 10.1007/s00417-007-0568-7.
[40] B. Sullenger, R. Woodruff, and D. M. Monroe, "Potent Anticoagulant Aptamer Directed against Factor IXa Blocks Macromolecular Substrate Interaction," *J. Biol. Chem.*, vol. 287, no. 16, pp. 12779–12786, Apr. 2012, doi: 10.1074/jbc.M111.300772.
[41] A. V. Lakhin, V. Z. Tarantul, and L. V. Gening, "Aptamers: Problems, Solutions and Prospects," *Acta Naturae*, vol. 5, no. 4, pp. 34–43, 2013.
[42] J. Zhou and J. J. Rossi, "Cell-type-specific, Aptamer-functionalized Agents for Targeted Disease Therapy," *Mol. Ther. Nucleic Acids*, vol. 3, no. 6, p. e169, Jun. 2014, doi: 10.1038/mtna.2014.21.
[43] H. Kaur, J. G. Bruno, A. Kumar, and T. K. Sharma, "Aptamers in the Therapeutics and Diagnostics Pipelines," *Theranostics*, vol. 8, no. 15, pp. 4016–4032, Jul. 2018, doi: 10.7150/thno.25958.
[44] S. Ni *et al.*, "Chemical Modifications of Nucleic Acid Aptamers for Therapeutic Purposes," *Int. J. Mol. Sci.*, vol. 18, no. 8, Aug. 2017, doi: 10.3390/ijms18081683.
[45] M. Blind and M. Blank, "Aptamer Selection Technology and Recent Advances," *Mol. Ther. Nucleic Acids*, vol. 4, no. 1, p. e223, Jan. 2015, doi: 10.1038/mtna.2014.74.
[46] P. Kalra, A. Dhiman, W. C. Cho, J. G. Bruno, and T. K. Sharma, "Simple Methods and Rational Design for Enhancing Aptamer Sensitivity and Specificity," *Front. Mol. Biosci.*, vol. 5,

May 2018, doi: 10.3389/fmolb.2018.00041.
[47] B. N. Gawande *et al.*, "Selection of DNA aptamers with two modified bases," *Proc. Natl. Acad. Sci.*, vol. 114, no. 11, pp. 2898–2903, Mar. 2017, doi: 10.1073/pnas.1615475114.
[48] J. C. Rohloff *et al.*, "Nucleic Acid Ligands With Protein-like Side Chains: Modified Aptamers and Their Use as Diagnostic and Therapeutic Agents," *Mol. Ther. - Nucleic Acids*, vol. 3, p. e201, Jan. 2014, doi: 10.1038/mtna.2014.49.
[49] S. Kraemer *et al.*, "From SOMAmer-Based Biomarker Discovery to Diagnostic and Clinical Applications: A SOMAmer-Based, Streamlined Multiplex Proteomic Assay," *PLoS ONE*, vol. 6, no. 10, Oct. 2011, doi: 10.1371/journal.pone.0026332.
[50] A. Vater and S. Klussmann, "Turning mirror-image oligonucleotides into drugs: the evolution of Spiegelmer® therapeutics," *Drug Discov. Today*, vol. 20, no. 1, pp. 147–155, Jan. 2015, doi: 10.1016/j.drudis.2014.09.004.
[51] R. M. Boomer, S. D. Lewis, J. M. Healy, M. Kurz, C. Wilson, and T. G. McCauley, "Conjugation to Polyethylene Glycol Polymer Promotes Aptamer Biodistribution to Healthy and Inflamed Tissues," *Oligonucleotides*, vol. 15, no. 3, pp. 183–195, Sep. 2005, doi: 10.1089/oli.2005.15.183.
[52] R. Wang *et al.*, "Using modified aptamers for site specific protein–aptamer conjugations †Electronic supplementary information (ESI) available: All experimental details are written as a separate section in the SI materials. These include the synthetic procedures, testing protocols etc. They are written in detail and are complete. See DOI: 10.1039/c5sc02631h," *Chem. Sci.*, vol. 7, no. 3, pp. 2157–2161, Mar. 2016, doi: 10.1039/c5sc02631h.
[53] C. H. Lee, S.-H. Lee, J. H. Kim, Y.-H. Noh, G.-J. Noh, and S.-W. Lee, "Pharmacokinetics of a Cholesterol-conjugated Aptamer Against the Hepatitis C Virus (HCV) NS5B Protein," *Mol. Ther. Nucleic Acids*, vol. 4, no. 10, p. e254, Oct. 2015, doi: 10.1038/mtna.2015.30.
[54] "Construction of an Aptamer Modified Liposomal System Targeted to Tumor Endothelial Cells." https://www.jstage.jst.go.jp/article/bpb/37/11/37_b14-00338/_article (accessed Jun. 25, 2020).
[55] M. Vorobyeva, P. Vorobjev, and A. Venyaminova, "Multivalent Aptamers: Versatile Tools for Diagnostic and Therapeutic Applications," *Molecules*, vol. 21, no. 12, Nov. 2016, doi: 10.3390/molecules21121613.
[56] J. Qian, X. Lou, Y. Zhang, Y. Xiao, and H. T. Soh, "Generation of Highly Specific Aptamers via Micromagnetic Selection," *Anal. Chem.*, vol. 81, no. 13, pp. 5490–5495, Jul. 2009, doi: 10.1021/ac900759k.
[57] K. M. Ahmad, S. S. Oh, S. Kim, F. M. McClellen, Y. Xiao, and H. T. Soh, "Probing the Limits of Aptamer Affinity with a Microfluidic SELEX Platform," *PLoS ONE*, vol. 6, no. 11, Nov. 2011, doi: 10.1371/journal.pone.0027051.
[58] M. Darmostuk, S. Rimpelova, H. Gbelcova, and T. Ruml, "Current approaches in SELEX: An update to aptamer selection technology," *Biotechnol. Adv.*, vol. 33, no. 6, Part 2, pp. 1141–1161, Nov. 2015, doi: 10.1016/j.biotechadv.2015.02.008.
[59] H. Hasegawa, N. Savory, K. Abe, and K. Ikebukuro, "Methods for Improving Aptamer Binding Affinity," *Molecules*, vol. 21, no. 4, Mar. 2016, doi: 10.3390/molecules21040421.
[60] M. Takahashi *et al.*, "High throughput sequencing analysis of RNA libraries reveals the influences of initial library and PCR methods on SELEX efficiency," *Sci. Rep.*, vol. 6, p. 33697, Sep. 2016, doi: 10.1038/srep33697.
[61] M. Jing and M. T. Bowser, "A Review of Methods for Measuring Aptamer-

ProteinEquilibria," *Anal. Chim. Acta*, vol. 686, no. 1–2, pp. 9–18, Feb. 2011, doi: 10.1016/j.aca.2010.10.032.
[62] S. Challa, S. Tzipori, and A. Sheoran, "Selective Evolution of Ligands by Exponential Enrichment to Identify RNA Aptamers against Shiga Toxins," *J. Nucleic Acids*, vol. 2014, 2014, doi: 10.1155/2014/214929.
[63] N. S. Hamedani and J. Müller, "Capillary Electrophoresis for the Selection of DNA Aptamers Recognizing Activated Protein C," in *Nucleic Acid Aptamers: Selection, Characterization, and Application*, G. Mayer, Ed. New York, NY: Springer New York, 2016, pp. 61–75.
[64] X. Lou *et al.*, "Micromagnetic selection of aptamers in microfluidic channels," *Proc. Natl. Acad. Sci.*, vol. 106, no. 9, pp. 2989–2994, Mar. 2009, doi: 10.1073/pnas.0813135106.
[65] S. Catuogno and C. L. Esposito, "Aptamer Cell-Based Selection: Overview and Advances," *Biomedicines*, vol. 5, no. 3, Aug. 2017, doi: 10.3390/biomedicines5030049.
[66] N. Ardjomandi *et al.*, "Identification of an Aptamer Binding to Human Osteogenic-Induced Progenitor Cells," *Nucleic Acid Ther.*, vol. 23, no. 1, pp. 44–61, Feb. 2013, doi: 10.1089/nat.2012.0349.
[67] D. Ruiz Ciancio, M. R. Vargas, W. H. Thiel, M. A. Bruno, P. H. Giangrande, and M. B. Mestre, "Aptamers as Diagnostic Tools in Cancer," *Pharmaceuticals*, vol. 11, no. 3, Sep. 2018, doi: 10.3390/ph11030086.
[68] C. Cheng, Y. H. Chen, K. A. Lennox, M. A. Behlke, and B. L. Davidson, "In vivo SELEX for Identification of Brain-penetrating Aptamers," *Mol. Ther. — Nucleic Acids*, vol. 2, no. 1, p. e67, Jan. 2013, doi: 10.1038/mtna.2012.59.
[69] H. Wang *et al.*, "In Vivo SELEX of an Inhibitory NSCLC-Specific RNA Aptamer from PEGylated RNA Library," *Mol. Ther. Nucleic Acids*, vol. 10, pp. 187–198, Dec. 2017, doi: 10.1016/j.omtn.2017.12.003.
[70] M. Sola *et al.*, "Aptamers Against Live Targets: Is In Vivo SELEX Finally Coming to the Edge?," *Mol. Ther. - Nucleic Acids*, vol. 21, pp. 192–204, Sep. 2020, doi: 10.1016/j.omtn.2020.05.025.
[71] J. Cruz-Toledo *et al.*, "Aptamer base: a collaborative knowledge base to describe aptamers and SELEX experiments," *Database J. Biol. Databases Curation*, vol. 2012, Feb. 2012, doi: 10.1093/database/bas006.
[72] Y. Zhang, B. S. Lai, and M. Juhas, "Recent Advances in Aptamer Discovery and Applications," *Molecules*, vol. 24, no. 5, Mar. 2019, doi: 10.3390/molecules24050941.
[73] K. Shao, W. Ding, F. Wang, H. Li, D. Ma, and H. Wang, "Emulsion PCR: a high efficient way of PCR amplification of random DNA libraries in aptamer selection," *PloS One*, vol. 6, no. 9, p. e24910, 2011, doi: 10.1371/journal.pone.0024910.
[74] F. Tolle, J. Wilke, J. Wengel, and G. Mayer, "By-Product Formation in Repetitive PCR Amplification of DNA Libraries during SELEX," *PLOS ONE*, vol. 9, no. 12, p. e114693, Dec. 2014, doi: 10.1371/journal.pone.0114693.
[75] "Platelet Derived Growth Factor AA - an overview | ScienceDirect Topics." https://www.sciencedirect.com/topics/neuroscience/platelet-derived-growth-factor-aa (accessed Jun. 26, 2020).
[76] E. Mandelkow and E.-M. Mandelkow, "Kinesin motors and disease," *Trends Cell Biol.*, vol. 12, no. 12, pp. 585–591, Dec. 2002, doi: 10.1016/S0962-8924(02)02400-5.
[77] N. J. Bryant, R. Govers, and D. E. James, "Regulated transport of the glucose transporter GLUT4," *Nat. Rev. Mol. Cell Biol.*, vol. 3, no. 4, pp. 267–277, Apr. 2002, doi: 10.1038/nrm782.

[78] T. Schütze *et al.*, "Probing the SELEX Process with Next-Generation Sequencing," *PLOS ONE*, vol. 6, no. 12, p. e29604, Dec. 2011, doi: 10.1371/journal.pone.0029604.
[79] M. Cho *et al.*, "Quantitative selection and parallel characterization of aptamers," *Proc. Natl. Acad. Sci.*, vol. 110, no. 46, pp. 18460–18465, Nov. 2013, doi: 10.1073/pnas.1315866110.
[80] R. K. Mosing, S. D. Mendonsa, and M. T. Bowser, "Capillary Electrophoresis-SELEX Selection of Aptamers with Affinity for HIV-1 Reverse Transcriptase," *Anal. Chem.*, vol. 77, no. 19, pp. 6107–6112, Oct. 2005, doi: 10.1021/ac050836q.
[81] J. Yang and M. T. Bowser, "CE-SELEX selection of catalytic DNA aptamers for a small molecule porphyrin target," *Anal. Chem.*, vol. 85, no. 3, pp. 1525–1530, Feb. 2013, doi: 10.1021/ac302721j.
[82] E. Ouellet, J. H. Foley, E. M. Conway, and C. Haynes, "Hi-Fi SELEX: A high-fidelity digital-PCR based therapeutic aptamer discovery platform," *Biotechnol. Bioeng.*, vol. 112, no. 8, pp. 1506–1522, Aug. 2015, doi: 10.1002/bit.25581.
[83] E. Ouellet, E. T. Lagally, K. C. Cheung, and C. A. Haynes, "A simple method for eliminating fixed-region interference of aptamer binding during SELEX," *Biotechnol. Bioeng.*, vol. 111, no. 11, pp. 2265–2279, Nov. 2014, doi: 10.1002/bit.25294.
[84] H. Qu, A. T. Csordas, J. Wang, S. S. Oh, M. S. Eisenstein, and H. T. Soh, "Rapid and Label-Free Strategy to Isolate Aptamers for Metal Ions," *ACS Nano*, vol. 10, no. 8, pp. 7558–7565, Aug. 2016, doi: 10.1021/acsnano.6b02558.
[85] D. Breitsprecher, N. Schlinck, D. Witte, S. Duhr, P. Baaske, and T. Schubert, "Aptamer Binding Studies Using MicroScale Thermophoresis," in *Nucleic Acid Aptamers: Selection, Characterization, and Application*, G. Mayer, Ed. New York, NY: Springer New York, 2016, pp. 99–111.
[86] C. Entzian and T. Schubert, "Studying small molecule–aptamer interactions using MicroScale Thermophoresis (MST)," *Methods*, vol. 97, pp. 27–34, Mar. 2016, doi: 10.1016/j.ymeth.2015.08.023.
[87] J. Hoinka, A. Berezhnoy, Z. E. Sauna, E. Gilboa, and T. M. Przytycka, "AptaCluster - A Method to Cluster HT-SELEX Aptamer Pools and Lessons from its Application," *Res. Comput. Mol. Biol. Annu. Int. Conf. RECOMB Proc. RECOMB Conf. 2005-*, vol. 8394, pp. 115–128, 2014, doi: 10.1007/978-3-319-05269-4_9.
[88] B. J. O'Grady, J. X. Wang, S. L. Faley, D. A. Balikov, E. S. Lippmann, and L. M. Bellan, "A Customizable, Low-Cost Perfusion System for Sustaining Tissue Constructs," *SLAS Technol. Transl. Life Sci. Innov.*, vol. 23, no. 6, pp. 592–598, Dec. 2018, doi: 10.1177/2472630318775059.
[89] K. Germer, M. Leonard, and X. Zhang, "RNA aptamers and their therapeutic and diagnostic applications," *Int. J. Biochem. Mol. Biol.*, vol. 4, no. 1, pp. 27–40, Mar. 2013.
[90] K.-N. Kang and Y.-S. Lee, "RNA Aptamers: A Review of Recent Trends and Applications," in *Future Trends in Biotechnology*, J.-J. Zhong, Ed. Berlin, Heidelberg: Springer Berlin Heidelberg, 2013, pp. 153–169.
[91] A. W. Kahsai *et al.*, "Conformationally selective RNA aptamers allosterically modulate the β2-adrenoceptor," *Nat. Chem. Biol.*, vol. 12, no. 9, pp. 709–716, Sep. 2016, doi: 10.1038/nchembio.2126.
[92] P. Ray and R. R. White, "Cell-SELEX Identifies a 'Sticky' RNA Aptamer Sequence," *Journal of Nucleic Acids*, 2017. https://www.hindawi.com/journals/jna/2017/4943072/ (accessed Dec. 05, 2017).
[93] R. J. van Vuuren, M. H. Visagie, A. E. Theron, and A. M. Joubert, "Antimitotic drugs in

the treatment of cancer," *Cancer Chemother. Pharmacol.*, vol. 76, pp. 1101–1112, 2015, doi: 10.1007/s00280-015-2903-8.
[94] G. M. Chin and R. Herbst, "Induction of apoptosis by monastrol, an inhibitor of the mitotic kinesin Eg5, is independent of the spindle checkpoint," *Mol. Cancer Ther.*, vol. 5, no. 10, pp. 2580–2591, Oct. 2006, doi: 10.1158/1535-7163.MCT-06-0201.
[95] M. E. Tanenbaum, L. Macůrek, A. Janssen, E. F. Geers, M. Alvarez-Fernández, and R. H. Medema, "Kif15 cooperates with eg5 to promote bipolar spindle assembly," *Curr. Biol. CB*, vol. 19, no. 20, pp. 1703–1711, Nov. 2009, doi: 10.1016/j.cub.2009.08.027.
[96] A. S. Khalil *et al.*, "Kinesin's cover-neck bundle folds forward to generate force," *Proc. Natl. Acad. Sci.*, vol. 105, no. 49, pp. 19247–19252, Dec. 2008, doi: 10.1073/pnas.0805147105.
[97] "HiScribe™ T7 Quick High Yield RNA Synthesis Kit | New England Biolabs." https://www.neb.ca/detail.php?id=e2050 (accessed Jun. 25, 2020).
[98] R. W. Carthew and E. J. Sontheimer, "Origins and Mechanisms of miRNAs and siRNAs," *Cell*, vol. 136, no. 4, pp. 642–655, Feb. 2009, doi: 10.1016/j.cell.2009.01.035.
[99] K. Tatiparti, S. Sau, S. K. Kashaw, and A. K. Iyer, "siRNA Delivery Strategies: A Comprehensive Review of Recent Developments," *Nanomaterials*, vol. 7, no. 4, Apr. 2017, doi: 10.3390/nano7040077.
[100] I. V. Chernikov, V. V. Vlassov, and E. L. Chernolovskaya, "Current Development of siRNA Bioconjugates: From Research to the Clinic," *Front. Pharmacol.*, vol. 10, 2019, doi: 10.3389/fphar.2019.00444.
[101] D. Sleep, J. Cameron, and L. R. Evans, "Albumin as a versatile platform for drug half-life extension," *Biochim. Biophys. Acta BBA - Gen. Subj.*, vol. 1830, no. 12, pp. 5526–5534, Dec. 2013, doi: 10.1016/j.bbagen.2013.04.023.
[102] D. Bumcrot, M. Manoharan, V. Koteliansky, and D. W. Y. Sah, "RNAi therapeutics: a potential new class of pharmaceutical drugs," *Nat. Chem. Biol.*, vol. 2, no. 12, pp. 711–719, Dec. 2006, doi: 10.1038/nchembio839.
[103] H. Dana *et al.*, "Molecular Mechanisms and Biological Functions of siRNA," *Int. J. Biomed. Sci. IJBS*, vol. 13, no. 2, pp. 48–57, Jun. 2017.
[104] A. J. Pratt and I. J. MacRae, "The RNA-induced Silencing Complex: A Versatile Gene-silencing Machine," *J. Biol. Chem.*, vol. 284, no. 27, pp. 17897–17901, Jul. 2009, doi: 10.1074/jbc.R900012200.
[105] S.-H. Chen and G. Zhaori, "Potential clinical applications of siRNA technique: benefits and limitations," *Eur. J. Clin. Invest.*, vol. 41, no. 2, pp. 221–232, 2011, doi: 10.1111/j.1365-2362.2010.02400.x.
[106] M. Dominska and D. M. Dykxhoorn, "Breaking down the barriers: siRNA delivery and endosome escape," *J. Cell Sci.*, vol. 123, no. 8, pp. 1183–1189, Apr. 2010, doi: 10.1242/jcs.066399.
[107] N. Gupta, D. B. Rai, A. K. Jangid, D. Pooja, and H. Kulhari, "Nanomaterials-Based siRNA Delivery: Routes of Administration, Hurdles and Role of Nanocarriers," *Nanotechnol. Mod. Anim. Biotechnol.*, pp. 67–114, Mar. 2019, doi: 10.1007/978-981-13-6004-6_3.
[108] S. M. Sarett *et al.*, "Lipophilic siRNA targets albumin in situ and promotes bioavailability, tumor penetration, and carrier-free gene silencing," *Proc. Natl. Acad. Sci.*, vol. 114, no. 32, pp. E6490–E6497, Aug. 2017, doi: 10.1073/pnas.1621240114.
[109] S. Kruspe and P. H. Giangrande, "Aptamer-siRNA Chimeras: Discovery, Progress, and Future Prospects," *Biomedicines*, vol. 5, no. 3, p. 45, Aug. 2017, doi: 10.3390/biomedicines5030045.

[110] P. Sivakumar, S. Kim, H. C. Kang, and M. S. Shim, "Targeted siRNA delivery using aptamer-siRNA chimeras and aptamer-conjugated nanoparticles," *WIREs Nanomedicine Nanobiotechnology*, vol. 11, no. 3, p. e1543, 2019, doi: 10.1002/wnan.1543.
[111] J. Zhou and J. J. Rossi, "Therapeutic Potential of Aptamer-siRNA Conjugates for Treatment of HIV-1," *BioDrugs Clin. Immunother. Biopharm. Gene Ther.*, vol. 26, no. 6, pp. 393–400, Dec. 2012, doi: 10.2165/11635350-000000000-00000.
[112] C. Tao, Y. J. Chuah, C. Xu, and D.-A. Wang, "Albumin conjugates and assemblies as versatile bio-functional additives and carriers for biomedical applications," *J. Mater. Chem. B*, vol. 7, no. 3, pp. 357–367, Jan. 2019, doi: 10.1039/C8TB02477D.
[113] H. En and D. Cl, "Harnessing Albumin as a Carrier for Cancer Therapies," *Advanced drug delivery reviews*, May 2018. https://pubmed.ncbi.nlm.nih.gov/30012492/ (accessed Jun. 25, 2020).
[114] H. Y. Kong and J. Byun, "Screening and Characterization of a Novel RNA Aptamer That Specifically Binds to Human Prostatic Acid Phosphatase and Human Prostate Cancer Cells," *Mol. Cells*, vol. 38, no. 2, pp. 171–179, Feb. 2015, doi: 10.14348/molcells.2015.2272.
[115] G. M. Stovall *et al.*, "In Vitro Selection Using Modified or Unnatural Nucleotides," *Curr. Protoc. Nucleic Acid Chem. Ed. Serge Beaucage Al*, vol. 56, p. 9.6.1-9.6.33, Mar. 2014, doi: 10.1002/0471142700.nc0906s56.
[116] C. L. Esposito, S. Catuogno, G. Condorelli, P. Ungaro, and V. de Franciscis, "Aptamer Chimeras for Therapeutic Delivery: The Challenging Perspectives," *Genes*, vol. 9, no. 11, Oct. 2018, doi: 10.3390/genes9110529.
[117] M. Takenaka, Y. Okumura, T. Amino, Y. Miyachi, C. Ogino, and A. Kondo, "DNA-duplex linker for AFM-SELEX of DNA aptamer against human serum albumin," *Bioorg. Med. Chem. Lett.*, vol. 27, no. 4, pp. 954–957, Feb. 2017, doi: 10.1016/j.bmcl.2016.12.080.
[118] J. P. Dassie *et al.*, "Systemic administration of optimized aptamer-siRNA chimeras promotes regression of PSMA-expressing tumors," *Nat. Biotechnol.*, vol. 27, no. 9, pp. 839–849, Sep. 2009, doi: 10.1038/nbt.1560.
[119] A. R. M. Bradbury, S. Sidhu, S. Dübel, and J. McCafferty, "Beyond natural antibodies: the power of in vitro display technologies," *Nat. Biotechnol.*, vol. 29, no. 3, pp. 245–254, Mar. 2011, doi: 10.1038/nbt.1791.
[120] T. Uchański *et al.*, "An improved yeast surface display platform for the screening of nanobody immune libraries," *Sci. Rep.*, vol. 9, no. 1, pp. 1–12, Jan. 2019, doi: 10.1038/s41598-018-37212-3.
[121] K. Sefah, D. Shangguan, X. Xiong, M. B. O'Donoghue, and W. Tan, "Development of DNA aptamers using Cell-SELEX," *Nat. Protoc.*, vol. 5, no. 6, pp. 1169–1185, Jun. 2010, doi: 10.1038/nprot.2010.66.
[122] X. X. Wang and E. V. Shusta, "The use of scFv-displaying yeast in mammalian cell surface selections," *J. Immunol. Methods*, vol. 304, no. 1–2, pp. 30–42, Sep. 2005, doi: 10.1016/j.jim.2005.05.006.
[123] J. Newton and S. L. Deutscher, "Phage peptide display," *Handb. Exp. Pharmacol.*, no. 185 Pt 2, pp. 145–163, 2008, doi: 10.1007/978-3-540-77496-9_7.
[124] G. Wang *et al.*, "Selection and characterization of DNA aptamer against glucagon receptor by cell-SELEX," *Sci. Rep.*, vol. 7, no. 1, pp. 1–10, Aug. 2017, doi: 10.1038/s41598-017-05840-w.
[125] T. Heitner, A. Moor, J. L. Garrison, C. Marks, T. Hasan, and J. D. Marks, "Selection of cell binding and internalizing epidermal growth factor receptor antibodies from a phage display

library," *J. Immunol. Methods*, vol. 248, no. 1–2, pp. 17–30, Feb. 2001, doi: 10.1016/s0022-1759(00)00340-9.
[126] "Selection of RNA aptamers against recombinant transforming growth factor-β type III receptor displayed on cell surface," *Biochimie*, vol. 88, no. 7, pp. 897–904, Jul. 2006, doi: 10.1016/j.biochi.2006.02.004.
[127] V. Askoxylakis *et al.*, "Peptide-based targeting of the platelet-derived growth factor receptor beta," *Mol. Imaging Biol.*, vol. 15, no. 2, pp. 212–221, Apr. 2013, doi: 10.1007/s11307-012-0578-7.
[128] M. Duan *et al.*, "Selection and characterization of DNA aptamer for metastatic prostate cancer recognition and tissue imaging," *Oncotarget*, vol. 7, no. 24, pp. 36436–36446, May 2016, doi: 10.18632/oncotarget.9262.
[129] M.-C. Mercier, M. Dontenwill, and L. Choulier, "Selection of Nucleic Acid Aptamers Targeting Tumor Cell-Surface Protein Biomarkers," *Cancers*, vol. 9, no. 6, Jun. 2017, doi: 10.3390/cancers9060069.
[130] J. W. Kim *et al.*, "Identification of DNA Aptamers toward Epithelial Cell Adhesion Molecule via Cell-SELEX," *Mol. Cells*, vol. 37, no. 10, pp. 742–746, Oct. 2014, doi: 10.14348/molcells.2014.0208.
[131] X. Wu *et al.*, "Cell-SELEX aptamer for highly specific radionuclide molecular imaging of glioblastoma in vivo," *PloS One*, vol. 9, no. 6, p. e90752, 2014, doi: 10.1371/journal.pone.0090752.
[132] L. A. Stern *et al.*, "Geometry and expression enhance enrichment of functional yeast-displayed ligands via cell panning," *Biotechnol. Bioeng.*, vol. 113, no. 11, pp. 2328–2341, Nov. 2016, doi: 10.1002/bit.26001.
[133] D. Dangaj *et al.*, "Novel recombinant human B7-H4 antibodies overcome tumoral immune escape to potentiate T cell anti-tumor responses," *Cancer Res.*, vol. 73, no. 15, pp. 4820–4829, Aug. 2013, doi: 10.1158/0008-5472.CAN-12-3457.
[134] K. Groff, J. Brown, and A. J. Clippinger, "Modern affinity reagents: Recombinant antibodies and aptamers," *Biotechnol. Adv.*, vol. 33, no. 8, pp. 1787–1798, Dec. 2015, doi: 10.1016/j.biotechadv.2015.10.004.
[135] D. Wang, J. M. Pascual, and D. De Vivo, "Glucose Transporter Type 1 Deficiency Syndrome," in *GeneReviews®*, M. P. Adam, H. H. Ardinger, R. A. Pagon, S. E. Wallace, L. J. Bean, K. Stephens, and A. Amemiya, Eds. Seattle (WA): University of Washington, Seattle, 1993.
[136] L. Szablewski, "Glucose Transporters in Brain: In Health and in Alzheimer's Disease," *J. Alzheimers Dis. JAD*, vol. 55, no. 4, pp. 1307–1320, 2017, doi: 10.3233/JAD-160841.
[137] M. Tang *et al.*, "Brain microvasculature defects and Glut1 deficiency syndrome averted by early repletion of the glucose transporter-1 protein," *Nat. Commun.*, vol. 8, no. 1, pp. 1–15, Jan. 2017, doi: 10.1038/ncomms14152.
[138] M. Mueckler and B. Thorens, "The SLC2 (GLUT) Family of Membrane Transporters," *Mol. Aspects Med.*, vol. 34, no. 0, pp. 121–138, 2013, doi: 10.1016/j.mam.2012.07.001.
[139] M. Mueckler and C. Makepeace, "Model of the Exofacial Substrate-Binding Site and Helical Folding of the Human Glut1 Glucose Transporter Based on Scanning Mutagenesis," *Biochemistry (Mosc.)*, vol. 48, no. 25, pp. 5934–5942, Jun. 2009, doi: 10.1021/bi900521n.
[140] E. H. Neal *et al.*, "A Simplified, Fully Defined Differentiation Scheme for Producing Blood-Brain Barrier Endothelial Cells from Human iPSCs," *Stem Cell Rep.*, vol. 12, no. 6, pp. 1380–1388, Jun. 2019, doi: 10.1016/j.stemcr.2019.05.008.

[141] E. S. Lippmann *et al.*, "Human Blood-Brain Barrier Endothelial Cells Derived from Pluripotent Stem Cells," *Nat. Biotechnol.*, vol. 30, no. 8, pp. 783–791, Aug. 2012, doi: 10.1038/nbt.2247.
[142] E. K. Brinkman, T. Chen, M. Amendola, and B. van Steensel, "Easy quantitative assessment of genome editing by sequence trace decomposition," *Nucleic Acids Res.*, vol. 42, no. 22, p. e168, Dec. 2014, doi: 10.1093/nar/gku936.
[143] J. C. Rosch, D. A. Balikov, F. Gong, and E. S. Lippmann, "A systematic evolution of ligands by exponential enrichment workflow with consolidated counterselection to efficiently isolate high-affinity aptamers," *Eng. Rep.*, vol. n/a, no. n/a, p. e12089, doi: 10.1002/eng2.12089.
[144] J. Hoinka, R. Backofen, and T. M. Przytycka, "AptaSUITE: A Full-Featured Bioinformatics Framework for the Comprehensive Analysis of Aptamers from HT-SELEX Experiments," *Mol. Ther. - Nucleic Acids*, vol. 11, pp. 515–517, Jun. 2018, doi: 10.1016/j.omtn.2018.04.006.
[145] C. S. Palmer, C. L. Cherry, I. Sada-Ovalle, A. Singh, and S. M. Crowe, "Glucose Metabolism in T Cells and Monocytes: New Perspectives in HIV Pathogenesis," *EBioMedicine*, vol. 6, pp. 31–41, Apr. 2016, doi: 10.1016/j.ebiom.2016.02.012.
[146] S. Kinet *et al.*, "Isolated receptor binding domains of HTLV-1 and HTLV-2 envelopes bind Glut-1 on activated CD4+ and CD8+ T cells," *Retrovirology*, vol. 4, p. 31, May 2007, doi: 10.1186/1742-4690-4-31.
[147] P. J. Thul *et al.*, "A subcellular map of the human proteome," *Science*, vol. 356, no. 6340, May 2017, doi: 10.1126/science.aal3321.
[148] S. Meyer *et al.*, "Development of an Efficient Targeted Cell-SELEX Procedure for DNA Aptamer Reagents," *PLOS ONE*, vol. 8, no. 8, p. e71798, Aug. 2013, doi: 10.1371/journal.pone.0071798.
[149] K. Pleiko, L. Saulite, V. Parfejevs, K. Miculis, E. Vjaters, and U. Riekstina, "Differential binding cell-SELEX method to identify cell-specific aptamers using high-throughput sequencing," *Sci. Rep.*, vol. 9, no. 1, pp. 1–12, May 2019, doi: 10.1038/s41598-019-44654-w.
[150] J. N. Zadeh *et al.*, "NUPACK: Analysis and design of nucleic acid systems," *J. Comput. Chem.*, vol. 32, no. 1, pp. 170–173, 2011, doi: 10.1002/jcc.21596.
[151] W. M. Pardridge, R. J. Boado, and C. R. Farrell, "Brain-type glucose transporter (GLUT-1) is selectively localized to the blood-brain barrier. Studies with quantitative western blotting and in situ hybridization," *J. Biol. Chem.*, vol. 265, no. 29, pp. 18035–18040, Oct. 1990.
[152] S. Hauptmann *et al.*, "Glucose transporter GLUT1 in colorectal adenocarcinoma cell lines is inversely correlated with tumour cell proliferation," *Anticancer Res.*, vol. 25, no. 5, pp. 3431–3436, Oct. 2005.
[153] L. Mahraoui *et al.*, "Presence and differential expression of SGLT1, GLUT1, GLUT2, GLUT3 and GLUT5 hexose-transporter mRNAs in Caco-2 cell clones in relation to cell growth and glucose consumption.," *Biochem. J.*, vol. 298, no. Pt 3, pp. 629–633, Mar. 1994.
[154] R. Ueki, A. Ueki, N. Kanda, and S. Sando, "Oligonucleotide-Based Mimetics of Hepatocyte Growth Factor," *Angew. Chem. Int. Ed.*, vol. 55, no. 2, pp. 579–582, 2016, doi: 10.1002/anie.201508572.
[155] B. Schmierer and C. S. Hill, "TGFβ–SMAD signal transduction: molecular specificity and functional flexibility," *Nat. Rev. Mol. Cell Biol.*, vol. 8, no. 12, pp. 970–982, Dec. 2007, doi: 10.1038/nrm2297.